Cellular phenotyping of paediatric airways disease

A thesis submitted to Imperial College London for the degree of Master of Philosophy

By

Hamdi Abdi Hassan, MSc

Inflammation, Repair and Development Section

National Heart and Lung Institute

Imperial College London

Declaration of Originality

I hereby declare that all the scientific work described in this thesis was conducted or directly supervised by myself, apart from the following exceptions. Bronchoscopy and phlebotomy procedures for the collection of paediatric bronchoalveolar lavage fluid and blood samples were performed by the clinicians Elizabeth Scotney and Katie Bonner. In chapter 3 blood collection from healthy adult volunteers in the lab was performed by Gill Martin. Samples acquired on the Fortessa III were conducted by Elizabeth Scotney, Katie Bonner, Ashley Hoffland and myself. In chapter 3, the autofluorescence extraction protocol was developed by Cytek Biosciences. The R programming script applied in chapter 5 was assisted by Kyle Mincham.

Copyright Declaration

The copyright of this thesis rests with the author. Unless otherwise indicated, its contents are licensed under a Creative Commons Attribution-Non-Commercial 4.0 International Licence (CC BY-NC). Under this licence, you may copy and redistribute the material in any medium or format. You may also create and distribute modified versions of the work. This is on the condition that: you credit the author and do not use it, or any derivative works, for a commercial purpose. When reusing or sharing this work, ensure you make the licence terms clear to others by naming the licence and linking to the licence text. Where a work has been adapted, you should indicate that the work has been changed and describe those changes. Please seek permission from the copyright holder for uses of this work that are not included in this licence or permitted under UK Copyright Law.

Acknowledgements

Firstly, I would like to thank my supervisors Professor Clare Lloyd, Professor Sejal Saglani and Dr. James Harker for their expert guidance and academic support during this MPhil. Their dedicated supervision has been fundamental in the completion of this thesis. I gratefully acknowledge the National Heart and Lung institute for funding my studentship.

I would like to additionally thank Dr. James Harker for introducing me to flow cytometry and always taking the time to simplify the basics of any subject. Many thanks to Dr. Franz Puttur for the immense support and training in the lab. I would also like to acknowledge all the IRD lab members and students who helped me along the way by troubleshooting protocols and equipment.

I would like to express my gratitude to the Saglani paediatrics research team for their hard work and coordination. The recruitment of patients and collection of samples could not have been achieved without them. Thank you to Liz Scotney who I shared many late evenings processing samples with.

I would also like to thank my Mum and Dad for their constant support and encouragement. Thank you for always uplifting me and reminding me that there is more to life. Finally, thank you to my aunt and uncle who were very supportive of me during my time in London.

Abstract

As one-third of preschool wheeze (PSW) children progress to school-age asthma, the early-life period (1- 3 years old) offers a window of opportunity to better characterise the immune profile of preschool wheezers that may progress to school-aged asthma.

The aim of this thesis was to phenotype the immune heterogeneity of paediatric airways disease. In doing so, it was hypothesised that children with severe PSW have a distinct airway and blood immune cell profile compared to non-wheezing disease controls. Obtaining optimal airway samples from young children remains challenging. Thus, a complex multiparameter spectral cytometry approach measuring 34-parameters was developed using adult bronchoalveolar lavage (BAL) and blood samples, to determine the cellular phenotype of most immune cell subsets. This showed the technique could be used for both conventional analysis of immune cell populations or unbiased clustering.

Conventional analysis revealed that PSWs had several distinct immune phenotypes compared to children with lower respiratory tract infections (LRTI) and severe therapy-resistant asthma (STRA). PSWs displayed reduced airway $CD8^+$ $CD25^+$ $CD127^-$ T cells compared to LRTIs. Additionally, circulating $CD15^+$ neutrophils and $CD14^+$ $CD16^-$ classical monocytes were decreased in PSWs relative to LRTIs. There was a notable positive correlation between peripheral $CD14^+$ $CD16^-$ cells and the number of bacterial infections in children with PSW. Furthermore, $CD4^+$ $CD25^+$ $CD127^-$ T cells were markedly reduced in PSWs blood compared to both STRA and LRTIs.

Unbiased analysis revealed multiple differentially expressed immune populations in blood and BAL, that were not highlighted by conventional analysis. For example, airway “cluster 100” described as $CD3^+$, $TCR\alpha\beta^+$, $CD8^+$, $CD103^+$, $CD69^+$ cells were decreased in PSW and STRA compared to LRTIs. This confirmed that unsupervised analysis can elucidate exclusive subsets that may be overlooked during conventional flow cytometry gating.

Collectively, high parameter immune cell phenotyping can identify unique immunological profiles in PSW children compared to non-wheeze disease controls and automated analysis can uncover unique immune cell subsets that were overlooked in standard flow gating.

Table of Contents

Declaration of Originality **2**

Copyright Declaration **3**

Acknowledgements **4**

Abstract **5**

Table of Contents **7**

List of figures **10**

List of figures **11**

List of figures **12**

List of tables **12**

Chapter 1. Introduction **13**

1.1 Lung homeostasis 14

1.2 Asthma 15

1.3 Asthma heterogeneity 15

1.4 Preschool wheeze 17

1.5 Severe therapy resistant asthma 19

1.6 Asthma pathogenesis in childhood 20

1.7 Immune responses in early life airways disease 21

1.7.1 Th2 cells in asthma 21

1.7.2 Eosinophils 22

1.7.3 Dendritic cells 23

1.7.4 Neutrophils 23

1.7.5 ILCs in asthma 24

1.8 Hypothesis 25

1.9 Aims 26

Chapter 2. Materials and methods **27**

2.1 Paediatric patients 28

2.2 Sample processing 28

2.2.1 Blood processing 28

2.2.2 BAL processing 28

2.3 Cell counts 29

2.3.1 Live cells 29

2.3.2 Differential cell counts....29
2.4 Spectral flow cytometry....30
2.5 Antibody titrations....30
2.6 Aurora panel components....31
2.7 Staining protocol....33
2.8 Flow data analysis....33
2.9 Data statistics....34

Chapter 3. Optimisation of 34-colour Aurora spectral cytometry panel....35

3.1 Aurora spectral cytometer....36
3.2 Hypothesis....38
3.3 Aims....38
3.4 Results....38
3.4.1 A 34-parameter flow cytometry approach for investigating airway and peripheral immune cells....38
3.4.2 Aurora panel antibody titrations....41
3.4.3 Fluorescence-minus panel controls....46
3.4.4 Comparison of a 1-step versus 3-step staining protocol....53
3.4.5 Autofluorescence identification and removal in spectral cytometry....55
3.4.6 Comparison of spectral and conventional flow cytometry....64
3.5 Discussion....68

Chapter 4. Cellular phenotyping of peripheral and airway immune cells in childhood airways disease....73

4.1 Introduction....74
4.2 Hypothesis....74
4.3 Aims....75
4.4 Results....75
4.4.1 Study design of patient recruitment and overview of immune profile....75
....79
4.4.2 Comprehensive gating strategy and distribution of immune cells....80
4.4.3 Phenotyping of peripheral and airways lymphocytes....87
4.4.4 Composition of innate lymphocytes in circulation and BAL fluid....95
4.4.5 Distribution of B cells and association with IgE....97
4.4.6 Quantification of eosinophils and correlation with clinical phenotypes....100
4.4.7 Frequency of neutrophils and association with infections....105
4.4.8 Macrophage phenotypes and expression of co-stimulatory molecules....107
4.4.9 Monocyte subsets and association with bacterial and viral infections....110
4.4.10 Distribution of DC subsets and expression of co-stimulatory signals....112
4.4.11 Characterisation of rare lineage negative cells expressing CRTH2 and CD127
....114
4.5 Discussion....117
4.6 Conclusion....125

Chapter 5. Unbiased analysis of airway and peripheral immune cells....127

5.1 Introduction....128
5.2 Hypothesis....129

5.3 Aims 129
5.4 Results 130
5.4.1 Experimental workflow of unsupervised clustering and data analysis 130
5.4.2 Unsupervised clustering of blood immune cells revealed 10 unique populations 132
5.4.3 Phenotyping of blood leukocyte clusters using differential marker expressions. 134
5.4.4 Automated clustering uncovered sixteen peripheral populations that were differentially expressed in PSWs compared to children with LRTI and STRA 136
5.4.5 Unbiased analysis discovered three circulating immune populations that were differentially expressed in children with STRAs compared to LRTI disease controls .. 139
5.4.6 Phenotyping of blood leukocyte clusters using differential marker expressions. 141
5.4.7 Subjective gating of peripheral immune cell clusters identified by unbiased analysis 145
5.4.8 Unsupervised analysis of BAL immune cells identified 10 different populations 150
5.4.9 Phenotyping of BAL leukocyte clusters using differential marker expressions ... 152
5.4.10 Objective analysis detected four airway immune populations that were differentially expressed in PSWs compared to non-wheeze children 154
5.4.11 Phenotyping of BAL leukocyte clusters using differential marker expressions. 157
5.4.12 Supervised gating of airway immune cell clusters identified by unbiased analysis 160
5.5 Discussion 166
5.6 Conclusion 169
Chapter 6. Final discussion 170
6.1 General discussion 171
6.2 Spectral cytometry can be used to accurately identify 33 immunological surface markers simultaneously 172
6.3 Preschool wheeze children have a distinct immune cell profile compared to non-wheezers 173
6.4 Automated analysis can detect distinct immune cell clusters overlooked by manual gating 175
6.5 Conclusion 176
7. References 177

List of figures

Figure	Title	Page
Fig 1.1	Diagram of asthma phenotypes	17
Fig 1.2	Diagram of the trajectory of respiratory diseases in early life	19
Fig 3.1	Illustration of the Aurora subpanel components and staining procedure	40
Fig 3.2	Merged plots of lymphocyte marker titrations to determine suitable antibody concentration	42
Fig 3.3	Representative plot of myeloid markers serial dilutions	44
Fig 3.4	Visualization of antibody dilutions for granulocyte and macrophage specific markers	45
Fig 3.5	Illustration of the Aurora staining protocol	47
Fig 3.6	Visualization of panel 1 markers CD4 and TCRαβ in fluorescence-minus-panel controls using blood	48
Fig 3.7	Flow plots of panel 2 markers CD14 and CD38 expression in fluorescence-minus-panel controls using blood	50
Fig 3.8	Scatter plots of fluorescence-minus-panel controls for macrophage and neutrophil markers in a BAL sample	52
Fig 3.9	Comparison of the one-step versus a three-steps staining protocol with a 33-colour panel in blood	54
Fig 3.10	Autofluorescence removal workflow and identification of AF populations in blood	57
Fig 3.11	Selection of median autofluorescence populations in peripheral blood for autofluorescence removal	59
Fig 3.12	Identification and removal of autofluorescent populations in BAL samples	61
Fig 3.13	Flow frequencies of cell types pre and post AF extraction	63
Fig 3.14	Aurora gating strategy	65
Fig 3.15	Fortessa gating strategy	66
Fig 3.16	Comparison of cell frequencies in matched blood and BAL samples acquired on the Aurora and Fortessa flow cytometers	67
Fig 4.1	Study design of patient recruitment and phenotyping method	77
Fig 4.2	Gating strategy for BAL immune cells using the Aurora panel	81
Fig 4.3	Naïve $CD4^+$ T cells are reduced in STRA blood compared to PSW and non-asthmatic children	89
Fig 4.4	Airway $CD4^+$ T cell subsets are comparable between PSW and STRA children	90
Fig 4.5	Circulating $CD8^+$ T cell subsets are comparable between PSW and STRA children	92
Fig 4.6	Airway $CD8^+$ $CD25^+$ $CD127^-$ cells were significantly reduced in PSW and STRA compared to LRTI patients	93

List of figures

Figure	Title	Page
Fig 4.7	Peripheral NKT cells are increased in STRA children relative to PSW and LRTI	96
Fig 4.8	Circulating IgD^+ B cells are decreased in STRA patients	99
Fig 4.9	STRA children have increased frequency of blood eosinophils compared to LRTI	101
Fig 4.10	PSW patients exhibited a positive correlation between circulating eosinophils and serum IgE quantity	102
Fig 4.11	There is no difference in peripheral eosinophils or serum IgE levels in PSW or STRA subjects grouped by atopic disposition	104
Fig 4.12	Peripheral neutrophils are lower in PSW and STRA children relative to LRTI	106
Fig 4.13	Airway macrophage frequencies are similar between children with PSW and STRA	109
Fig 4.14	Classical monocytes are reduced in PSW blood compared to controls	111
Fig 4.15	Airway $CD1c^+$ dendritic cells displayed decreased PD-1 expression in STRA children	113
Fig 4.16	Gating strategy for Lineage negative ILCs using the Aurora panel	115
Fig 4.17	Circulating and airway $CRTH2^+$ $CD127^+$ ILC subsets are comparable between disease groups	116
Fig 5.1	Summary of experimental pipeline for data acquisition and unbiased analysis	131
Fig 5.2	The number of unique metaclusters in blood paediatric samples	133
Fig 5.3	Heatmap of blood immune cell metaclusters defined by marker expressions	135
Fig 5.4	The proportion of significantly different immune cell clusters in PSW blood compared to LRTIs	137
Fig 5.5	The frequency of markedly different leukocyte clusters in PSW blood compared to STRAs	138
Fig 5.6	The frequency of markedly different immune cell clusters in STRA blood compared to LRTIs	140
Fig 5.7	Heatmap illustration of blood immune cell clusters outlined by marker expressions	143
Fig 5.8	Gating strategy for peripheral immune cell clusters 83 and 46	147
Fig 5.9	The frequency of altered immune cell populations in PSW and STRA blood	148
Fig 5.10	Gating strategy and proportion of peripheral immune cell cluster 77	149
Fig 5.11	The number of unique metaclusters in BAL paediatric samples	151

List of figures

Figure	Title	Page
Fig 5.12	Heatmap of BAL immune cell metaclusters defined by marker expressions	153
Fig 5.13	The proportion of notably different immune cell types in PSW BAL compared to LRTI and STRAs	155
Fig 5.14	The frequency of altered immune cell populations in STRA BAL compared to LRTIs	156
Fig 5.15	Heatmap illustration of BAL immune cell clusters outlined by marker expressions	158
Fig 5.16	Gating strategy for BAL immune cell cluster 100	162
Fig 5.17	The proportion of differential immune cell populations in PSW and STRA BAL compared to LRTIs	163
Fig 5.18	Gating strategy for BAL immune cell clusters 61 and 85	164
Fig 5.19	Comparisons of gated BAL immune cell clusters between PSW and STRA BAL	165

List of tables

Table	Title	Page
2.1	List of antibody serial dilutions	30
2.2	List of flow antibodies	32
4.1	Demographics of paediatric STRA, PSW, and LRTI patients	78
4.2	Demographics of paediatric disease patients' white blood cell count compared to healthy children	79
4.3	Aurora markers used to identify the cell types	82
4.4	Antigens recognized by each antibody on the Aurora panel	86
4.5	Blood T cell frequencies from paediatric cohorts	94
4.6	BAL T cell frequencies from paediatric cohorts	94
5.1	The cell phenotypes and disease types of the significantly altered clusters in blood unbiased analysis	144
5.2	The cell phenotypes and disease types of the significantly altered clusters in BAL unbiased analysis	159

Chapter 1. Introduction

1.1 Lung homeostasis

The primary function of the human lungs is to conduct gas exchange whilst preserving lung homeostasis when exposed to environmental stimuli. As humans inhale 5 to 8 litres of air per minute, the lungs are susceptible to non-pathogenic and pathogenic molecules which can lead to inflammation and pulmonary diseases[1]. To manage these conditions, the lungs need to remove debris, launch inflammatory responses, expediate tissue repair following damage and modulate cell turnover without interrupting gas exchange[2]. Thus, to maintaining lung homeostasis, highly specialized lung resident cells known as alveolar macrophages and epithelial cells are considered essential in shaping the immune response[1].

Furthermore, most of what is known about human lung homeostasis is deduced from animal studies or tissue samples extracted from human lungs. However, research on human samples are difficult to interpret as factors such as lifestyle and genetic variability can influence results[2].

Numerous respiratory diseases have been associated with an imbalance in lung homeostasis. In chronic obstructive pulmonary disease (COPD), primary infection by pathogenic bacteria trigger inflammation and mucus secretion. This damages the respiratory epithelium which weakens the innate immune response, ultimately exposing the lungs to subsequent infections such as haemophilus influenzae colonization[3].

In pneumonia, lung inflammation is primarily caused by invading pathogens within the lower respiratory tract. In response, the immune system coordinates defence against microbes by mobilising resident cells and recruited cells to the

site of infection. This leads to excessive lung inflammation which can cause tissue damage. An inability to control this host immune response can develop in to sepsis. Thus, to reinforce tissue repair, the lung environment must be able to counteract the inflammation whilst also maintaining gas exchange processes[4].

1.2 Asthma

Asthma is a chronic inflammatory disease of the airways characterised by chest tightness, airflow obstruction, coughing and wheeze[5]. Globally it affects over 300 million people and is increasing in prevalence amongst children [6,7]. This respiratory condition varies in severity ranging from mild to severe, with the latter accounting for 5% of patients with asthma[7]. According to the Global Strategy for Asthma (GINA) report, severe asthma is defined as asthma that remains uncontrolled despite receiving maximal therapy and adherence plan[5]. Children with severe asthma have a poor quality of life, an increased morbidity, mortality and exhaust over 50% of the UK Asthma healthcare budget[7,8].

1.3 Asthma heterogeneity

Asthma is a heterogenous disease with different underlying phenotypes and endotypes. Phenotypes are defined as observable characteristics based on clinical and physiological features, whereas endotypes describe the pathological mechanisms underlying the clinical presentations at a molecular level such as Type 2 (T2) high or low asthma[9]. The most common asthma phenotypes are allergic, non-allergic and late-onset asthma. Allergic asthma

which frequently emerges in early life, relates to a family history of allergic disease such as rhinitis or eczema and atopic sensitization[10]. More than 85% of children with severe asthma are severely atopic, which is distinguished by multiple sensitizations to outdoor and indoor allergens and elevated specific immunoglobulin E (IgE) levels in serum. Both early-onset allergic asthma and sensitization are associated with severe asthma progression into adulthood[11]. Patients with this phenotype exhibit eosinophilic airway inflammation in their induced sputum prior to treatment and respond to inhaled corticosteroid (ICS) therapy[10].

The non-allergic phenotype encompasses patients whose asthma is not affiliated with allergy and account for <15% of paediatric severe asthma. Environmental stimuli such as parental smoking and lower respiratory tract infections are risk factor connected with this subtype[12]. The immune profile of these subjects can vary between eosinophilic, neutrophilic or a paucigranulocytic phenotype [10].

Adult-onset asthma is mainly non-allergic, and patients possess reduced sensitivity to corticosteroid therapy, as eosinophilic inflammation and nasal polyposis persist with high doses of ICS. Associated risk factors include smoking and obesity particularly in women[11]. An outline of these asthma phenotypes is summarised in **Fig 1.1**.

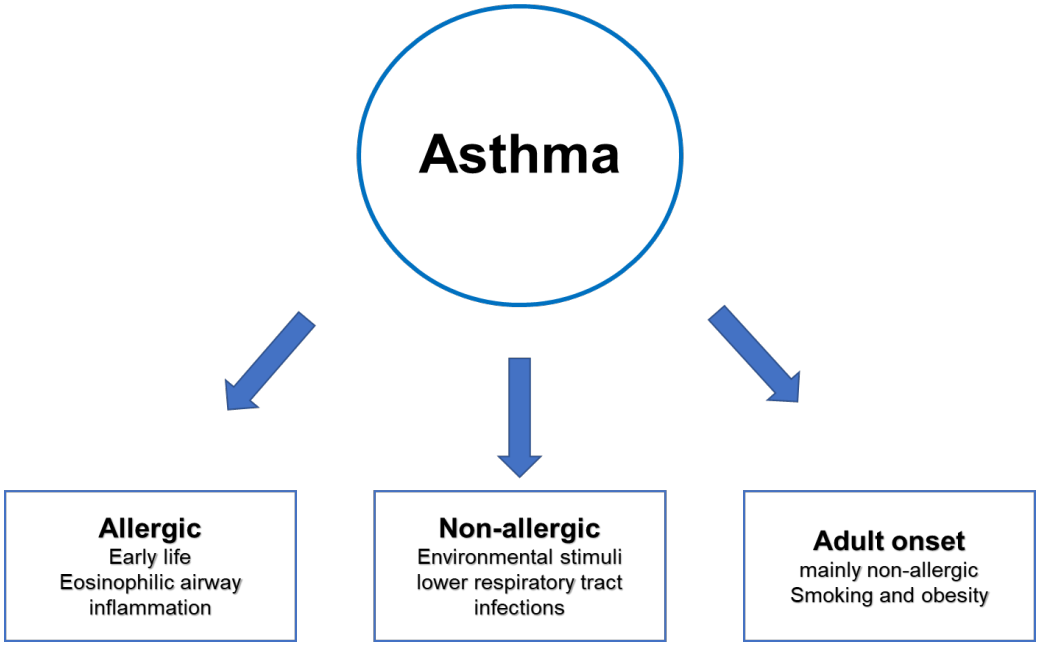


Fig 1.1 Diagram of asthma phenotypes

Diagram shows the different types of asthma characterised by global patient cohort studies. Phenotypes differ by age of onset, atopic predisposition, environmental causes and type of inflammation.

1.4 Preschool wheeze

Although phenotyping early-onset asthma is complex, wheezing is the primary clinical manifestation in preschool children. While half of all children experience wheezing before the age of 5, one-third progress to school-age asthma. Thus this early-life period between 1- 3 years offers a window of opportunity to better characterise the immune profile of preschool wheezers

(PSWs) that may go on to develop school-aged asthma[13]. The progression to asthma is associated with numerous factors, the strongest association being; atopy, increased number of wheezing episodes, simultaneous coughing, prematurity and maternal asthma during pregnancy[14]. An outline of the trajectory of respiratory disease in early life is summarised in **Fig 1.2**.

PSWs are categorised into two groups termed episodic viral wheeze (EVW) and multiple-trigger wheeze (MTW) which are treated differently based on their clinical phenotypes. EVWs are administered intermittent therapy using short-acting bronchodilators, whereas MTWs are mainly prescribed ICS[15]. However, the long-term use of steroids in such a young population can increase side effects thus highlighting a demand for alternative biomarkers for PSWs. A plethora of associative data demonstrate the influence of respiratory infections on wheeze persistence, whereby 85% of PSWs had positive bacterial cultures, 65% had presence of viral pathogens and 55% had both bacterial and viral infections. The most common viral pathogens were rhinovirus and adenovirus whereas the most frequent bacterial strains included streptococcus pneumonia and Moraxella[16]. Furthermore, endobronchial biopsies from PSWs showed an abundance of tissue eosinophils in the submucosa, regardless of atopy[17]. Moreover, Robinson et al. (2019) reported that increased neutrophils in the bronchoalveolar lavage (BAL) fluid are associated with a presence of airway bacterial pathogens in MTWs, while there was no correlation between airway eosinophils and infection[16].

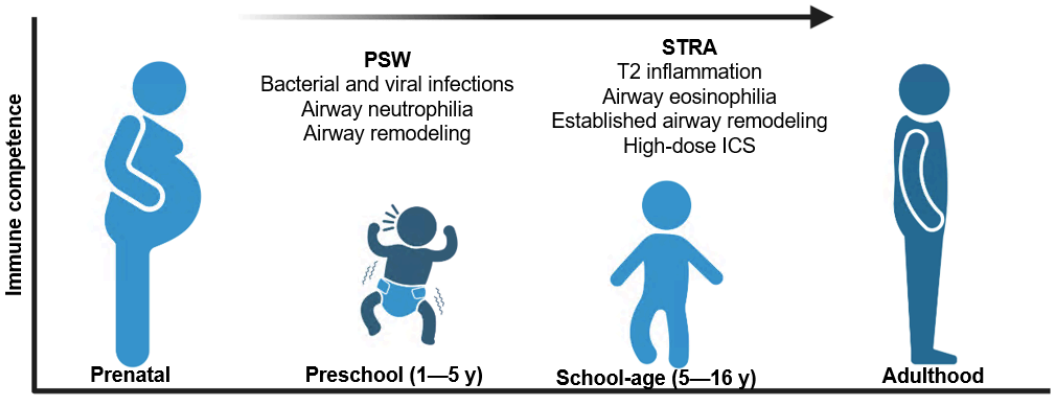


Fig 1.2 Diagram of the trajectory of respiratory diseases in early life

Population-based observational studies found that maternal uncontrolled asthma increases the risk of early-onset persistent asthma. Half of preschool children with wheeze are diagnosed with school-age asthma by 17 years of age. School-age severe asthma is defined by multiple aeroallergen sensitization, airway eosinophilia and airway type 2 mediators.

1.5 Severe therapy resistant asthma

Severe therapy-resistant asthma (STRA) falls under the category of problematic severe asthma (PSA) which is an umbrella term that encompasses children between 6 – 16 years of age with persistent asthma symptoms whilst receiving maximal therapy[18]. To accurately diagnose STRA, children with PSA undergo a detailed assessment of modifiable factors such as allergen exposure and adherence plan, to differentiate difficult-to-treat asthma and mild asthma from STRA[8]. The remaining patients with poor asthma control after addressing comorbid conditions, inhaler technique and environmental stimuli, are classified as STRA and undergo invasive

bronchoscopy to phenotype their airway pathology for a suitable add-on treatment[8, 19].

1.6 Asthma pathogenesis in childhood

In early life, children with allergen sensitisation regularly exhibit elevated airway tissue eosinophilia linked with increased reticular basement membrane thickening (RBM). Alternatively, PSW children unaffected by allergen sensitization, possess airway bacterial infections connected with neutrophilia[17]. Furthermore, clinical trials in PSWs given ICS have alleviated exacerbations and symptoms but failed to rectify lung function decline and airway hyperresponsiveness (AHR)[17]. Airway remodelling is described as a hallmark feature of established asthma and has been observed in severe PSWs as early as 3 to 5 years of age. Additionally, increased airway smooth muscle has been detected in PSWs by 2 years of age[17].

Children with STRA predominantly exhibit T2 inflammation characterised by eosinophilia which is induced by epithelial cytokines interleukin (IL) - 33, IL-25 and thymic stromal lymphopoietin (TSLP) and maintained by T2 cytokines IL-4, IL-5 and IL-13. These cytokines are produced by a range of cells including T helper 2 (Th2) cells, group 2 innate lymphoid cells (ILC2s) and eosinophils[20]. In paediatric asthma research however, T2 cytokines were rarely detectable in STRA BAL fluid[8]. Non-invasive biomarkers that are regularly used to determine eosinophilic inflammation are blood and sputum eosinophil counts, level of serum IgE and fractional exhaled nitric oxide (FeNO). There is a direct relationship between eosinophilic inflammation and FeNO level which is implemented to pinpoint asthmatic patients that may respond to ICS[20].

Currently, the treatment for severe asthma involves ICS combined with long-acting beta 2 agonists (LABA). However, children with STRA require additional add-on therapies to achieve symptom control and reduce exacerbations. Thus, biologics have been developed to target T2 inflammatory pathways and alleviate steroid use. Although biologics are common for adult asthmatics, they are less regular in children because the underlying mechanisms are not necessarily the same for paediatric asthma. At present, omalizumab and mepolizumab are the only two biologics approved for use in children between 6 – 18 years with allergic asthma. Omalizumab is a monoclonal antibody that immobilizes peripheral IgE resulting in decreased IgE receptors on mast cells and dendritic cells, consequently diminishing Th2 inflammation. However due to the restricted IgE criteria for this biologic, one third of paediatric patients are ineligible and an additional third remain unresponsive[18,12]. On the other hand, mepolizumab is an anti-IL-5 antibody which inhibits IL-5 stimulated eosinophil activation, albeit confirmation of safety and efficacy in children was mainly extrapolated from adult clinical trials[18].

1.7 Immune responses in early life airways disease

1.7.1 Th2 cells in asthma

Exposure to microbes and allergens can lead to epithelial barrier dysfunction whereby molecules infiltrate the epithelial tissue, destabilising tight junctions. Impaired epithelial cells secrete the alarmins IL-33 and TSLP[21] which induce dendritic cells (DCs). The DCs process the allergen and travel to the lung draining lymph nodes to deliver the antigen peptides to naïve $CD4^+$ T cells via

major histocompatibility complex (MHC) 2 molecule, thus prompting Th2 cell differentiation and proliferation. Distinct Th2 subsets are produced comprising effector T cells, central memory and tissue-resident memory (TRM) T cells[22]. Newly differentiated Th2 cells migrate to the damaged lung tissue sites to release T2 cytokines IL-4, IL-5 and IL-13 leading to T2 inflammatory responses[23,22]. IL-4 and IL-13 drive B-cell immunoglobulin class switching from IgM to IgE which is a key player in allergic sensation. Furthermore, IgE associates with a mast cell receptor triggering degranulation which in turn promotes goblet cell hyperplasia and airway smooth muscle constriction. IL-5 facilitates eosinophil activation and survival[22]. $CD4^+$ $CRTH2^+$ Th2 cells were observed to be elevated in the blood of severe asthmatics relative to mild asthmatics and were connected with lower lung function results[24].

1.7.2 Eosinophils

Eosinophils mature in the bone marrow and egress into the peripheral blood following IL-5 signalling. Subsequently, eosinophils adhere to the endothelium and are guided by the chemokines eotaxin I, II and III to migrate into the lung tissue. Activated eosinophils excrete inflammatory proteins including major basic protein (MBP) and eosinophil peroxidase (EPO) which perpetuate airway injury in T2 asthma[22]. Research has established that an increase in eosinophils in the airways correlates with airflow obstruction. An increase in peripheral (>150 cells/μl) and sputum (>2%) eosinophils indicate type 2 inflammation and possibility of asthma exacerbations[22].

1.7.3 Dendritic cells

DCs are fundamental antigen-presenting cells (APC) that bridge the gap between the innate and adaptive cells in T2 immune responses. During inflammatory conditions, the human airways contain three distinct DC subsets which express different surface receptors. Type 1 DCs (cDC1s) express CD141 and are involved in antigen presentation to $CD8^+$ T cells, and therefore participate in the antiviral response. T2 DCs (cDC2s) express CD1c and are crucial for the initiation of Th2 differentiation in allergic asthma[25]. While DC2s have a superior capacity to take up allergens compared DC1s, both subsets can elicit Th2 cytokines and were augmented in the blood[26], induced sputum[27] and BAL fluid[28] of adult allergic asthmatics following allergen exposure relative to controls. In addition, plasmacytoid (pDCs) are implicated in antiviral immune response and immunological tolerance by stimulating T regulatory (Treg) cell differentiation[25].

1.7.4 Neutrophils

Neutrophils are a crucial element of the innate immune system and are the most abundant leukocyte in the peripheral blood accounting for up to 70%[29]. Contrary to adults, neutrophil quantity and phagocytosis activity is reduced in children[30]. Neutrophil recruitment is set in motion when pathogen associated molecular patterns (PAMPs) induce specific receptors that initiate the secretion of pro-inflammatory mediators such as CXCL-8[31]. Although neutrophils are released from the bone marrow into the periphery and recruited to damaged tissue by chemoattractant signalling[29], there is a population that

is naturally resident in the lungs during steady state[31]. It is presumed that these airway neutrophils are maintained by the overexpression of chemokine receptor CXCR4 which associates with the ligand CXCL12 that is also expressed by endothelial cells in the lungs[31]. Activated neutrophils perform an array of effector functions ranging from degranulation of proteolytic enzymes to pathogen clearance by phagocytosis[31].

While the T2-high asthma endotype is well documented in adults, there is growing research to support the existence of T2-low asthma which is associated with neutrophilia[32]. Patients with neutrophilic asthma display reduced atopy and FeNO levels. Robinson et al. (2021) recently demonstrated using clustering analysis that PSW children with positive BAL bacterial cultures had substantially higher BAL neutrophils[15]. Furthermore, it has also been established that lung neutrophils are significantly elevated in children with respiratory syncytial virus (RSV) and rhinovirus infections. Thus neutrophils are heavily implicated in viral-induced asthma exacerbations and wheeze in early life[31]. In contrast, STRA children do not possess elevated neutrophils in their BAL fluid[33].

1.7.5 ILCs in asthma

ILCs are a rare innate immune population that inhabit mucosal environments and mimic T effector cells by producing cytokines[34]. These cells differentiate into three subsets based on their transcription factor expression and cytokine production. ILC1s are characterised by the expression of transcription factor T-bet and production of Th1 cytokine interferon-gamma, whereas ILC2s are

distinguished by the GATA-3 transcription factor and secretion of Th2 cytokines IL-5 and IL-13. ILC3s on the other hand display RORγt transcription factor expression and release IL-17 and IL-22 cytokines[35].

ILC2 are elevated in the blood, sputum and BAL fluid of children and adults with severe asthma[36,37]. Like Th2 cells, ILCs can be directly induced by epithelial-derived IL-33 and TSLP and amplify T2 inflammation leading to further lung injury[22,32]. ILCs do not express conventional lineage markers of other immune cells and can be classified by the expression of $CRTH2^{+}$ and $CD127^{+}$ surface markers[35,30]. Using these immune-phenotypes, Nagakumar et al. (2019) illustrated an increased presence of sputum and airway ILC2s in STRA children compared to disease controls with lower respiratory tract infections[33]. Moreover peripheral and sputum ILC2s from STRA children were determined to be steroid sensitive following a longitudinal study and *in vitro* treatment with systemic steroids[37].

1.8 Hypothesis

The overall hypothesis of this thesis is that children with severe preschool wheeze have a distinct airway and blood immune cell profile compared to non-wheezing disease controls. As the pathophysiology and immunology of paediatric asthma phenotypes are not well understood, it is necessary to examine immune cells in a range of paediatric respiratory disease groups. To investigate a wide variety of cells and their sub-phenotypes in limited bronchoalveolar lavage volumes, an advanced spectral flow cytometry approach was implemented using the Aurora cytometer.

1.9 Aims

1. Optimise a 34-multicolour flow panel to identify immune cell subsets in blood and bronchoalveolar lavage fluid
2. Phenotype the immune heterogeneity of paediatric airways disease and integrate clinical information
3. Conduct automated analysis to distinguish immune cell clusters between childhood airways diseases

Chapter 2. Materials and methods

2.1 Paediatric patients

Children aged between 1 to 16 years old were recruited. Wheeze or severe asthma diagnosis was confirmed by doctors following a detailed checklist and clinical tests. For non-asthmatic controls, children with LRTIs undergoing elective bronchoscopy were consented to provide BAL fluid. Clinical data was collected by clinicians and obtained from the Inform database. All bronchoscopies undertaken in children were part of standard clinical protocols and samples for research were obtained with ethical permission and written, informed parental consent. The samples were obtained with the Research Ethics Council reference number 15/LO/1885.

2.2 Sample processing

2.2.1 Blood processing

Blood was collected in an anti-coagulant EDTA (Ethylenediaminetetraacetic acid) coated tube and transferred to a 50ml falcon tube. Red blood cell (RBC) lysis buffer (8.26g of NH_4Cl, 1.19g of $NaHCO_3$ and 200µl of 0.5M, pH8 EDTA) was added at a 1:10 ratio (1ml blood: 10ml RBC) and incubated for 15min on a roller. Sample was topped up with equal volume of PBS and centrifuged at 1800 rpm for 5min in a 50ml falcon tube to pellet the cells. Cells were washed in 10ml PBS again before resuspending in 1ml of FACS buffer (500ml PBS, 2% fetal bovine serum and 2mM EDTA).

2.2.2 BAL processing

Whole BAL was obtained by instilling 1ml/kg (maximum of 40mls/aliquot) of sterile saline via a bronchoscope into the right middle lobe. The sample was

accumulated from 3 washes. An aliquot was filtered through a 70µm cell strainer and centrifuged in a 50ml falcon tube at 1800 rpm for 2 min, 4°C. The supernatant was separated and stored in -80°C. If the pellet is too bloody, an RBC lysis step was performed for 5min and cells were washed in PBS. The cell pellet was resuspended in 1ml FACS buffer for downstream steps.

2.3 Cell counts

2.3.1 Live cells

To count live cells for flow cytometry, cells were stained with Trypan Blue (1:10 or 1:2) to label dead cells. The solution was transferred into a haemocytometer chamber. The average of two squares and the dilution factor was used to calculate total leukocytes per ml.

2.3.2 Differential cell counts

Approximately 5 x 10^4 cells in 100µl FACS buffer was loaded into a cyto-funnel attached to a charged microslide (Thermo Fisher). A cytospin was conducted using a cytocentrifuge for 4min at 400 rpm. The slide was left to air dry to allow cells to adhere and then fixed in 100% methanol for 5min. The Kwik Diff Stain Kit from Thermo Scientific is utilized to stain immune cells. The slide was first submerged five times in the red Solution 2 and rinsed in a water bath two times. This was followed by three dips in the blue solution 3 and rinsed again. After air drying for 24 hours, the cells were covered with ~700µl of DPX mounting medium and preserved with a coverslip. The slide was viewed under a microscope after drying. To quantify cell types, neutrophils, eosinophils, macrophages and lymphomononuclear cells were differentiated by nucleus

morphology staining and size. Roughly 200-300 cells were counted, and the proportion of each cell type was enumerated as a percentage of total cells

2.4 Spectral flow cytometry

The Aurora spectral cytometer was purchased from Cytek and utilized in the acquisition and phenotyping of blood and BAL cells. It is equipped with a 5-laser system and 64 fluorescence channels to facilitate our 34-colour panel. Typically, 500,000 – 1 x 10^6 cells were stained for acquisition.

2.5 Antibody titrations

To determine suitable antibody concentrations, serial dilutions were conducted at 1:5, 1:20, 1:50 and 1:100. The 33 fluorophore conjugated antibodies were prepared in groups of 11, using a U-bottom 96 well plate.

Dilution Factor	**Mixture**
1:5	40ul FACS + 10ul of antibody
1:20	30ul FACS + 10ul 1:5
1:50	31.5ul FACS + 3.5ul 1:5
1:100	24ul FACS + 6ul 1:20

Table 2.1 List of antibody serial dilutions

1. For the 1:5 dilution, 40µl of FACS buffer was combined with 10µl of antibody, in the first well and mixed.
2. Then 10µl of the 1:5 dilution was transferred to the second well containing 30µl of FACS buffer to make 1:20 dilution.

3. Next, 3.5µl of the 1:5 dilution was added to the third well to make 1:50 titration.
4. For the 1:100 titration, 6µl of the 1:20 dilution was resuspended in 24µl of FACS buffer. $1x10^6$ cells were plated into a separate U-bottom 96-well plate in an identical format to the antibody titrations plate.
5. Cells were centrifuged at 2000 rpm for 2min at 4°C and 25µl of each antibody titration and resuspend into wells containing cells.
6. The plate was covered in foil and incubated in the fridge for 30min. Following a wash step in PBS, the cells were fixed in 1% paraformaldehyde (PFA) for 10min and washed again with PBS.
7. Cells were resuspended in 150µl FACS buffer and stored at 4ºC until flow acquisition.
8. Single-colour Ultra-comp ebeads purchased from Thermofisher were prepared using the same reagents and incubation steps to be comparable controls to the cells.

2.6 Aurora panel components

Antibodies were purchased from Biolegend, BD Bioscience and Thermo-Fisher. Live/dead (L/D) Blue stain was acquired from Thermo-Fisher and is reconstituted in DMSO and stored in 3µl aliquots in -20°C. A fresh aliquot is reconstituted each day for staining cells in 1X PBS in a 1:1000 dilution. Anti-CD32 antibody is included to block Fc receptors.

Laser	Fluorophore	Antigen	Clone	Vendor	Dilution
UV	BUV395	CD69	FN50	BD Biosciences	1;20
	BUV496	CD8	RPA-T8	BD Biosciences	1;100
	BUV563	CD45RA	HI100	BD Biosciences	1;100
	BUV661	CD11c	B-ly6	BD Biosciences	1;100
	BUV737	CD56	NCAM16.2	BD Biosciences	1;100
	BUV805	CD3	UCHT1	BD Biosciences	1;100
	Live/Dead Blue	Dead cells		ThermoFisher	
Violet	BV421	IgD	IA6-2	Biolegend	1;100
	Super Bright 436	CD16	3G8	ThermoFisher	1;100
	eFluor450	CD25	CD25-4E3	ThermoFisher	1;100
	BV480	CD20	2H7	BD Biosciences	1;100
	BV510	CD127	A019D5	Biolegend	1;50
	BV570	HLA-DR	L243	Biolegend	1;100
	BV605	CD28	CD28.2	Biolegend	1;100
	BV650	CD38	HB-7	Biolegend	1;100
	BV711	CD15	W6D3	Biolegend	1;100
	BV750	PD1	EH12.2H7	Biolegend	1;100
	BV785	CD206	15-2	Biolegend	1;20
Blue	BB515	CXCR5	RF8B2	BD Biosciences	1;50
	AF488	Siglec 8	837535	R&D systems	1;100
	Spark Blue 550	CD4	SK3	Biolegend	1;100
	PerCP	CD161	HP-3G10	Biolegend	1;20
	BB700	CD27	M-T271	BD Biosciences	1;100
	PerCP Cy5.5	CD45	HI30	Thermofisher	1;25
	PeCP eFlour710	CD86	IT2.2	ThermoFisher	1;100
Yellow/ Green	PE	CD141	M80	Biolegend	1;20
	PeDz594	TCR g/d	B1	Biolegend	1;100
	PECy5	TCR a/b	IP26	Biolegend	1;100
	PECy7	CD11b	ICRF44	Biolegend	1;100
Red	APC	CD123	6H6	Biolegend	1;100
	A647	CRTH2	BM16	Biolegend	1;100
	Spark NIR 685	CD14	63D3	Biolegend	1;100
	APC R700	CD1c	F10/21A3	BD Biosciences	1;100
	APC Cy7	CD103	Ber-ACT8	Biolegend	1;100
Purified	Pure	CD32	6C4	ThemoFIsher	1;100

Table 2.2 List of flow antibodies

2.7 Staining protocol

First 1 x 10^6 cells resuspended in FACS buffer were plated into a V-bottom 96 well plate for staining and at least 5 x 10^5 cells were allocated to the unstained control for sample unmixing. The plate was spun at 2100 rpm with FACS buffer for 2 min and the supernatant was discarded. Then 25µl of the L/D Blue was added to each well and mixed by pipetting. The L/D control was prepared by heat killing 2.5 x 10^5 cells at 60°C for 10min and divided into two wells. Only one well is stained with Live-dead Blue and both wells are combined after fixation. Cells were incubated for 20min at 4°C, then washed with PBS and spun to remove supernatant. Then 30µl of the antibody cocktail was added per 1 x 10^6 cells for 30 mins at 4°C. For the multicolour panel controls, six additional wells of cells are included to stain with single panel 1, panel 2, panel 3, or panel combinations 1+2, 1+3, and 2+3. The plate of cells was wrapped in foil and incubated in the fridge for 30min. Following this, two wash steps were carried out with FACS buffer. Cells were then fixed with 50µl of 1% PFA for 10min in the dark. After a wash step with PBS, cell pellets were resuspended in 200µl FACS buffer and left in the fridge until flow acquisition.

2.8 Flow data analysis

All flow data was generated by the Aurora cytometer and SpectroFlo software. For autofluorescence (AF) removal, flow cytometry files were imported back into SpectroFlo to visualize populations on the AF channel and create AF tags for unmixing. AF spectra was assessed using FCS express and GraphPad Prism. Flow data was analysed using the FlowJo software and cell frequencies were plotted and represented as line graphs using GraphPad. Dimension

reduction and unbiased analysis was performed in R studio using flow cytometry files containing gated cells that were CD45 positive, that were exported from the FlowJO software. The coding scripts utilised were published by CyTOF[38] and the open software Bioconductor[39].

2.9 Data statistics

All statistics analyses were conducted in GraphPad Prism software. Data was interpreted as non-parametric distributions. Mann-Whitney U test was applied to comparisons between two groups. For comparisons between three groups Kruskal-Wallis test, followed by the Dunn's multiple comparisons test was used. Differences were considered significant if p-value was less than 0.05. Correlation analysis was carried out the by non-parametric Spearman correlation approach.

Chapter 3. Optimisation of 34-colour Aurora spectral cytometry panel

3.1 Aurora spectral cytometer

The Aurora 5-laser instrument was launched by Cytek Bioscience in 2019[40]. The configuration consists of an ultraviolet, violet, blue, yellow-green and red laser system combined with 64 detector channels for fluorescence that can detect emission spectra between 365 – 829nm and can separate up to 40 fluorophores[40,41]. The five-laser system has a distinctive optical framework whereby the lasers are spatially separated as they enter the flow cell to prevent cross-laser excitation of dyes that are excited by multiple laser lines. The lasers are assigned to a designated detector array assembled from avalanche photodiodes (APDs) which encompass up to 16 detector channels. APDs are currently the preferred choice for high sensitivity detection as they can examine much narrower bandwidth ranges than photomultiplier tubes and exhibit a higher quantum efficiency across a wider wavelengths range of 400 – 1100nm which accommodates most fluorophores frequently utilized. Owing to this, the Aurora has a smaller footprint, less background noise and is more thermostable in comparison to traditional flow machines[40].

The aim of spectral cytometry is to capture the whole emission spectrum of a fluorophore generated by all five lasers using the built-in 64 detector channels. Individual fluorophores are then isolated based on their emission across this entire spectrum through a process called spectral deconvolution/unmixing. In doing so, the Aurora cytometer can segregate fluorophores with close emission peaks but dissimilar secondary emissions, thus allowing extra flexibility for panel design. In comparison conventional flow cytometry assigns a specific wavelength of light passes through an wavelength restricted optical filter generated after laser excitation to an individual fluorophore.

Fluorescence spillover in a multicolour stained sample is corrected by a mathematical algorithm in Aurora software called spectral unmixing which requires an unstained sample and single-stain controls. This means, unlike conventional flow cytometry, this algorithm can also subtract baseline fluorescence of cells in the mixed sample using the tissue-specific unstained sample and assigns a parameter which is beneficial for extremely autofluorescent tissue[40].

Autofluorescence (AF) is an intrinsic feature in all cells whereby endogenous biological molecules emit fluorescence. These biomolecules include flavins and NADPH which fluoresce in the absence of a fluorophore, when excited with laser light. Studies show that small lymphocytes are less autofluorescent that large macrophages which possess high side scatter, indicating that a high degree of granularity is related to AF[42]. Adjusting for AF eliminates these background signals that may obscure dim markers emanating light at a similar wavelength[40].

Spectral cytometry via the Cytek Aurora, can therefore substantially increase the number of markers that can be measured on a single cell compared to traditional flow cytometry, while correcting for cellular characteristics like AF that might obscure marker expression. It is therefore optimal for work where sample size is limited, such as when working with paediatric samples. Therefore, by combining all these aspects, a multicolour panel was developed with a rigorous staining protocol to efficiently phenotype the immune profile of paediatric airway and blood samples.

3.2 Hypothesis

A 34-colour panel of extracellular surface proteins can characterise key immune cells within peripheral blood and BAL samples.

3.3 Aims

1. Establish optimal working concentrations of 33 fluorophore-conjugated antibodies
2. Determine an efficient staining method which conserves fluorophore integrity
3. Identify and extract autofluorescent populations in unstained blood and BAL samples
4. Compare cell frequency data from matched samples acquired by spectral and conventional flow cytometry

3.4 Results

3.4.1 A 34-parameter flow cytometry approach for investigating airway and peripheral immune cells

A key focus of this thesis was to define multiple immune cell types in the blood and airways of children with wheeze and non-wheeze. The volume of samples taken in paediatric cohorts is extremely limited for clinical and ethical reasons This is particularly relevant for samples of the airways, which are obtained by invasive bronchoscopy. This is only carried out in children for clinical reasons, placing a natural limit on donor numbers, and cellular yield available for research purposes, especially once clinically relevant assays are accounted

for, can often be low. High resolution, low volume assays, such as multiparameter flow described here, are therefore particularly valuable. The panel was designed to address the following:

1. Define key immune cell subsets in the restricted airways and peripheral blood of patients.
2. Differentiate between activation and stimulatory status of distinct subsets of cells.
3. Explore rare cell types during disease

A 34-colour panel was designed consisting of 33-flouorphore conjugated antibodies and a blue-Live/Dead stain to characterize viable leukocytes (lymphocytes, granulocytes and myeloid cells). These markers include those that distinguish all major immune cell populations, their activation status and functional identity. Broadly speaking the markers could be split into three subpanels related to their expression pattern, useful for quality control of the full 33 fluorophore panel. Panel 1 consisted of T cell markers **(Fig. 3.1A)**, Panel 2 included B cell and activation markers **(Fig. 3.1B)**, whilst Panel 3 mainly comprised granulocyte and myeloid markers **(Fig. 3.1C)**. To ensure that all proteins were efficiently characterised, markers known to be highly expressed were conjugated to dim fluorophores (e.g. CD8-BUV496) whereas less expressed proteins were coupled to fluorophores with high excitation yield (e.g. CD123-APC).

A

Panel 1

Fluorophore	Antigen
BUV496	CD8
BUV563	CD45RA
BUV805	CD3
eFluor450	CD25
BV510	CD127
BV605	CD28
BV750	PD1
Spark Blue 550	CD4
PECy5	TCRab
A647	CRTH2
APC Cy7	CD103

B

Panel 2

Fluorophore	Antigen
BUV395	CD69
BUV737	CD56
BV421	IgD
BV480	CD20
BV650	CD38
BB515	CXCR5
BB700	CD27
PeCP eFlour710	CD86
PeDz594	TCRgd
Spark NIR685	CD14

C

Panel 3

Fluorophore	Antigen
BUV661	CD11c
SuperBright436	CD16
BV570	HLA-DR
BV711	CD15
BV785	CD206
AF488	Siglec 8
PerCP	CD161
PerCP Cy5.5	CD45
PE	CD141
PECy7	CD11b
APC	CD123
AR700	CD1c

Fig 3.1. Illustration of the Aurora subpanel components and staining procedure

Table of markers in **A)** Panel 1, **B)** Panel 2, **C)** Panel 3. Anti-CD32 was added to each antibody mix to block Fc receptor interactions.

3.4.2 Aurora panel antibody titrations

To set up the high-parameter panel, antibody titrations were performed to ascertain the optimum concentration of each antibody that displays a distinct positive signal at the lowest dilution. By doing so, this method accomplished sufficient staining and minimized costs. Titrations ranging between 1 in 5 to 1 in 100 (e.g., CD11b-BUV737 50ug/ml) were conducted in sets. Lymphocytes are an abundant population in peripheral blood[43], therefore were readily identifiable, and most of the lymphocyte markers analysed in blood samples showed a clear positive population even at the 1 in 100 dilution **(Fig. 3.2)**. For some less well detected surface proteins, higher titrations were selected i.e. CD127 (1:50), CD69 (1:20) and CD161 (1:20).

Likewise, to optimize the myeloid markers on the panel, serial dilutions were conducted and antibody concentrations that produced discrete populations were selected **(Fig. 3.3)**. The remaining markers were grouped into panel 3 and subsequently titrated to establish optimal dilutions **(Fig. 3.4A, B)**. As panel 3 contains the macrophage surface receptor CD206, a BAL fluid sample was utilized to depict immune cells with a positive CD206 signal **(Fig. 3.4C)**. Pooled cells from the serial dilutions indicated that CD206 signal decreases post 1:20 titration.

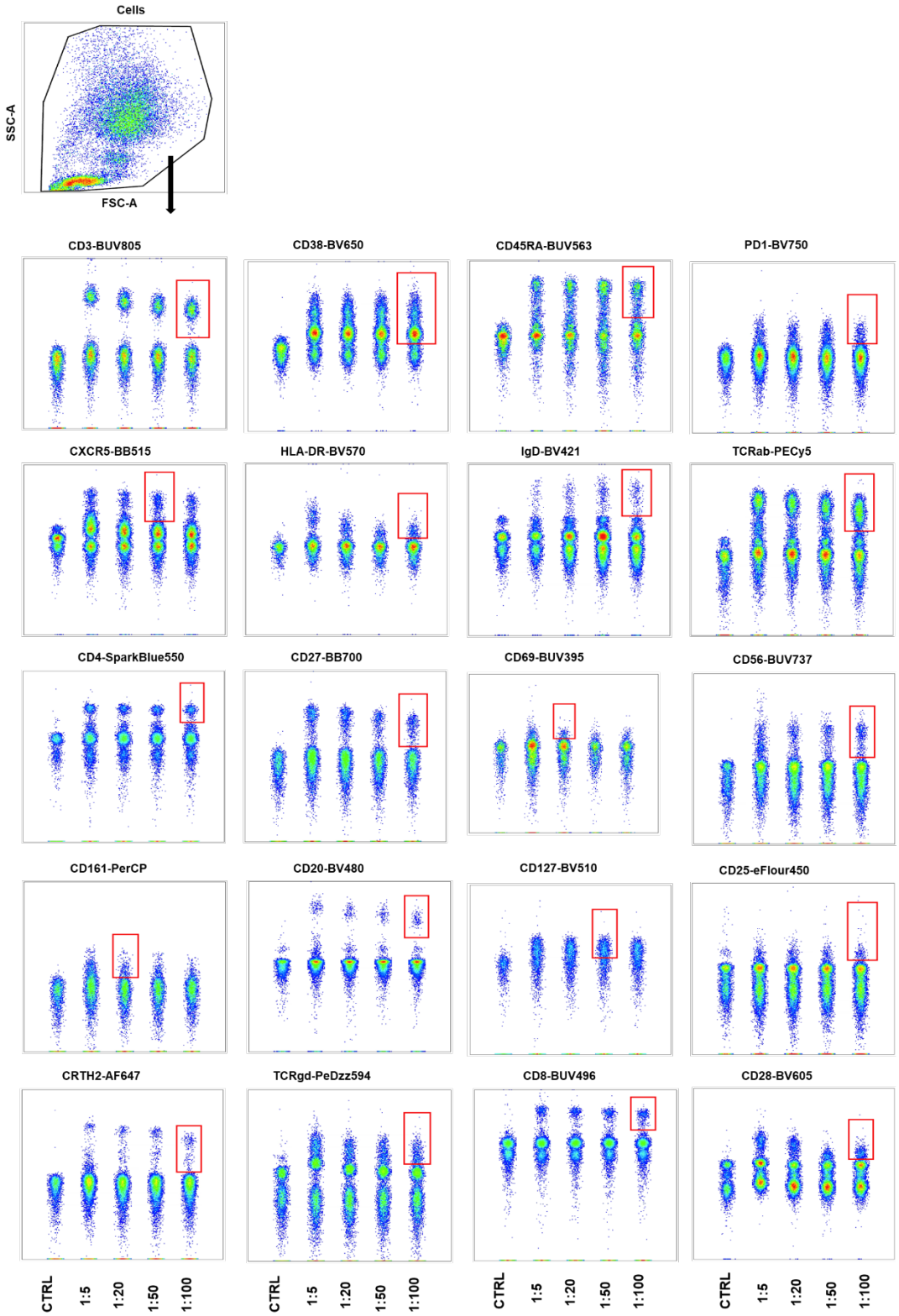

Cells
SSC-A
FSC-A
CD3-BUV805
CD38-BV650
CD45RA-BUV563
PD1-BV750
CXCR5-BB515
HLA-DR-BV570
IgD-BV421
TCRab-PECy5
CD4-SparkBlue550
CD27-BB700
CD69-BUV395
CD56-BUV737
CD161-PerCP
CD20-BV480
CD127-BV510
CD25-eFlour450
CRTH2-AF647
TCRgd-PeDzz594
CD8-BUV496
CD28-BV605
CTRL
1:5
1:20
1:50
1:100

Fig 3.2. Merged plots of lymphocyte marker titrations to determine suitable antibody concentration

Schematic of merged plots from individually stained and unstained blood cells from healthy adults. Blood cells were processed and $1x10^6$ cells were plated in a U-bottom 96-well plate. Cells were washed with PBS and stained with 25µl of each antibody titration for 30min. Cells were fixed with 1% PFA, washed with PBS and stored in FACS buffer. Samples were acquired on the Aurora cytometer. All cells were gated and assessed for staining at 1:5, 1:20, 1:50 and 1:100 dilution.

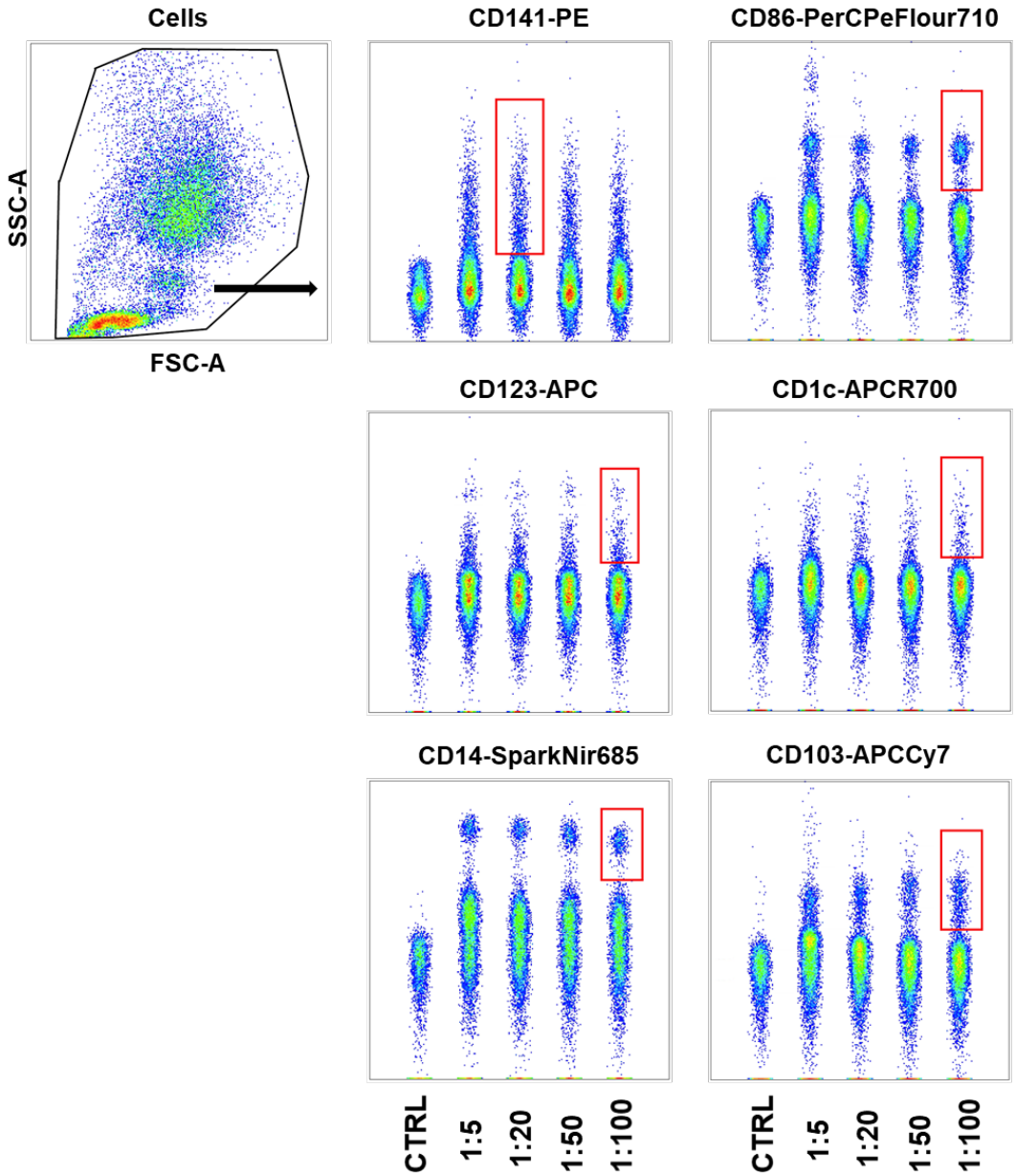


Fig 3.3. Representative plot of myeloid markers serial dilutions
Flow events were pooled from unstained and stained blood cells. Dilution factors for each myeloid marker were compared. Blood cells were processed and $1x10^6$ cells were plated in a U-bottom 96-well plate. Cells were washed with PBS and stained with 25µl of each antibody titration for 30min. Cells were fixed with 1% PFA, washed with PBS and stored in FACS buffer. Samples were acquired on the Aurora cytometer.

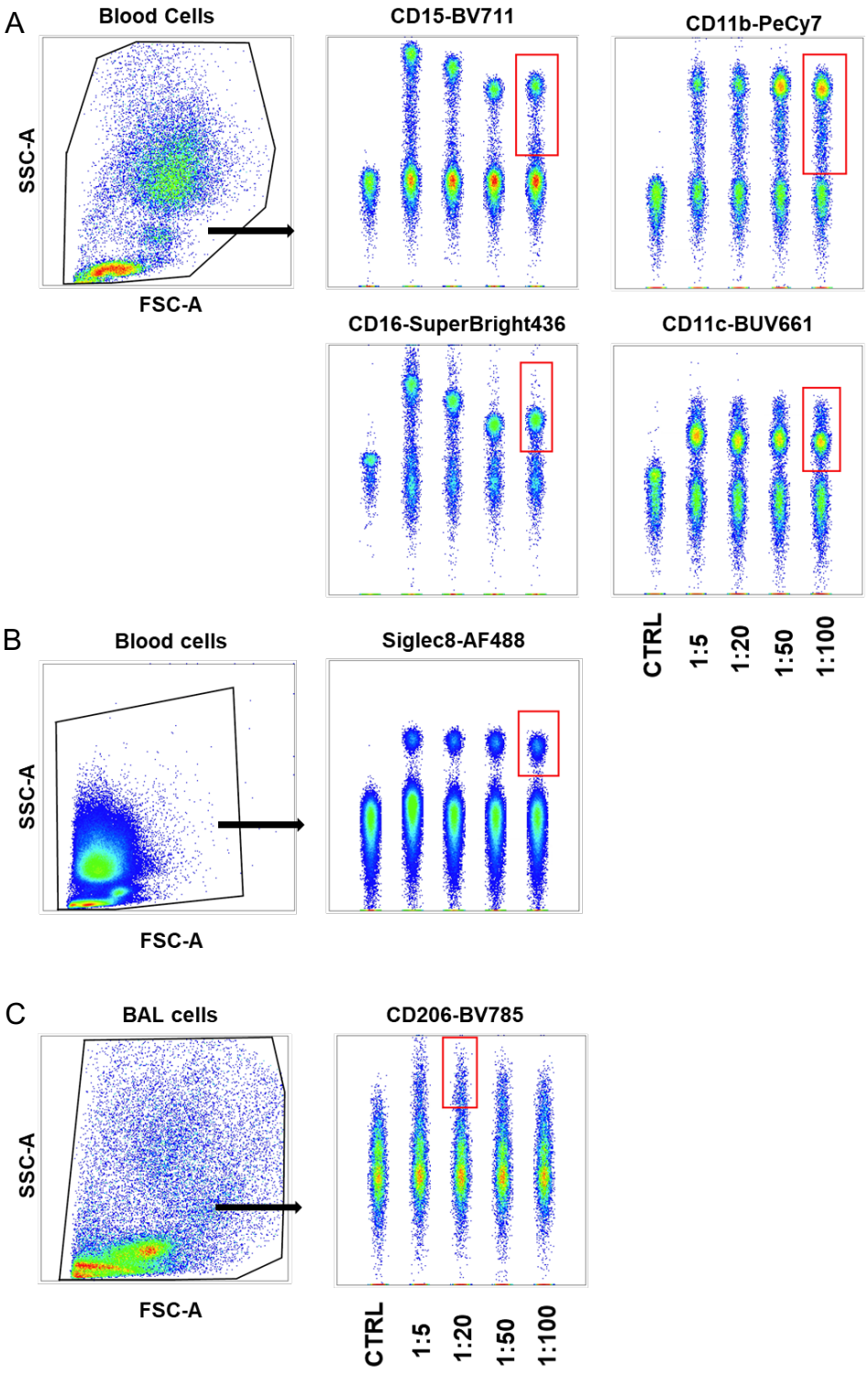

A
Blood Cells
SSC-A
FSC-A
CD15-BV711
CD11b-PeCy7
CD16-SuperBright436
CD11c-BUV661
CTRL
1:5
1:20
1:50
1:100
B
Blood cells
SSC-A
FSC-A
Siglec8-AF488
C
BAL cells
SSC-A
FSC-A
CD206-BV785
CTRL
1:5
1:20
1:50
1:100

Fig 3.4. Visualization of antibody dilutions for granulocyte and macrophage specific markers
Schematic of flow gating and antibody titrations for **A)** granulocytes, **B)** eosinophils and **C)** macrophages. Blood cells were processed and $1x10^6$ cells were plated. Cells were washed with PBS, stained with 25µl of each antibody titration for 30min followed by fixation with 1% PFA. Samples washed with PBS and acquired on the Aurora cytometer in FACS buffer.

3.4.3 Fluorescence-minus panel controls

Traditional flow cytometry routinely implements fluorescence minus one (FMOs) controls, which contain every marker on the panel minus one[41]. This method is advantageous in highlighting signal spillover of markers into unrelated channels and facilitates accurate gating of the positive and negative populations. However, the high cell yield required, and the technical variation associated with preparing 33 individual antibody cocktails is error prone and limits feasibility. To overcome this difficulty, while still screening for non-specific spillover, the 33 antibodies were divided into three subpanels categorized by cell types, thus creating three cocktails of 11 antibodies each. In the staining protocol, cells were incubated with combinations of these subpanels and compared to cells stained with the complete panel **(Fig. 3.5)**. Combinations of two subpanels allowed the visualization and identification of any irregular or indistinguishable signals between markers. For example, CD4 and TCRαβ marker signals were analysed to evaluate Panel 1 controls. Firstly, the lymphocyte population was gated, followed by removal of doublet cells **(Fig. 3.6A)**. Marker expression was compared across a blood sample stained

with different panel combinations. Unstained cells showed where the negative population sits and confirmed that there was no spectral spillover **(Fig. 3.6B)**. Panel 1 staining indicated that 31% and 35% of lymphocytes were TCRαβ^{+} and double CD4^{+} TCRαβ^{+} respectively **(Fig. 3.6C)**. As expected, panel 2 and panel 3 that lacked TCRαβ and CD4 antibodies did not show a positive signal **(Fig. 3.6D, E)**. Analysis of the multiple panel combinations revealed no interference from other markers and the frequencies remain similar when panel 1 stain is added to the cells **(Fig. 3.6F, G, H, I)**.

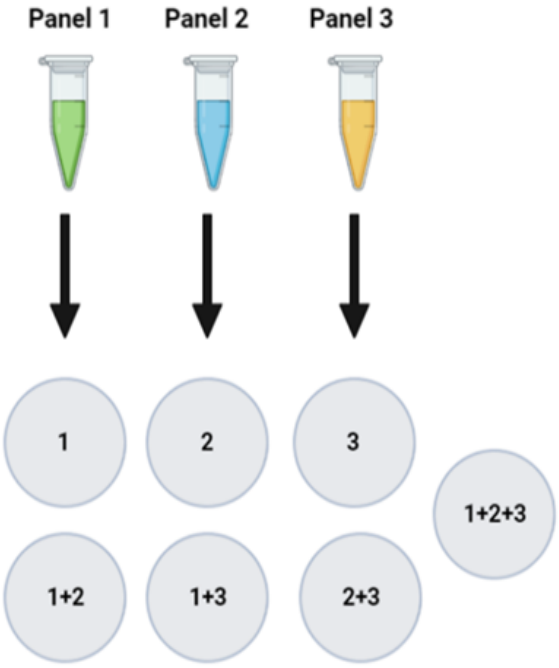


Fig 3.5. Illustration of the Aurora staining protocol
Diagram of the subpanels staining protocol. Blood or BAL cells were processed as described in methods. 1 x10 ^{6} cells were plated in each well and incubated with live-dead blue, washed with PBS and followed by the designated antibody mixture. Wells receiving more than one cocktail were washed at intervals with PBS. After staining, cells were fixed in 1% PFA for 10min and washed again with PBS. Cells were stored in FACS buffer and acquired on the Aurora.

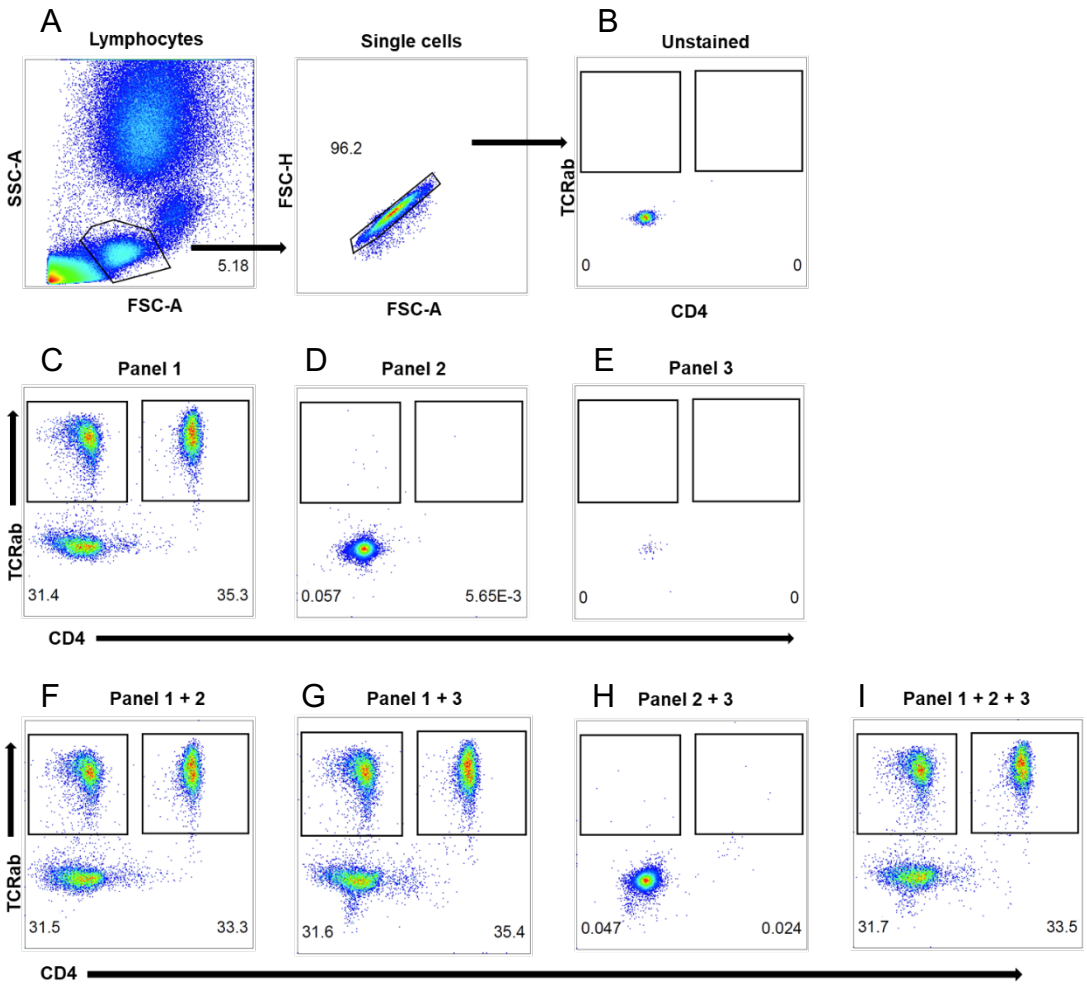


Fig 3.6. Visualization of panel 1 markers CD4 and TCRαβ in fluorescence-minus-panel controls using blood

1 x10 ^{6} cells were plated in each well and incubated with live-dead blue for 20min. Cells were stained with 30µl of the antibody cocktail for 30min. Wells receiving more than one cocktail were washed at intervals with PBS. After staining, cells were fixed in 1% PFA for 10min and washed again with PBS. Cells were stored in FACS buffer and acquired on the Aurora. **A) L**ymphocyte gating and debris exclusion. **B)** Unstained control, **C)** Panel 1 controls, **D)** Panel 2 controls, **E)** Panel 3 controls, **F)** Panel 1+ 2 controls, **G)** Panel 1+ 3 controls, **H)** Panel 2+3 controls and **I)** Panel 1+ 2+3 staining.

Likewise, when examining markers found in panel 2 markers such as CD14 and CD38 could be used to gate a monocyte population across the various fluorescence-minus (FM) panel controls **(Fig. 3.7A)**. As CD14 and CD38 are designated to panel 2 only, unstained cells and samples stained with panel 1 or 3 alone did not exhibit any signal **(Fig. 3.7B, C, E, G)**. Panel 2 revealed that $CD38^+$ and dual $CD14^+$ $CD38^+$ expression accounted for 6% and 83% of monocytes respectively **(Fig. 3.7D)**, which was replicated in samples stained with panels 1+ 2, 2+3 and 1+2+3 **(Fig. 3.7F, H, I)**.

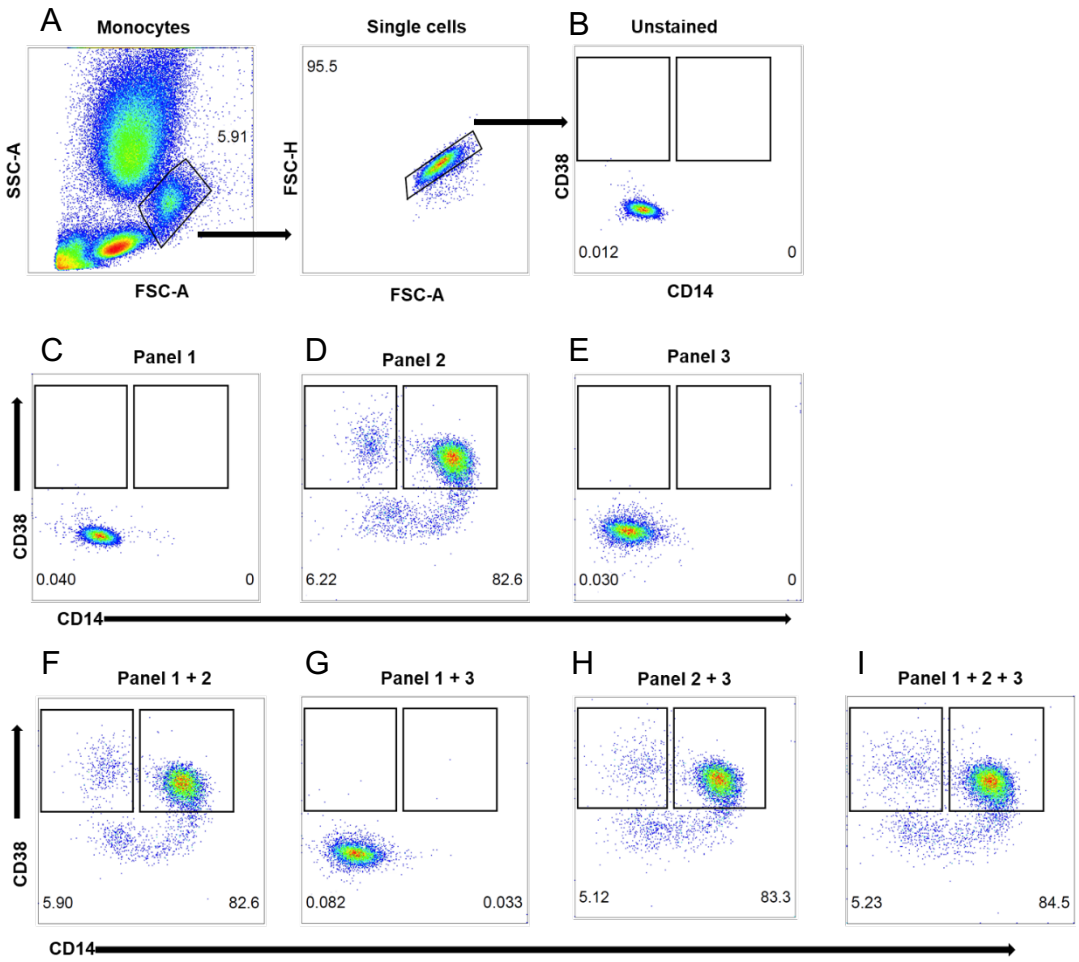


Fig 3.7. Flow plots of panel 2 markers CD14 and CD38 expression in fluorescence-minus-panel controls using blood

1 x10^6 cells were plated in each well and incubated with live-dead blue for 20min, washed and stained with 30µl of the antibody cocktail for 30min. Wells receiving more than one cocktail were washed at intervals with PBS. After staining, cells were fixed in 1% PFA for 10min and washed again with PBS. Cells were stored in FACS buffer and acquired on the Aurora. **A)** Monocyte gating and doublet exclusion. **B)** Unstained control, **C)** Panel 1 controls, **D)** Panel 2 controls, **E)** Panel 3 controls, **F)** Panel 1+ 2 controls, **G)** Panel 1+ 3 controls, **H)** Panel 2+3 controls and **I)** Panel 1+ 2+3 staining.

To inspect panel 3 antibody performance and integration with the remaining markers, a BAL sample was stained with the different subpanels. To highlight granulocytes and macrophages, a wide gate was drawn across cells with high side-scatter area and debris was excluded by single cell gating **(Fig. 3.8A)**. The neutrophil and macrophage populations are displayed on a scatter plot using CD15 and CD206 expression across the diverse subpanel compositions. Unstained cells were used to approximate the position of the positive signals **(Fig. 3.8B)**. The cells stained with the control panels 1 and 2 were void of CD15 and CD206 expression as anticipated **(Fig. 3.8C, D, F)**. Panel 3 staining illustrated that 25% and 55% of the population of interest were denoted by neutrophils and macrophages sequentially **(Fig. 3.8E)**. This was reproduced in the multi-panel combinations 1+3, 2+3 and 1+2+3 **(Fig. 3.8G, H, I)**.

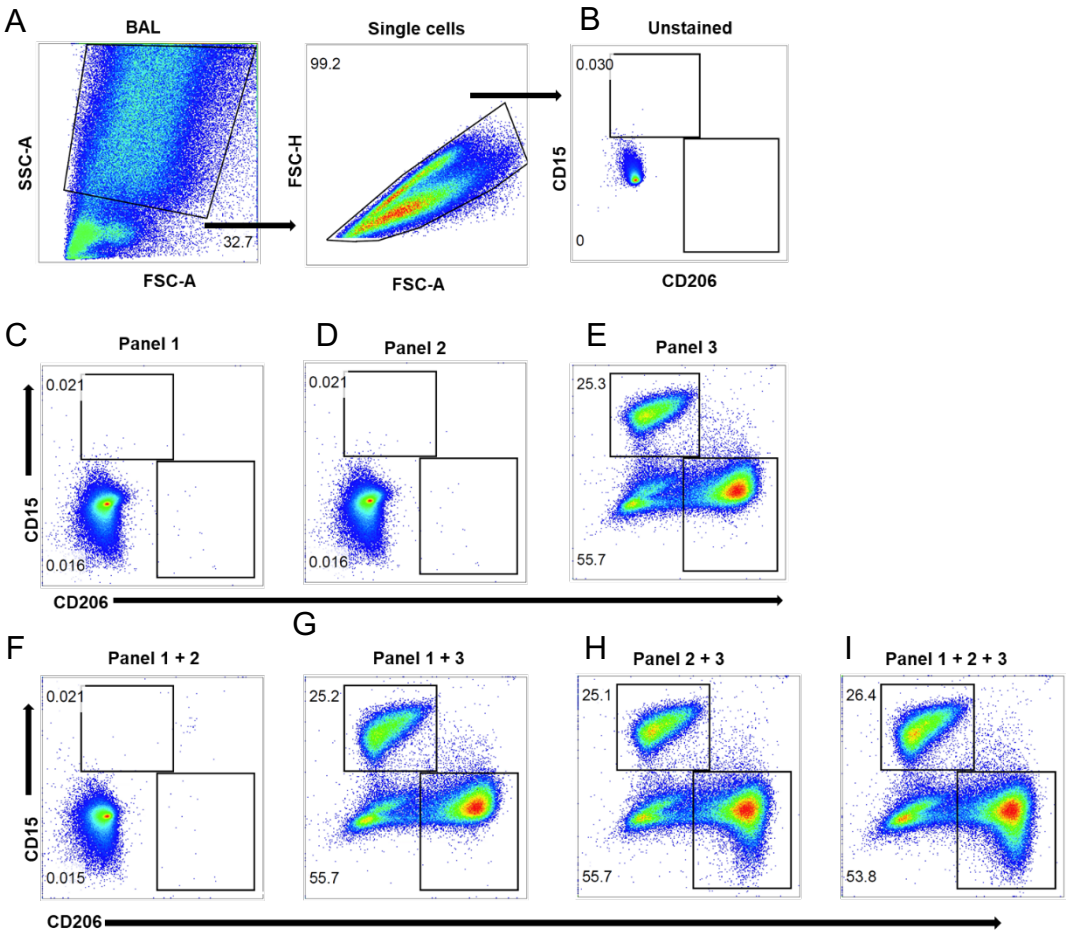


Fig 3.8. Scatter plots of fluorescence-minus-panel controls for macrophage and neutrophil markers in a BAL sample

1 x10^6 cells were plated in each well and incubated with live-dead blue for 20min, washed and stained with 30µl of the antibody cocktail for 30min. Wells receiving more than one cocktail were washed at intervals with PBS. After staining, cells were fixed in 1% PFA for 10min and washed again with PBS. Cells were stored in FACS buffer and acquired on the Aurora. **A)** Macrophage and neutrophil gating and doublet exclusion. **B)** Unstained control, **C)** Panel 1 controls, **D)** Panel 2 controls, **E)** Panel 3 controls, **F)** Panel 1+ 2 controls, **G)** Panel 1+ 3 controls, **H)** Panel 2+3 controls and **I)** Panel 1+ 2+3 staining.

3.4.4 Comparison of a 1-step versus 3-step staining protocol

Combining 33 fluorophores can lead to technical challenges, such as loss of antibody specificity (e.g. aggregation of polymer based fluorophores), reduced fluorescence due to spectral spread and nonspecific binding[44]. Therefore it was important to develop a methodical staining protocol. Given the complexity of spectral cytometry and the intricate algorithms applied to differentiate fluorescent spectra, two comprehensive staining techniques were tested. Leukocytes isolated from blood were either incubated with each subpanel sequentially or stained with a single cocktail containing all 33 antibodies and a number of key immune cells representing each sub-panel were analysed. Using this approach flow cytometry analysis showed that the 1-step and 3-step staining methods were comparable for $CD4^+$ and $CD45RA^+$ T cell subsets **(Fig. 3.9A, B)**, $CD56^+$ NK cells **(Fig. 3.9C)**, $CD15^+$ neutrophils **(Fig. 3.9D)**, IgD^+ B cells **(Fig. 3.9E)**, and $CD14^+$ monocytes **(Fig. 3.9F)**.

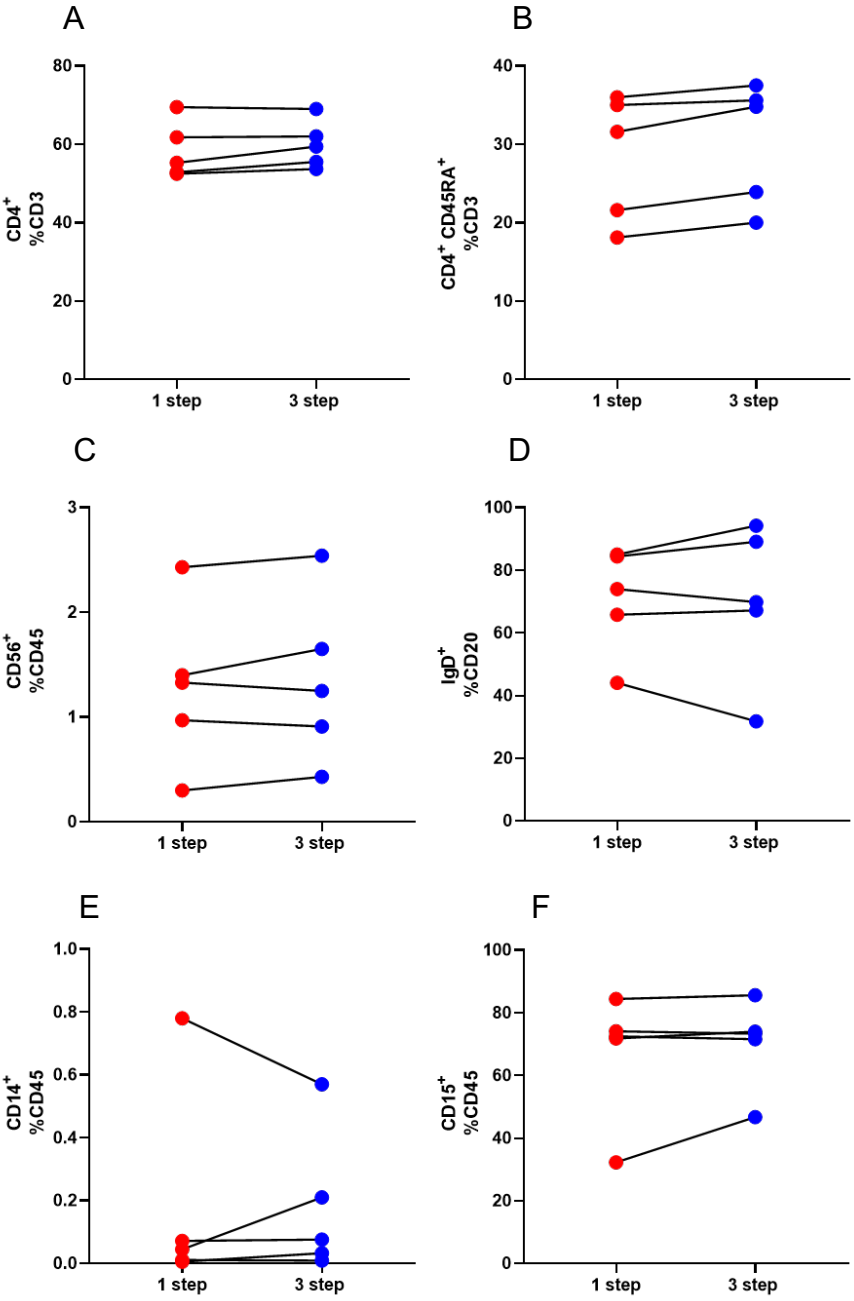


Fig 3.9. Comparison of the one-step versus a three-steps staining protocol with a 33-colour panel in blood

1 x10^6 cells were plated in each well and incubated with live-dead blue for 20min, washed and stained with 30µl of the antibody cocktail for 30min. Wells receiving more than one cocktail were washed at intervals with PBS. After staining, cells were fixed in 1% PFA for 10min and washed again with PBS. Cells were stored in FACS buffer and acquired on the Aurora. Flow cytometry percentage of **A)** $CD4^+$ cell, **B)** $CD45RA^+$ cells, **C)** $CD56^+$ cells, **D)** $CD15^+$ cells, **E)** IgD^+ cells and **F)** $CD14^+$ cells. Statistical significance was measured by unpaired, non-parametric Mann-Whitney U-Test.

3.4.5 Autofluorescence identification and removal in spectral cytometry

Live cells have an inherent AF which can obscure the signal of dim markers[45], thus making flow data analyses challenging. AF is produced by the existence of cellular granules and lipids, and is further magnified by the numerous laser excitations[46]. The presence of highly granulocytic neutrophils and eosinophils in blood and the abundance of AF macrophages in BAL fluid, necessitates an AF removal workflow. To facilitate this, the Aurora provides a parameter for AF, whereby a population can be identified in an unstained sample and taken as a reference control to extract AF and unmix the spectra. To determine AF signatures in blood and BAL samples, a framework was devised to outline the steps involved **(Fig. 3.10A)**. Using the SpectroFlo software, an unstained blood sample was unmixed using a library of single stain bead controls, and the leukocytes and debris negative cells were distinctively labelled **(Fig. 3.10B)**. Debris cells were utilized as a base control for the AF cells as they lack components known to contribute to AF, and thus could be considered as AF negative. Doublets were excluded, and the fluorophores were plotted against the AF channel **(Fig. 3.10C)**. Using BUV563 as an example, the appearance of positive and super negative populations in the unstained sample confirmed the presence of AF **(Fig. 3.10D)**. By gating and exporting these populations as individual flow cytometry files termed FCS files, they could then be imported back into the SpectroFlo experiment and listed as additional reference controls, alongside those for the individual fluorophores in the panel. The unmixing protocol was repeated using the same unstained sample and the resulting scatter plot of BUV563 showed that the AF populations were eliminated **(Fig. 3.10E)**. This method was applied to all

unstained samples acquired on the Aurora creating a bank of flow cytometry files of AF signatures. Four recurrent AF populations were observed across the unstained blood samples, which were assigned a number AF1 – AF4, based on their location on the scatter plot.

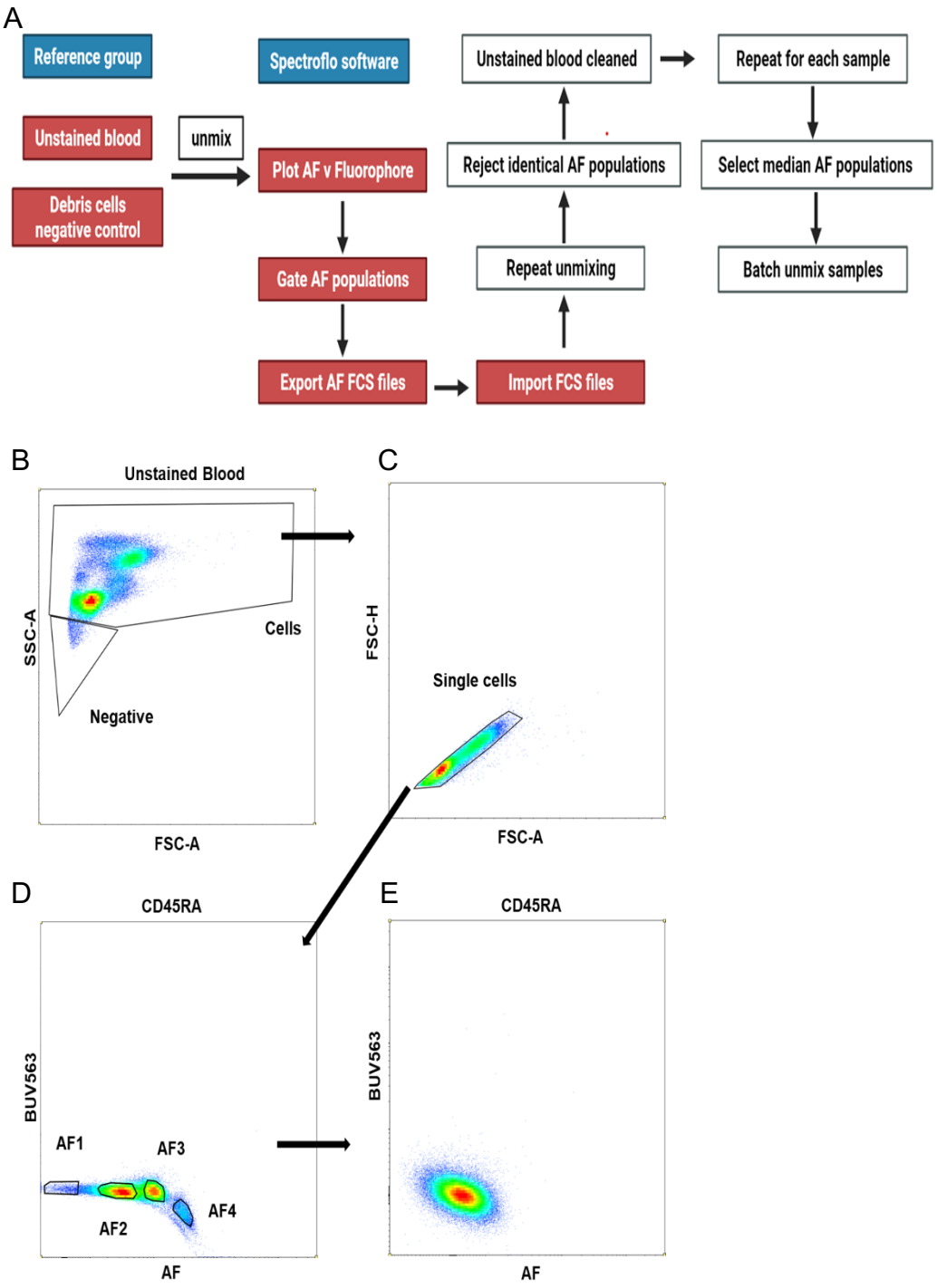


Fig 3.10. Autofluorescence removal workflow and identification of AF populations in blood

A) Diagram of AF removal workflow generated on the SpectroFlo software, Scatter plot of **B)** unstained cells, **C)** single cells, **D)** AF cells, **E)** cells post AF removal.

To develop a consistent, and appropriate, workflow for AF subtraction it was necessary to determine if the 4 AF populations observed in peripheral blood were consistent between donors or showed substantial donor to donor variance. The former allowing a single common AF reference to be used for all samples, the latter requiring individual donor AF to be calculated. The aurora has 64 detector channels and each AF file exhibits 64 variables corresponding to its spectra. Therefore, to determine the variance of AF populations between samples principal component plots (PCA) were constructed to visualize the multiple parameters **(Fig. 3.11)**. This also allowed selection of a representative median population for blood AF1 **(Fig. 3.11A)**, AF2 **(Fig. 3.11B)**, AF3 **(Fig. 3.11C)** and AF4 **(Fig. 3.11D)** which could be used to unmix samples. Next to unmix a batch of stained blood samples, these median AF signatures were added to the reference library as controls and a similarly index was generated to ensure they were distinctive enough to be spectrally unmixed (below 0.98) **(Fig. 3.11E)**. The four AF populations were overlaid on to the unstained cells they were extracted from to determine their cell type. AF1 appeared to be derived from lymphocytes **(Fig. 3.11F)** whereas AF2 signified neutrophils **(Fig. 3.11G)**. The forward and side scatter profiles of AF3 **(Fig. 3.11H)** and AF4 **(Fig. 3.11I)** suggesting they were of monocytes and eosinophils morphology, respectively.

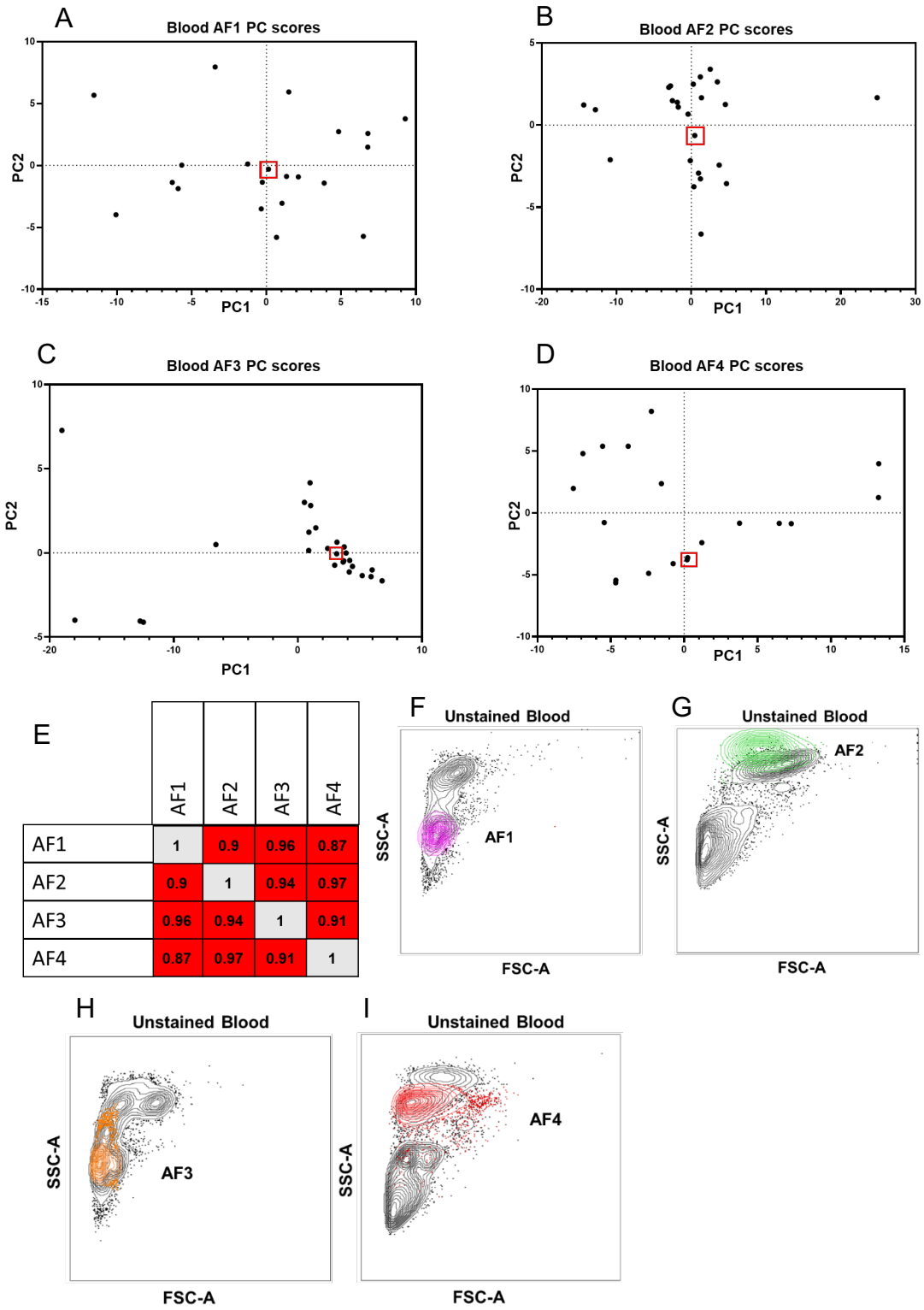


Fig 3.11. Selection of median autofluorescence populations in peripheral blood for autofluorescence removal

PCA plot of **A)** AF1 populations, **B)** AF2 populations, **C)** AF3 populations, **D)** AF4 populations. **E)** Similarity index of median AF populations. Scatter plot of **F)** AF1 signature, **G)** AF2 signature, **H)** AF3 signature and **I)** AF4 signature overlaid on unstained cells.

The same strategy was applied to BAL samples to extract autofluorescent signatures. Interestingly for BAL only three unique AF populations were identified by inspecting the AF channel against a fluorophore channel after unmixing the unstained sample **(Fig. 3.12A)**. PCA plots were applied to ascertain the median AF population for each cohort **(Fig. 3.12B, C, D)**. To unmix the batch of stained BAL samples, the similarity of BAF1 – BAF3 populations were verified to ensure the index was below 0.98 **(Fig. 3.12E)**. The three AF populations appeared to be representative of a lymphocytic and granulocytic phenotype based on their scatter plot localization **(Fig. 3.12F, G, H)**.

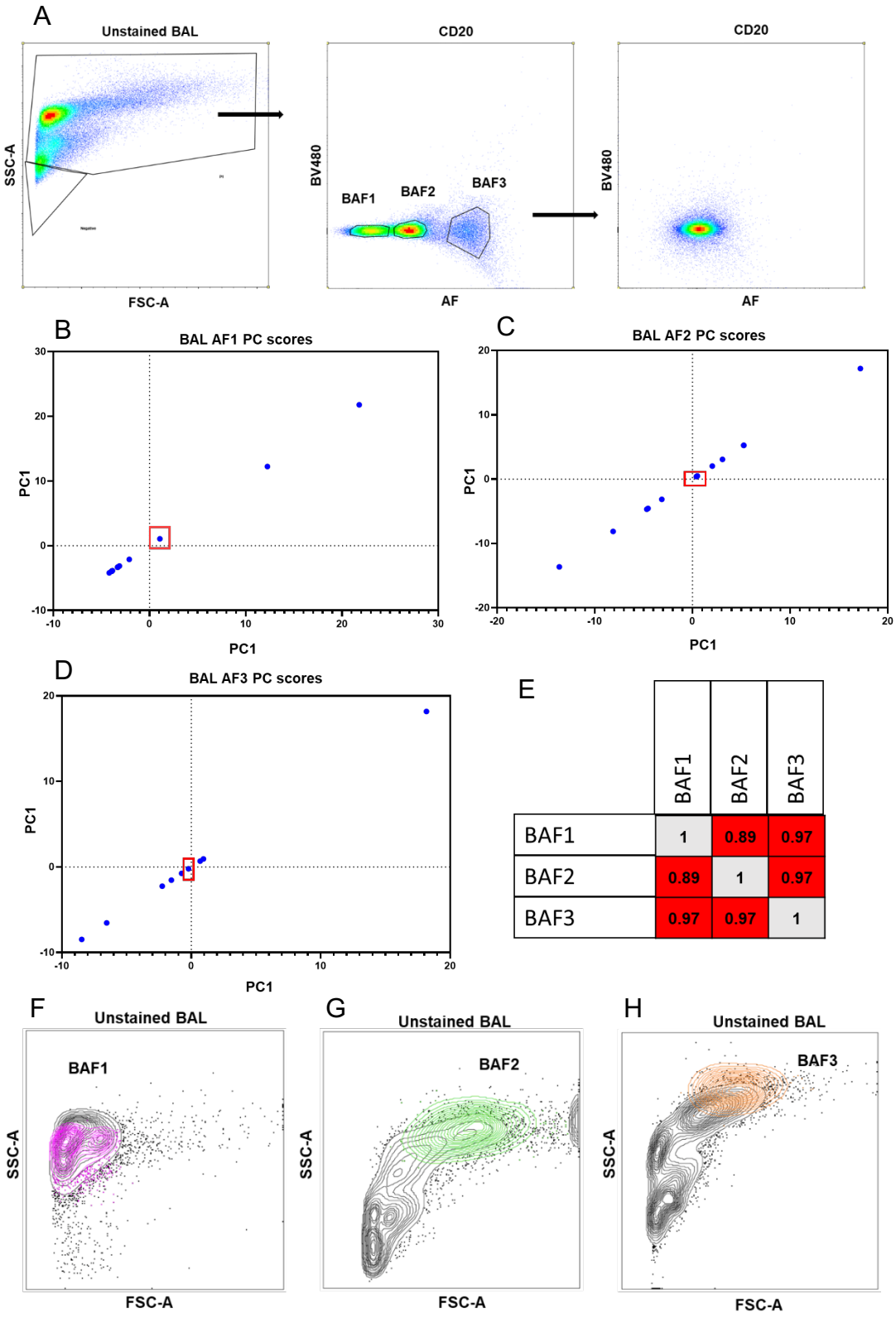

A
Unstained BAL
SSC-A
FSC-A
CD20
BV480
BAF1
BAF2
BAF3
AF
CD20
BV480
AF
B
BAL AF1 PC scores
PC1
PC1
C
BAL AF2 PC scores
PC1
PC1
D
BAL AF3 PC scores
PC1
PC1
E
BAF1
BAF2
BAF3
BAF1 1 0.89 0.97
BAF2 0.89 1 0.97
BAF3 0.97 0.97 1
F
Unstained BAL
BAF1
SSC-A
FSC-A
G
Unstained BAL
BAF2
SSC-A
FSC-A
H
Unstained BAL
BAF3
SSC-A
FSC-A

Fig 3.12. Identification and removal of autofluorescent populations in BAL samples
A) Gating illustration of AF populations. PCA plot of **B)** AF1 populations, **C)** AF2 populations and **D)** AF3 populations acquired from BAL samples. **E)** Similarity index of BAL median AF populations. Scatter plot of **F)** AF1 signature, **G)** AF2 signature, **H)** AF3 signature overlaid on unstained cells.

To determine whether autofluorescence extraction altered protein expression frequencies, the proportion of cell types pre and post AF removal were enumerated. Analysis of blood samples indicated that $CD15^+$, $CD3^+$ and Siglec-8^+ proportions were comparable **(Fig. 3.13A, B, C)**. Similarly, in BAL, there was no difference in the percentage of $CD206^+$, $CD3^+$ and $CD15^+$ cells following AF removal **(Fig. 3.13D, E, F)**.

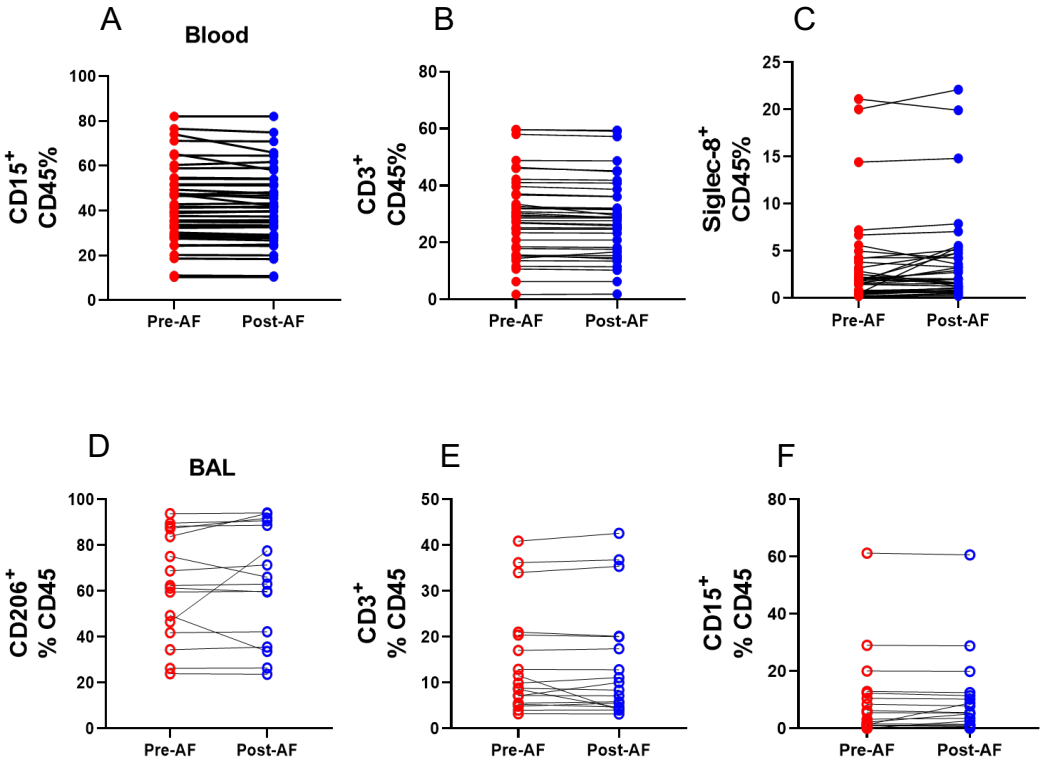


Fig 3.13. Flow frequencies of cell types pre and post AF extraction
1 x10^6 cells were plated in each well and incubated with live-dead blue for 20min, washed and stained with 30µl of the antibody cocktail for 30min. After staining, cells were fixed in 1% PFA for 10min and washed again with PBS. Cells were stored in FACS buffer and acquired on the Aurora. Frequency of **A)** $CD15^+$ cells, **B)** $CD3^+$ cells and **C)** Siglec-8^+ cells as a percentage of $CD45^+$ cells in blood. Proportion of **D)** $CD206^+$ cells, **E)** $CD3^+$ cells and **F)** $CD15^+$ cells as a percentage of $CD45^+$ cells in BAL.

3.4.6 Comparison of spectral and conventional flow cytometry

Finally, as the Aurora spectral cytometer is a relatively new approach, I validated the data with an existing well-established approach. To achieve this, all samples were acquired simultaneously using 12-marker panel on a conventional Fortessa flow cytometer. Given the limitations of the Fortessa panel, only a finite number of markers could be correlated using a matched gating strategy **(Fig. 3.14, 3.15)**. Analysis of blood samples revealed that most immune cell frequencies were similar in blood and BAL except for monocyte subsets. Heatmap illustrations showed that $CD14^+$ classical monocytes were significantly increased and $CD16^+$ nonclassical monocytes were significantly decreased in the Fortessa file compared to the matched Aurora file **(Fig. 3.16A)**. In BAL, the $CD16^+$ proportions were increased in the Aurora relative to the Fortessa data **(Fig. 3.16B)**. These differences could be due to a fluorophore and clone differences between both panels.

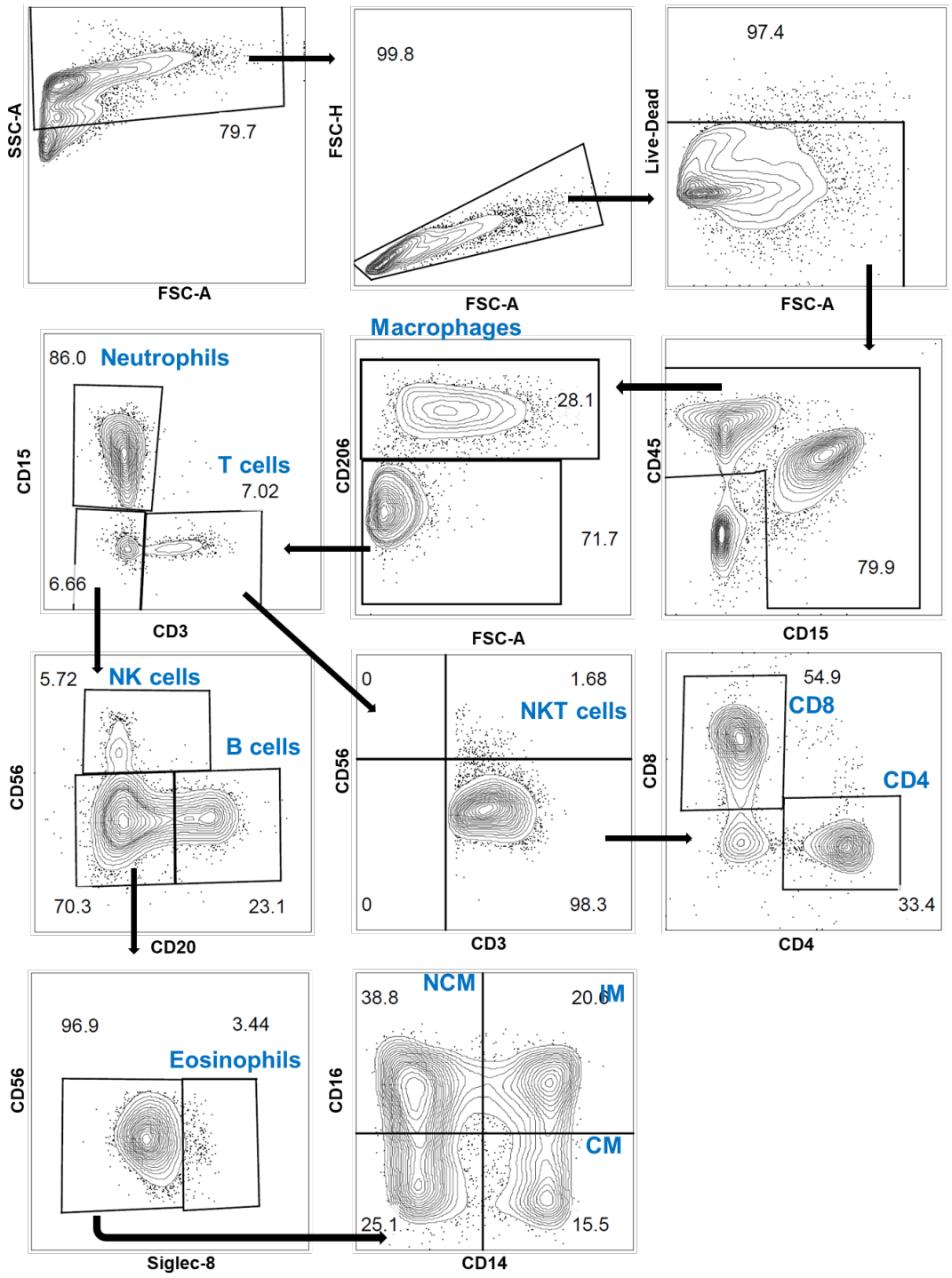


Fig 3.14. Aurora gating strategy

Representative flow cytometry gating strategy for BAL cell types defined on the Fortessa panel and replicated on the Aurora. The diagram shown is from a sample analysed on the Aurora cytometer.

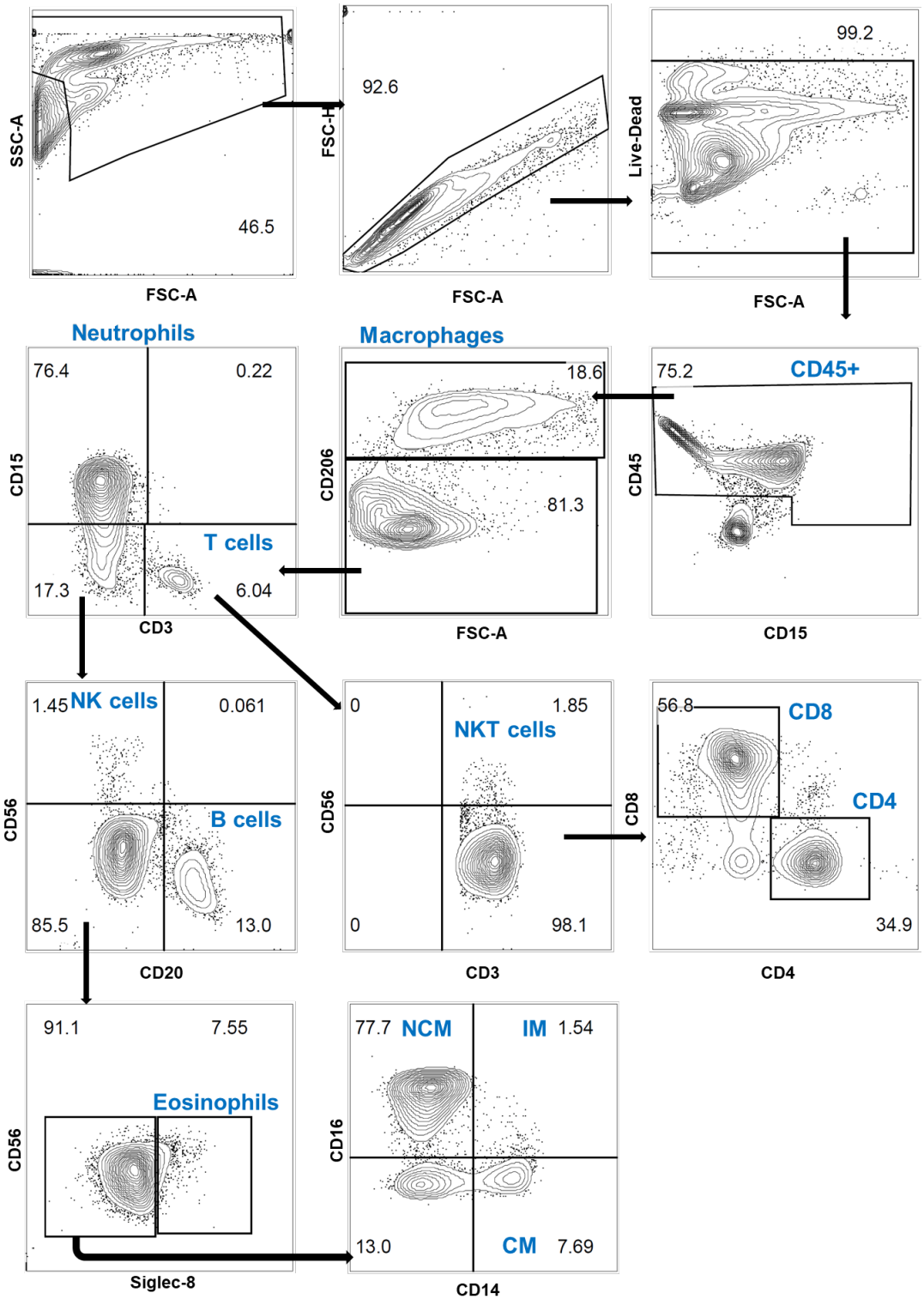


Fig 3.15. Fortessa gating strategy
Representative flow cytometry gating strategy for BAL cell types defined on the Fortessa panel. The diagram shown is from a sample analysed on the Fortessa III cytometer.

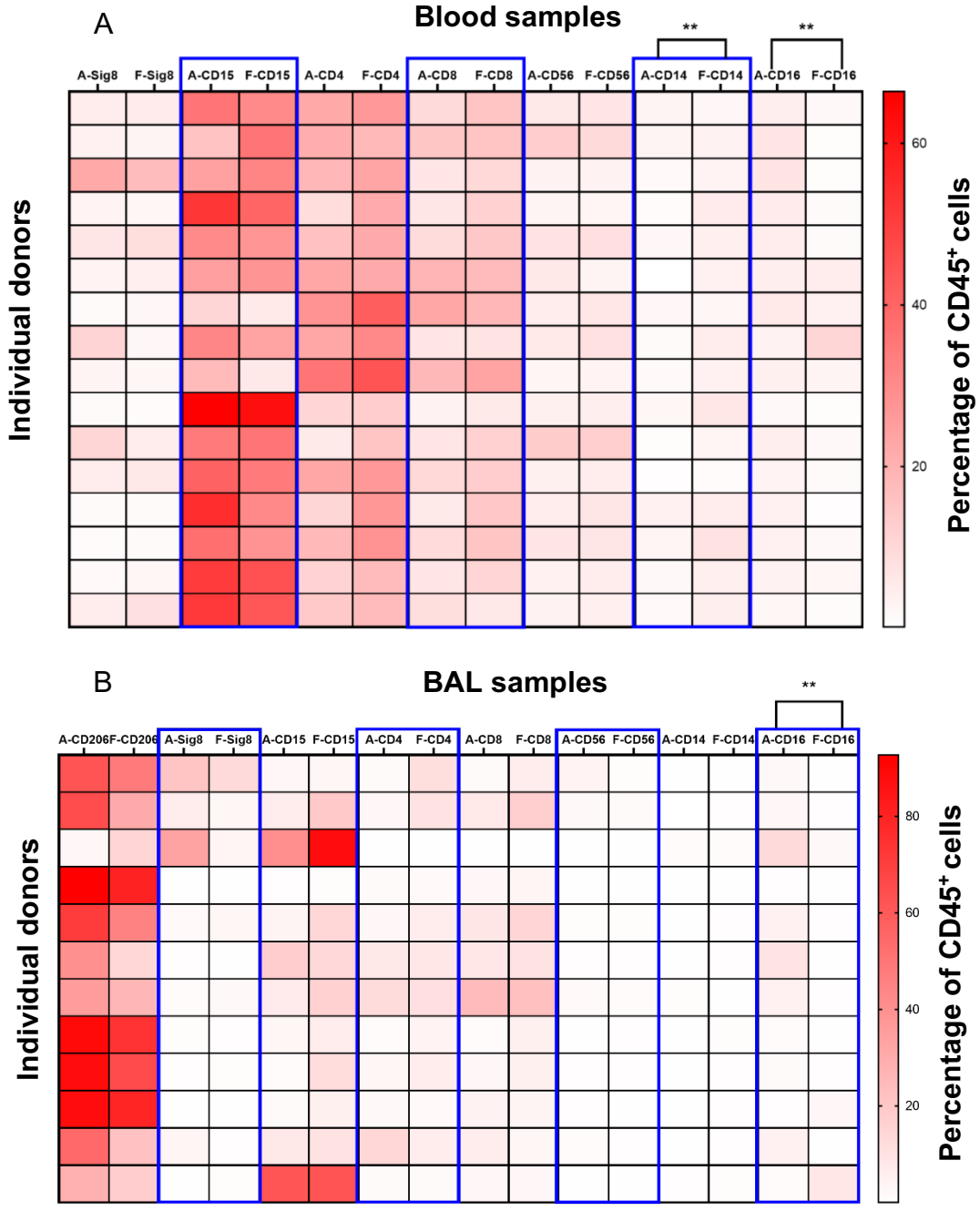


Fig 3.16. Comparison of cell frequencies in matched blood and BAL samples acquired on the Aurora and Fortessa flow cytometers

Samples from paediatric donors in this study were processed. 1 x10^6 cells were plated in each well and incubated with live-dead blue for 20min, washed and stained with 30µl of the antibody cocktail for 30min. After staining, cells were fixed in 1% PFA for 10min and washed again with PBS. Cells were resuspended in FACS buffer for flow cytometry. Heatmap of immune cell proportions in **A)** Blood **B)** BAL samples acquired on the Aurora (A) and Fortessa (F). Statistical significance was measured by Kruskal Wallis test + Dunn's multiple comparison test. Significance value presented * < 0.05, **<0.01, ***< 0.001. ****< 0.0001.

3.5 Discussion

The aim of this chapter was to establish a multi-parameter flow panel capable of phenotyping key immune cell types within peripheral blood and BAL fluid. To this end the 5-laser Aurora spectral cytometer was implemented.

The findings of this chapter showed that spectral cytometry can be used to accurately identify 33 immunological surface markers simultaneously. As paediatric samples are precious, preliminary experiments were conducted using blood from healthy adult volunteers and ample supply of BAL fluid was obtained from an adult patient with Idiopathic pulmonary fibrosis. Antibody titrations showed that most of the lymphocyte surface antigens were detectable at 1 in 100 dilutions. Certain lymphocyte associated markers that required higher concentrations to obtain a distinct signal resolution were CXCR5, CD69, CD161 and CD127. This could be due to the lower affinity of the antibodies used to identify these markers or the lower protein density of these markers on the cells analysed[47]. Certainly, many of the markers for which higher concentrations of antibodies were required are activation markers, which may have relatively low expression in the circulation of healthy adult volunteers but may be elevated in clinical samples from individuals with inflammatory or infectious disease. Likewise, myeloid-derived proteins revealed that positive populations were mostly distinguishable at 1 in 100 dilutions except for CD141-PE which was assigned a 1 in 20 titrations.

Flow data analysis of BAL cells stained with serial dilutions of the macrophage marker CD206, displayed that the signal resolution of $CD206^{+}$ cells decline after 1 in 20. It is well documented that macrophages are the most abundant population in healthy BAL fluid[48] and are extremely autofluorescent with

adhesive attributes[42]. Therefore, a higher concentration of antibody may be required to capture a clear positive signal.

Subdivided panels provide an alternative to FMOs for a 33-colour panel. As an alternative to FMOs, the high-parameter panel is often subdivided into three smaller panels. However, this approach does have limitations in terms of certainty. The Aurora panel contains 34 fluorophores, some of which have high emission wavelengths (PE-Dazzle 594) and similar signatures (APC and A647). These factors create spreading error which is present after spectral unmixing, making it difficult to determine where a positive population begins. Some measures were applied to minimize the spreading error generated by fluorophores. Co-expressed markers such as CD3 and CD4 were conjugated to distinguishable fluorophores BUV805 and Spark Blue 550 respectively. Highly similar fluorophores were placed on unrelated cell types to avoid gating them together (CD123-APC and CRTH2-A647). Fluorophores that cause extensive spreading error were assigned to markers that are rarely expressed (TCRγδ – PE Dazzle 594)[49,50,51].

Furthermore, the removal of multiple markers simultaneously (panel 1, 2 or 3) can obscure the potential spread of fluorophores[52]. Using these FM-panel controls masks the contribution of each fluorophore to the spreading error in a scatter plot of two markers. Therefore, individual FMOs are more accurate in positioning gating boundaries. Nevertheless, obtaining enough peripheral immune cells to run FMOs for a 34-colour panel would require multiple donors, split across sessions which would lead to technical variability and cannot be performed regularly. This approach would also be impossible for paediatric BAL cells. Although single stain controls are utilized for the spectral unmixing

algorithm, they can also be used to visualise the positive signals, albeit beads are not a perfect representation of human cells.

In addition, both blood and BAL samples are processed to prepare clean viable cell suspensions for staining. As airway samples are mixed with mucus[53], more stringent steps are taking to filter and wash BAL fluid reducing cell yield. The repeated washing leads to cell loss[54], therefore it is suggested to plate at least a million cells. However, cell recovery from paediatric samples can be unpredictable, which highlights a major advantage of the Aurora. Given its high-level of sensitivity and signal resolution, immunophenotyping samples with low cell counts is achievable[52].

While the Aurora provides an advanced approach for single cell analysis, the post-acquisition modifications are laborious, particularly dealing with AF removal in continuous patient samples. A major complication to consider in human samples is that AF varies with cell type and disease. Specifically in BAL fluid, macrophages are highly autofluorescent causing a nonuniform distribution of AF between cell types within a sample[55]. Thus, an extensive protocol was required to determine the AF contributed by each cell type in blood and BAL. To achieve this, the AF in each donor's unstained sample was analysed using the unmixing workflow described in this chapter. Our findings showed that three and four distinct AF populations were discovered in unstained BAL and blood samples respectively.

Based on the forward and side scatter features of the AF populations, this suggested that they represented lymphocytes, neutrophils, eosinophils and macrophages. To accelerate the AF extraction workflow, a library of median

AF populations was created for each tissue using a batch of donor samples. Assessment of stained cell frequencies pre and post AF removal indicated that protein fluorescence is unaffected.

While this batch unmixing protocol is practical for clinical studies, overtime individual sample variance may lead to inaccuracies. For example, AF of immune cell populations will vary based on inflammation status[56] and may lead to imperfect AF removal and unmixing of markers such as CD206 and CD16 which are expressed by highly autofluorescent macrophages.

Most cell type proportions in blood and BAL were comparable between the two flow cytometry systems. However, comparison of $CD14^+$ and $CD16^+$ gated populations acquired by conventional and spectral flow were dissimilar and could be contributed to clone or fluorophore differences between the panels. For example, CD14 on the aurora was produced by the clone 63D3 whereas on the Fortessa, CD14 was generated by the clone M5E2. Different clones of antibodies can bind to different epitopes on a single antigen, and therefore will have dissimilar affinity and performance when comparing stained populations[57]. The abundance of epitopes may also be influenced by disease type and ethnicity which is variable in patient cohorts.

As previously highlighted, a 34-colour panel will exhibit more spreading error than a 12-colour panel. Furthermore, on the Fortessa instrument, each detector is assigned to a single fluorophore and compensation is applied to eliminate spillover[41]. This does not apply in spectral cytometry as all detectors are used to capture the whole spectrum of each fluorophore, thus there are multiple fluorophores in the detector[41]. In conventional flow cytometry, the

simplicity of a 12-colour panel allows the selection of uncomplicated fluorophores. Whereas a 34-colour panel must make use of all commercially available fluorophores and therefore is exposed to more complexities. Thus, it is possible that with the spectral cytometry approach, the gating for minute $CD14^+$ and $CD16^+$ monocyte populations may not be precise due to overlaps with the intermediate monocytes and the double negative population.

This experimental chapter provides some positive prospects for the future of multi-parameter flow cytometry. We have established a functional multicolour flow panel that can rapidly differentiate lymphocytes, granulocytes and myeloid cells in a single sample, devised an effective staining technique and developed an AF removal strategy for spectral cytometry. This approach surpasses the limitations of mass cytometry such as low sensitivity of less expressed markers, low flow rate of cells per second and an inability to recover cells for subsequent assays[58]. In clinical studies, samples are preserved for further functional analyses which highlights the major advantage of spectral cytometry in using a minute sample and sparing cells.

3.6 Conclusion

Taken together, the results presented here demonstrate a comprehensive high-parameter flow panel which can stain key immune subsets in blood and BAL samples and a functional AF extraction protocol which can be applied to clinical samples for deep phenotyping.

Chapter 4. Cellular phenotyping of peripheral and airway immune cells in childhood airways disease

4.1 Introduction

In chapter 3, a comprehensive multi-parameter flow panel allowing phenotyping multiple immune cell types within peripheral blood and BAL fluid was established. The panel was developed to overcome the limitations of paediatric samples and the scarcity of BAL cell yield. To delineate asthma and wheeze phenotypes, key immune cells introduced in chapter 3 were investigated in this study including T cells, NK and NKT cells, B cells, eosinophils, neutrophils, macrophages, monocytes, DCs and ILCs. This chapter presents the characterisation of these immune cells in the blood and airways, their activation status and correlations with clinical demographics.

Blood and BAL samples were chosen for this study because they offer various advantages for phenotyping disease pathogenesis. For example, peripheral blood is easily accessible and offers a wide variety of immune cells in large quantities. BAL samples provide discrete information on specialised immune cells relevant to respiratory diseases. Immune cell responses to asthma therapies are commonly investigated in both tissue types[18,12]. As our understanding of the early-life immune system is limited and asthma trajectory prediction is challenging[13], multi-parameter flow cytometry may offer a novel approach that allows more detailed immune phenotyping and improve patient diagnosis.

4.2 Hypothesis

Children with severe preschool wheeze have a distinct airway and blood immune cell profile compared to non-wheezing disease controls.

4.3 Aims

1. To phenotype the cellular profile of lower airways and blood in children with preschool wheeze, severe asthma and non-wheeze controls
2. To relate the cellular phenotypes of the disease cohorts with their clinical features

4.4 Results

4.4.1 Study design of patient recruitment and overview of immune profile

Forty children aged between 1 to 16 years with STRA, PSW or other respiratory infections were recruited from the Royal Brompton Hospital. Their clinical demographics are summarised in **Table 4.1**. STRA diagnosis was confirmed by doctors following a detailed clinical evaluation of underlying modifiable features including optimal adherence to maintenance asthma therapy[59]. Wheeze in preschool children (1- 5 years) was confirmed using clinical assessment and parental reports[16]. Children (1- 16 years) undergoing an elective clinically indicated bronchoscopy for recurrent lower respiratory tract infections were selected to represent a non-wheeze control group. Parents gave informed consent for additional blood and BAL samples to be used for research. Samples were processed in the lab using established methods (Chapter 2) and cell phenotypes were delineated using the Aurora spectral cytometer. Cytospins were prepared to give a rapid overview of cell distribution and morphology **(Fig. 4.1A)**. Proportions of total leukocytes in circulation and in BAL fluid between the disease groups were comparable,

although STRA children showed an increasing trend in total peripheral cells but a decrease in total airway leukocytes **(Fig. 4.1B, C)**. The paediatric disease patients' white blood cell count compared to healthy children are outlined in **Table 4.2.**

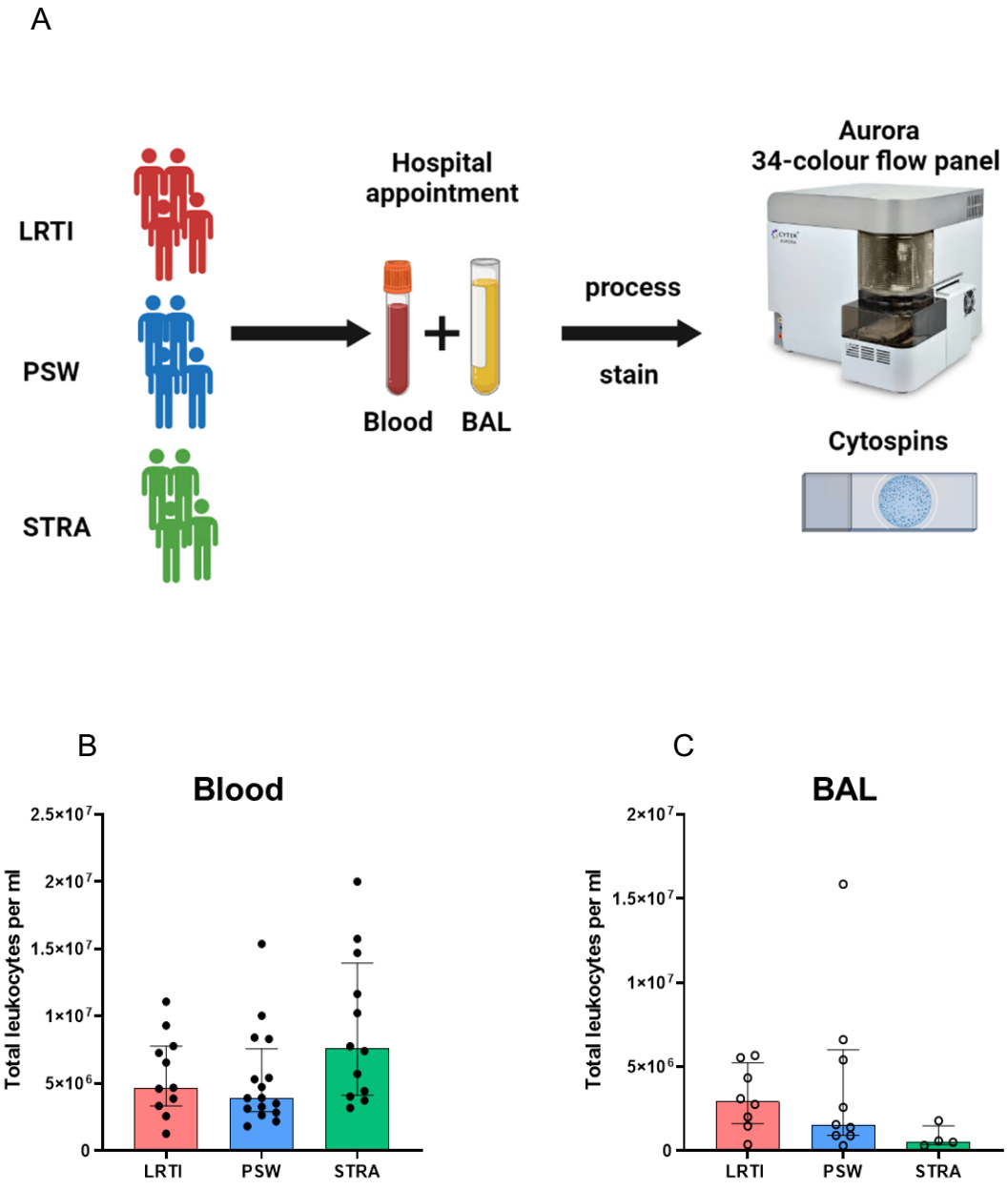


Fig 4.1. Study design of patient recruitment and phenotyping method **A)** Schematic of subject recruitment and sample processing methods. Number of total leukocytes in **B)** Blood and **C)** BAL samples. Statistical significance was measured by Kruskal Wallis test + Dunn's multiple comparison test.

Characteristics	STRA	PSW	LRTI
Subjects	12	17	11
Number of blood samples	12	17	11
Number of BAL samples	4	9	8
Volume of BAL recovered mL median (range)	11.9 (4.0 – 18.2)	5.7 (2.0 – 10.7)	11.4 (3.5 – 22.0)
Number of matched samples	4	9	8
Age (years) median (range)	12.17 (5.7-16.8)	2.42 (1.58-4.16)	3.9 (1.3 - 16.3)
Sex	6M : 6F	10M : 7F	7M : 4F
Atopic	8	5	0
ICS prescribed	12	16	2
Steroid dose per day equivalent to Budesonide median (range)	1000mcg (400 - 2000)	400mcg (100 - 400)	250mcg (100-400)
Serum IgE median IU/ml median (range)	1082.5 (15 - 4483)	24 (15 - 480)	20 (15 - 291)
Positive for bacterial pathogens	4 of 12 patients	7 of 17 patients	5 of 11 patients
Types of bacterial pathogens	S. aureus, C. diffluens, P. alcaligenes	S. pneumoniae, M. catarrhalis, S. aureus, H. influenzae,	S. pneumoniae, Aspergillus, S. aureus, M. catarrhalis
Positive for viral pathogens	1 of 12 patients	12 of 17 patients	5 of 11 patients
Type of viral pathogens	Rhinovirus, Enterovirus	Rhinovirus, Enterovirus, Parainfluenza 3, Adenovirus, Parechovirus, Parainfluenza 3 & 4	Rhinovirus, Enterovirus, Parainfluenza 3, Human metapneumovirus

Table 4.1. Demographics of paediatric STRA, PSW and LRTI patients

All patients were recruited when undergoing clinically indicated bronchoscopy. Number of BAL and blood samples collected are not matched. Data shown as median with range. STRA = severe therapy resistant asthma. PSW = preschool wheeze. LRTI = lower respiratory tract infections.

Characteristics	STRA	PSW	LRTI	Normal	Normal	Normal Females	Normal Males
Age (years)	6 – 17	2 – 4	1 – 16	1 – 6	6 – 12	12 – 18	12 – 18
White blood cell count ($x10^6$/mL)	3.2 – 20	1.8 – 15.4	1.25 – 11.1	5 – 17	4.5 – 14.5	4.5 – 13.0	4.5 – 13.0

Table 4.2. Demographics of paediatric disease patients' white blood cell count compared to healthy children
The normal children's reference ranges for white blood cell count were obtained from North Bristol NHS Trust. Data shown as a range.

4.4.2 Comprehensive gating strategy and distribution of immune cells

To characterise the relevant immune cell subsets in asthma and wheeze pathogenesis, a hierarchical gating strategy was devised using the Aurora 34-colour panel **(Fig. 4.2A)**. The list of markers gated to define each cell type and putative cell subsets are summarised in **Table 4.3**. The description of the antigens recognised by each antibody are highlighted in **Table 4.4**. The primary gating criteria used for each cell type consisted of; macrophages ($CD206^+$), neutrophils ($CD15^+$), eosinophils ($Siglec8^+$, $CD15^{+/-}$, $CD16^-$), T cells ($CD3^+$ $TCR\alpha\beta^+$ / $TCR\gamma\delta^+$ $CD4^+$ or $CD8^+$), NKT cells ($CD3^+$ $CD56^+$), NK cells ($CD56^+$) and B cells ($CD20^+$). Monocytes were categorised as $CD11b^+$, $HLA\text{-}DR^+$, $CD11c^+$ cells and split by $CD14^+$ or $CD16^+$ or dual positive expression. The remaining double negative population was examined for DC subsets using $CD1c^+$, CD123 and CD141 expression. ILC gating was adjusted to focus on the lymphoid population and is presented later. The cell types that are identified by the panel are presented in chapter 3 pages 29 – 32.

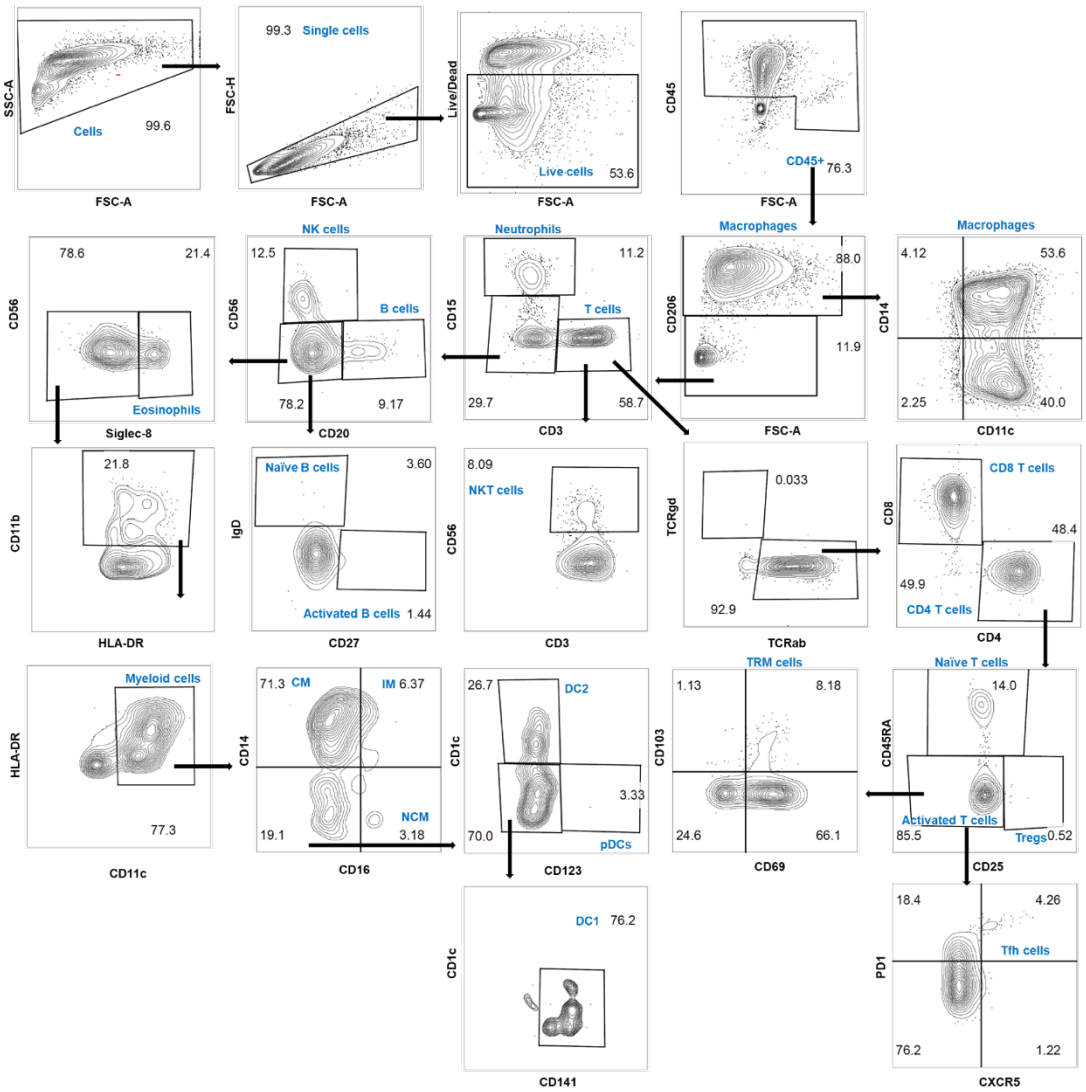


Fig 4.2. Gating strategy for BAL immune cells using the Aurora panel
Schematic of flow cytometry scatter plots showing immune cell gating strategy. All cells were selected using forward and side scatter. Doublets were removed by gating for single cells using FSC-A versus FSC-H. Live cells were selected as Live-Dead blue negative cells. Viable immune cells were defined as CD45 positive.

Cell type	Gated markers
CD4 T cells	$CD3^+$ $TCRab^+$ $CD4^+$
Naïve CD4	$CD3^+$ $TCRab^+$ $CD4^+$ $CD45RA^+$
CD4 Tregs	$CD3^+$ $TCRab^+$ $CD4^+$ $CD45RA^-$ $CD25^+$
CD4 TFH	$CD3^+$ $TCRab^+$ $CD4^+$ $CD45RA^-$ $CD25^-$ → $CXCR5^+$ $PD1^+$
CD4 TRM	$CD3^+$ $TCRab^+$ $CD4^+$ $CD45RA^-$ $CD25^-$ → $CD69^+$ $CD103^+$ or $CD69^+$ $CD103^-$
CD8 T cells	$CD3^+$ $TCRab^+$ $CD8^+$
Naïve CD8	$CD3^+$ $TCRab^+$ $CD8^+$ $CD45RA^+$
CD8 Tregs	$CD3^+$ $TCRab^+$ $CD8^+$ $CD45RA^-$ $CD25^+$
CD8 TF cells	$CD3^+$ $TCRab^+$ $CD8^+$ $CD45RA^-$ $CD25^-$ → $CXCR5^+$ $PD1^+$
CD8 TRM	$CD3^+$ $TCRab^+$ $CD8^+$ $CD45RA^-$ $CD25^-$ → $CD69^+$ $CD103^+$ or $CD69^+$ $CD103^-$
NKT cells	$CD3^+$ $CD56^+$
NK cells	$CD3^-$ $CD15^-$ $CD20^-$ $CD56^+$
B cells	$CD3^-$ $CD15^-$ $CD56^-$ $CD20^+$
Naïve B cells	$CD20^+$ IgD^+ $CD27^-$
Memory B cells	$CD20^+$ IgD^- $CD27^+$
Plasma cells	$CD20^-$ $CD38^+$ $CD27^+$
Eosinophils	$CD3^-$ $CD15^{low}$ $CD56^-$ $CD20^-$ Siglec-8^+
Neutrophils	$CD3^-$ $CD15^+$
Macrophages	$CD206^+$ → $CD14^+$ $CD11c^+$ or $CD11c^+$ $CD14^-$
Classical Monocytes	$CD3^-$ $CD15^-$ $CD56^-$ $CD20^-$ Siglec-8^- → $CD11b^+$ $HLA\text{-}DR^+$ $CD11c^+$ $CD14^+$
Intermediate Monocytes	$CD3^-$ $CD15^-$ $CD56^-$ $CD20^-$ Siglec-8^- → $CD11b^+$ $HLA\text{-}DR^+$ $CD11c^+$ $CD14^+$ $CD16^+$
Nonclassical Monocytes	$CD3^-$ $CD15^-$ $CD56^-$ $CD20^-$ Siglec-8^- → $CD11b^+$ $HLA\text{-}DR^+$ $CD11c^+$ $CD16^+$ $CD14^-$
T1 Dendritic cells	$CD3^-$ $CD15^-$ $CD56^-$ $CD20^-$ Siglec-8^- → $CD11b^+$ $HLA\text{-}DR^+$ $CD11c^+$ $CD14^-$ $CD16^-$ → $CD1c^-$ $CD123^-$ $CD141^+$
T2 Dendritic cellS	$CD3^-$ $CD15^-$ $CD56^-$ $CD20^-$ Siglec-8^- → $CD11b^+$ $HLA\text{-}DR^+$ $CD11c^+$ $CD14^-$ $CD16^-$ → $CD123^-$ $CD1c^+$
Plasmacytoid Dendritic cells	$CD3^-$ $CD15^-$ $CD56^-$ $CD20^-$ Siglec-8^- → $CD11b^+$ $HLA\text{-}DR^+$ $CD11c^+$ $CD14^-$ $CD16^-$ → $CD1c^-$ $CD123^+$
ILCs	Lymphoid cells → $CD3^-$ $CD15^-$ $CD20^-$ $CD56^-$ Siglec-8^- $CD11c^-$ $CD123^-$ → $CRTH2^+$ $CD127^+$

Table 4.3. Aurora markers used to identify the cell types
The list of markers gated to define the cell types and putative cell subsets. All cells were first gated as singlets, live and $CD45^+$. Next macrophages were separated using $CD206^+$ expression and the remaining cells were characterised using their relevant antigens.

Antigen	Description
CD69	Marker of T cell activation and tissue retention[60]
CD8	Glycoprotein expressed on cytotoxic T cells involved in antiviral immunity[61]
CD45RA	Glycoprotein expressed on naïve/resting T cells[62], B cells[63] and monocytes[64]
CD11c	Adhesion protein expressed on monocytes, macrophages, granulocytes, DCs, NK cells and subsets of T and B cells[65,66]
CD56	Cell adhesion molecule present on NK cells and T cells with cytotoxic capacity[67]
CD3	Antigen recognition and signal transduction receptor expressed on T cells[68]
IgD	Immunoglobulin expressed on naïve B cells and participates in cell maturation[69]
CD16	Cell surface molecule essential for cellular cytotoxicity by NK cells, and is expressed on macrophages and monocytes[70]
CD25	IL-2 receptor associated with cell proliferation and survival of regulatory T cells[71]
CD20	B cell differentiation antigen expressed throughout B cell development[72]
CD127	IL-7 transmembrane receptor expressed on effector T cells, NKT cells and ILCs[73]
HLA-DR	Antigen presenting molecule expressed on B cells, activated T cells, monocytes, macrophages and dendritic cells[74]
CD28	Co-stimulatory molecule involved in the activation of T cells during antigen presentation[75]

CD38	Activation marker involved in cell adhesion, migration and signal transduction. Highly expressed on plasma cells and activated T and B cells and NK cells[76]
CD15	Adhesion molecule found on neutrophils and mediates phagocytosis and chemotaxis[77]
PD1	Cell surface marker of exhaustion and apoptosis mostly expressed on activated T cells, B cells, and myeloid cells[78]
CD206	Pattern recognition receptor expressed on macrophages and DCs and mediates endocytosis and phagocytosis[79]
CXCR5	B cell and T follicular helper cells receptor for chemokines and regulates migration into the follicles[80]
Siglec-8	Surface protein expressed exclusively on eosinophils, mast cells and basophils. Receptor engagement results in eosinophil apoptosis, or inhibition of mast cell degranulation[81]
CD4	Receptor expressed on T cells that recognises antigens and participates in thymic differentiation, cell-cell interactions and signal transduction[82]
CD161	Stimulatory receptor expressed on NK cells, NKT and T cells[83]
CD27	Lymphocyte-specific co-stimulatory molecule that regulates activation and survival[84]
CD45	Common leukocyte antigen involved in in the regulation of cell differentiation[85]
CD86	Co-stimulatory molecule constrictively expressed on B cells, macrophages and dendritic cells[86,87]
CD141	CD141 is a cofactor in the protein C anticoagulant system and is found on DC1s which induce Th1 immune response[26]
TCRγδ	T cell receptor that recognises unprocessed antigens[88]

TCRαβ	T cell receptor that recognises antigens bound to MHC molecules[88]
CD11b	Integrin expressed on granulocytes, monocytes, macrophages and DCs that assists in cell migration and adhesion[89]
CD123	IL-3 receptor used for the identification of plasmacytoid DCs and basophils[90]
CRTH2	Inhibits apoptosis of Th2 cells and mediates the chemotaxis of CRTH2 expressing cells to the sites of allergic inflammation[91]
CD14	Pattern recognition receptor for gram-negative pathogens and highly expressed on monocytes and macrophages[92]
CD1c	Surface protein that presents antigens to T cells and used to define DC2 subset which mediate Th2 responses[25]
CD103	Integrin expressed on a subset of T cells and DCs which interacts with E-cadherin to mediate cell adhesion, migration, and lymphocyte homing[93]

Table 4.4. Antigens recognised by each antibody on the Aurora panel
A description of the role of each antigen and the cell types defined by their cognate antibody

4.4.3 Phenotyping of peripheral and airways lymphocytes

Next the cellular phenotype of each immune cell and differential frequencies between the disease groups was evaluated. With the array of surface markers available, the differentiation and activation status were analysed using FlowJo. It is accepted that $CD4^+$ T cells contribute to the pathology of asthma via the secretion of T2 cytokines IL-5 and IL-13[94] and that cytotoxic $CD8^+$ T cells drive immunity against viruses[95] which are common infections in preschool wheezers[16]. T cells were identified using $CD3^+$ and $TCR\alpha\beta^+$ co-expression and split between $CD4^+$ and $CD8^+$ populations. Examination of blood $CD4^+$ T cells showed no difference between the subject groups **(Fig. 4.3A)**, while a subset defined as naïve $CD45RA^+$ $CD4^+$ T cells were elevated in LRTI and PSWs compared to STRA children **(Fig. 4.3B)**. This decrease is associated with aging as studies show that thymic production of T cells peaks in the first year of life and naïve CD4 T cell export declines over time to a steady state[96].

There was increased $CD25^+$ $CD127^-$ $CD4^+$ T cells in the periphery of STRA and LRTI children as opposed to PSW **(Fig. 4.3C)**. This population likely represents Tregs, which are generally immunosuppressive[97]. There was no distinction in blood $CD4^+$ T cell populations expressing T follicular helper (TFH) cell markers $CXCR5^+$ and $PD\text{-}1^+$ however there were some children with pronounced populations that appeared as outliers **(Fig. 4.3D)**. As anticipated, all three disease cohorts had minimal frequency of circulating $CD4^+$ T cells expressing CD69 surface antigen **(Fig. 4.3E)**. Further assessment of the geometric mean fluorescence intensity (gMFI) of activation markers expressed on the $CD25^+$ $CD127^-$ $CD4^+$ subset revealed that only CD38 expression was augmented in PSW and LRTI children compared to STRA patients **(Fig. 4.3F)**.

This suggested that STRA individuals may have heightened $CD4^+$ immune activity. In contrast, total airway $CD4^+$ T cell populations were comparable between the study groups **(Fig. 4.4A)**.

Spectral cytometry analysis of the paediatric airways conveyed a minor composition of naïve $CD45RA^+$ **(Fig. 4.4B)** and $CD25^+$ $CD127^-$ $CD4^+$ populations **(Fig. 4.4C)** but an abundance of BAL T cells that displayed markers associated with TRMs ($CD69^+$ and $CD103^+$) **(Fig. 4.D, E)**. In summary these findings indicate that children with STRA and PSW have distinct peripheral CD4 T cell phenotypes but comparable airway immune profiles.

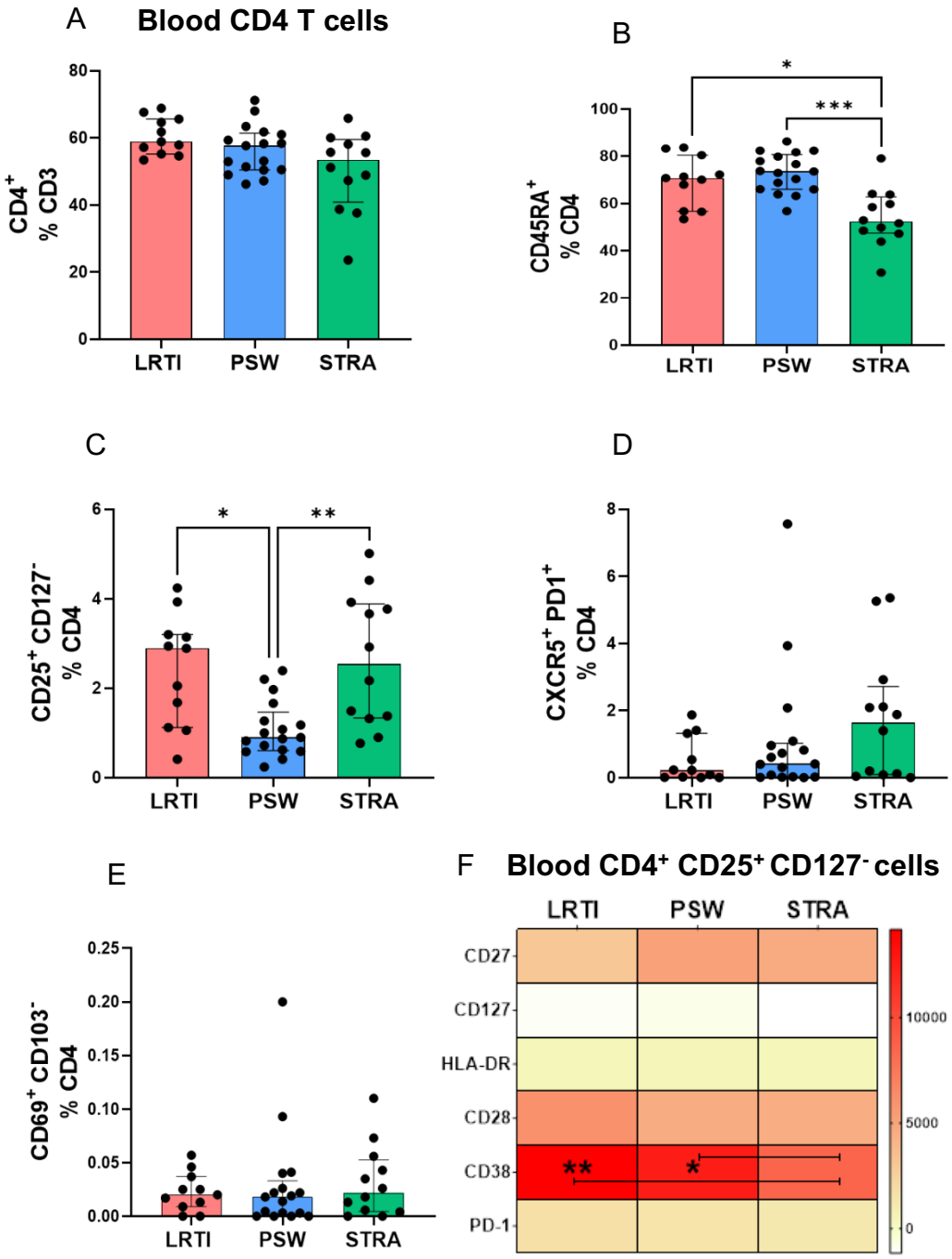


Fig 4.3. Naïve CD4⁺ T cells are reduced in STRA blood compared to PSW and non-asthmatic children

Proportion of blood **A)** CD4⁺ cells as a percentage of CD3⁺ T cells. **B)** CD45RA⁺ cells, **C)** CD25⁺ cells, **D)** CXCR5⁺ PD1⁺ cells and **E)** CD69⁺ cells as a percentage of CD4⁺ T cells. **F)** Heatmap of activation markers gMFIs expressed by CD4+ CD25+ CD127- cells. Statistical significance was measured by Kruskal Wallis test + Dunn's multiple comparison test. Significance value presented * < 0.05, **<0.01, ***< 0.001. ****< 0.0001.

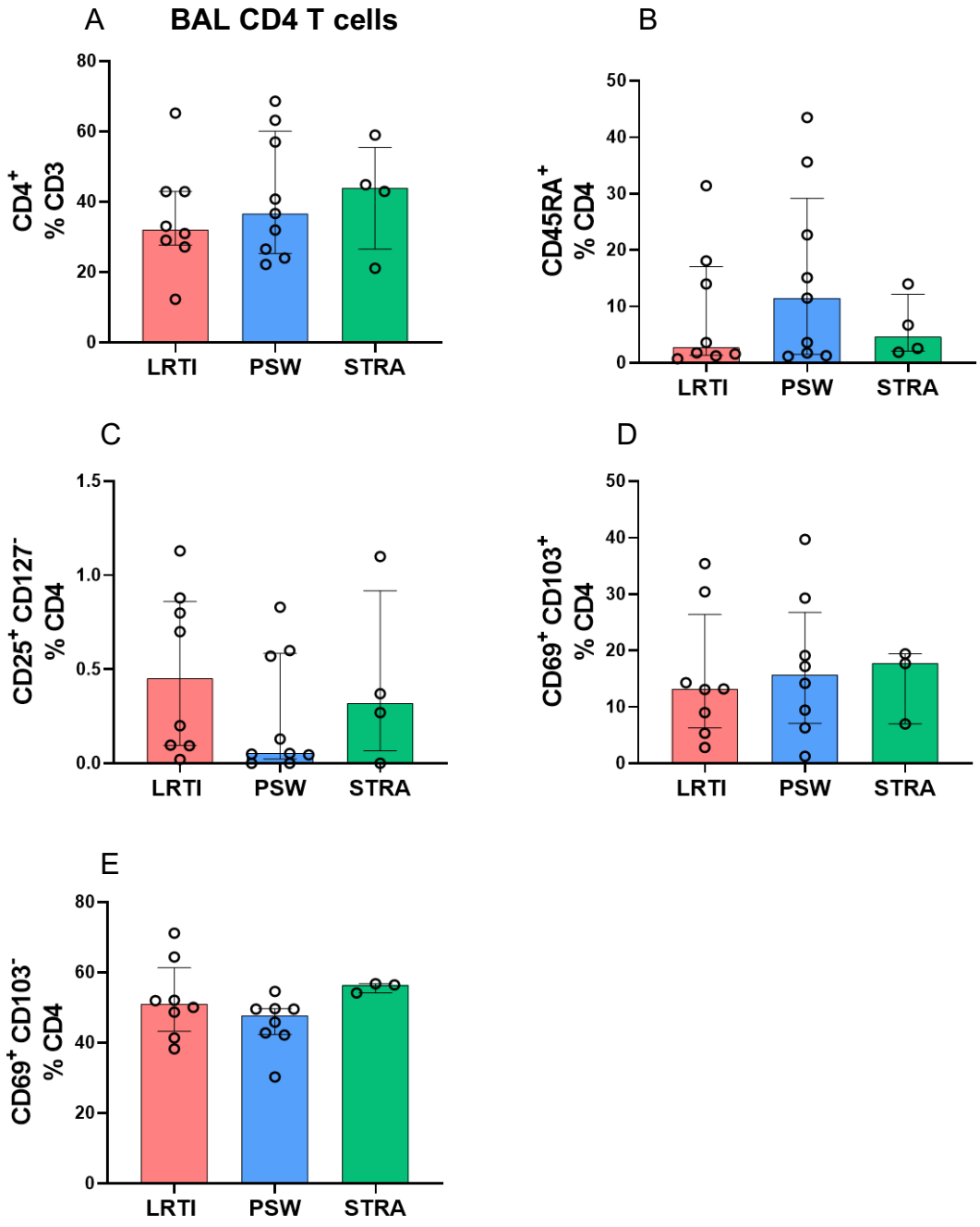


Fig 4.4. Airway CD4⁺ T cell subsets are comparable between PSW and STRA children

Proportion of BAL **A)** $CD4^+$ cells as a percentage of $CD3^+$ T cells. **B)** $CD45RA^+$ cells, **C)** $CD25^+$ cells, **D)** $CXCR5^+$ $PD1^+$ cells and **E)** $CD69^+$ $CD103^+$ and **F)** $CD69^+$ $C103^-$ cells as a percentage of $CD4^+$ T cells. Statistical significance was measured by Kruskal Wallis test + Dunn's multiple comparison test. Significance value presented * < 0.05, **<0.01, ***< 0.001. ****< 0.0001.

Assessment of peripheral $CD8^+$ T cells revealed that total CD8 cells were increased in STRA patients relative to children with LRTIs **(Fig. 4.5A)**. While there was no difference in circulating naïve $CD45RA^+$ **(Fig. 4.5B)**, $CD25^+$ $CD127^-$ **(Fig. 4.5C)** and $CD69^+$ $CD8^+$ T cell subsets **(Fig. 4.5E)**, the $CXCR5^+$ $PD\text{-}1^+$ subset was augmented in STRA children **(Fig. 4.5D)** which may have contributed to the expansion of their total $CD8^+$ T cell frequency.

Although the PSW and LRTI patients had a greater detection of respiratory viruses in BAL **(Table 4.1)**, total and naïve $CD45RA^+$ airway CD8 T cells were similar between the groups **(Fig. 4.6A, B)**. Interestingly the airways of non-wheeze patients with LRTI were enriched with a CD8 subset with a regulatory phenotype[98] expressing CD25 and low or negative CD127, relative to PSW and STRA children **(Fig. 4.6C)**. While there was no significant expression of T cell activation markers CD27, CD127, HLA-DR, PD-1 within this subset, there was an increasing trend in CD38 gMFI observed in LRTI and PSW patients **(Fig. 4.6F)**. Likewise, there was no substantial variance in $CD69^+$ subsets of BAL $CD8^+$ T cells **(Fig. 4.6D, E)**. The proportion and ratio of CD4 an CD8 T cells in the periphery and airways are enumerated in **Table 4.5** and **Table 4.6.**

Collectively, these results suggest that children with PSW and STRA have similar proportions of peripheral and airway $CD8^+$ T cells but have reduced $CD8^+$ regulatory profile in their airways relative to children with recurrent lung infections. Additionally, phenotyping of blood and BAL T cell types, showed that the blood is augmented with naïve $CD4^+$ and $CD8^+$ T cells, whereas the airways are enriched with cells that are CD69 and CD103 positive, representative of a TRM profile.

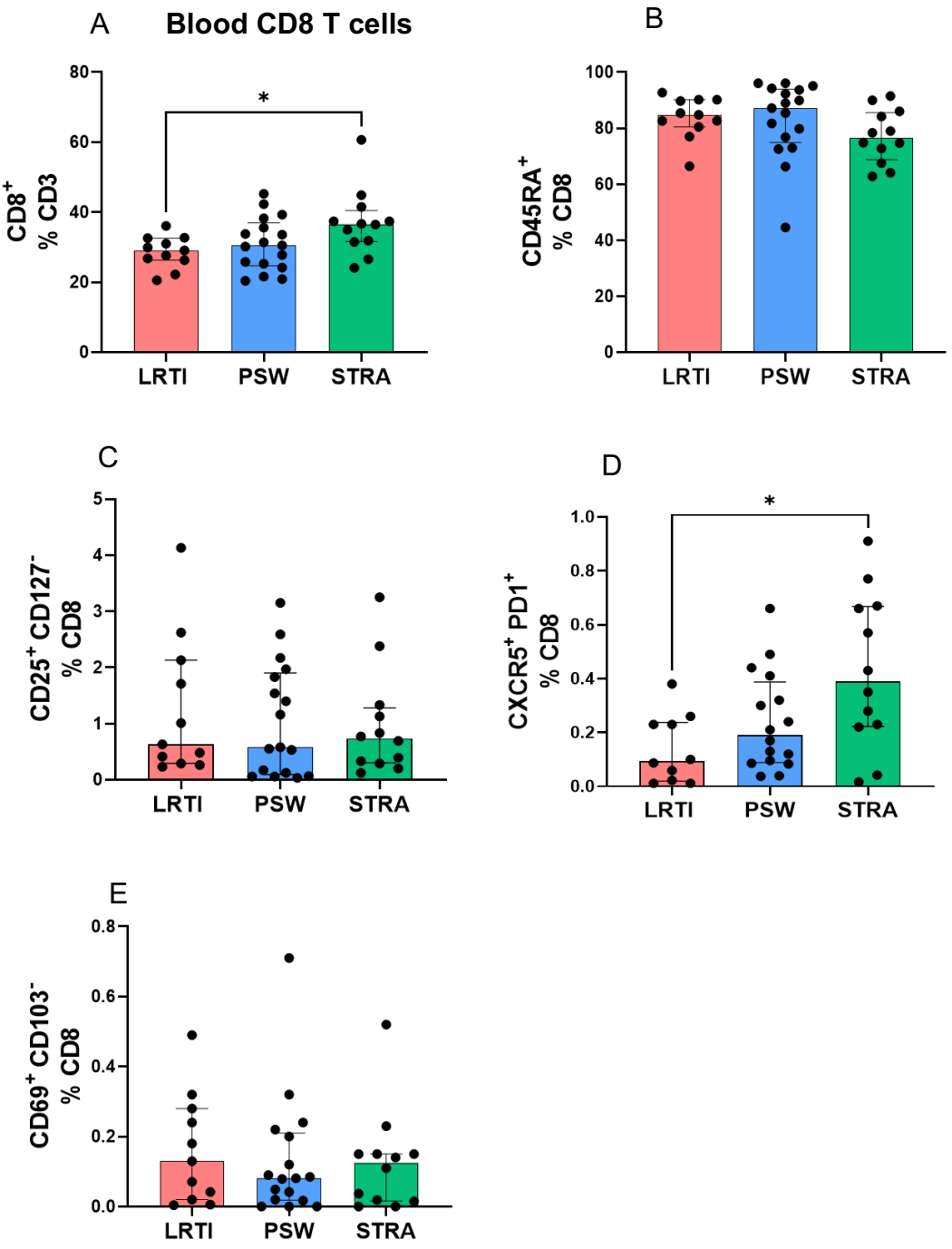


Fig 4.5. Circulating CD8⁺ T cell subsets are comparable between PSW and STRA children

Proportion of blood **A)** CD8⁺ cells as a percentage of CD3⁺ T cells. **B)** CD45RA⁺ cells, **C)** CD25⁺ cells, **D)** CXCR5⁺ PD1⁺ cells and **E)** CD69⁺ cells as a percentage of CD8⁺ T cells. Statistical significance was measured by Kruskal Wallis test + Dunn's multiple comparison test. Significance value presented * < 0.05, **<0.01, ***< 0.001. ****< 0.0001.

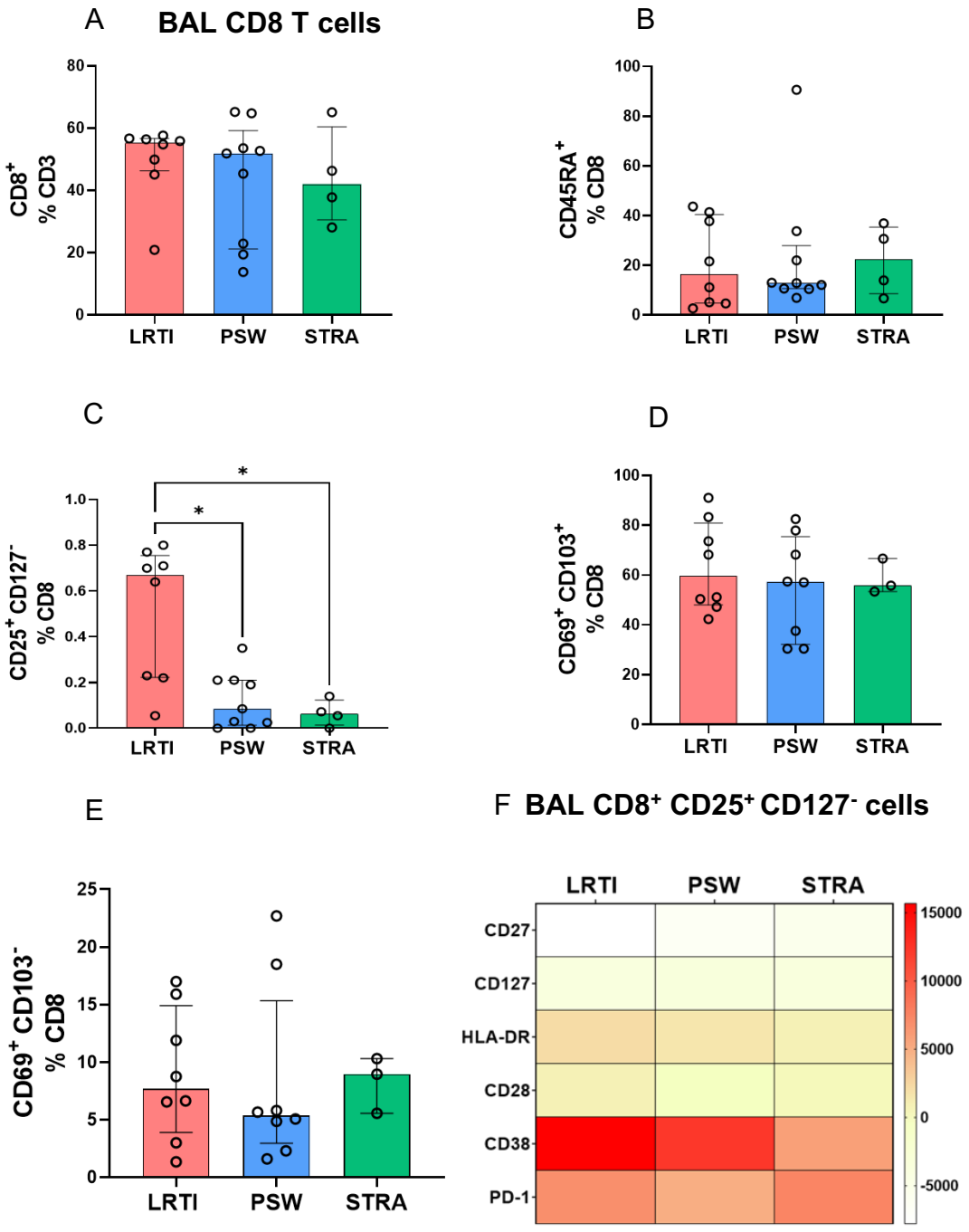


Fig 4.6. Airway $CD8^+$ $CD25^+$ $CD127^-$ cells were significantly reduced in PSW and STRA compared to LRTI patients

Proportion of BAL **A)** $CD8^+$ cells as a percentage of $CD3^+$ T cells. **B)** $CD45RA^+$ cells, **C)** $CD25^+$ cells, **D)** CXCR5$^+$ PD1$^+$ cells and **E)** $CD69^+$ $CD103^+$ and **F)** $CD69^+$ $C103^-$ cells as a percentage of $CD8^+$ T cells. **F)** gMFI of activation and inhibition markers on $CD8^+$ $CD25^+$ $CD127^-$ cells. Statistical significance was measured by Kruskal Wallis test + Dunn's multiple comparison test. Significance value presented * < 0.05, **<0.01, ***< 0.001. ****< 0.0001.

Blood % CD3	LRTI	PSW	STRA
CD4 median (range)	59 (53.4 – 68.8	57.7 (46.2 – 68)	53.35 (23.6 – 65.8)
CD8 median (range)	29.1 (20.6 – 36.2)	30.5 (20.4 – 45.3)	36.65 (24.1 – 60.7)
CD4/CD8	2.03	1.89	1.46

Table 4.5 Blood T cell frequencies from paediatric cohorts
Proportion of circulating CD4 and CD8 T cells as a percentage of $CD3^+$ cells obtained by flow cytometry. Data presented as median with range.

BAL % CD3	LRTI	PSW	STRA
CD4 median (range)	32.05 (12.3 – 65.2)	36.7 (22.2 – 68.6)	43.95 (21.1 – 59)
CD8 median (range)	55.35 (20.9 – 57.6)	51.9 (13.8 – 65.2)	42.05 (28.1 – 65.1)
CD8/CD4	1.73	1.41	0.96

Table 4.6. BAL T cell frequencies from paediatric cohorts
Proportion of airway CD4 and CD8 T cells as a percentage of $CD3^+$ cells obtained by flow cytometry. Data presented as median with range.

4.4.4 Composition of innate lymphocytes in circulation and BAL fluid

NK and NKT cells are innate lymphocytes which share the expression marker CD56[99]. NKT cells can express the full range of lymphocyte-associated cytokines and are implicated in the induction of airway hyperresponsiveness (AHR) in allergic asthma[99]. In contrast, NK cells are naturally cytotoxic and are capable of secreting cytokines[100]. Both cell types have been linked to asthma pathogenesis, and therefore their distribution in wheeze and early-onset asthma was investigated. Using CD3 and CD56 surface protein expression, NKT cells were found to be significantly increased in the blood of STRA children compared to children with PSW and non-asthmatics **(Fig. 4.7A)**. To further explore the difference in peripheral NKT cell phenotypes, the percentage of CD4 and CD8 expression on $CD3^+$ $CD56^+$ cells were examined. The results conveyed that while the peripheral distribution of NKT cells were predominantly $CD8^+$, children with PSW had elevated $CD4^+$ $CD3^+$ $CD56^+$ NKT cells compared to STRA individuals in circulation **(Fig. 4.7B, C)**. In contrast, there was no variance in the corresponding $CD3^+$ $CD56^+$ population in BAL fluid **(Fig. 4.7D)**. Quantification of NK cells using CD56 expression revealed comparable frequencies between disease groups in blood and BAL **(Fig. 4.7E, F)**.

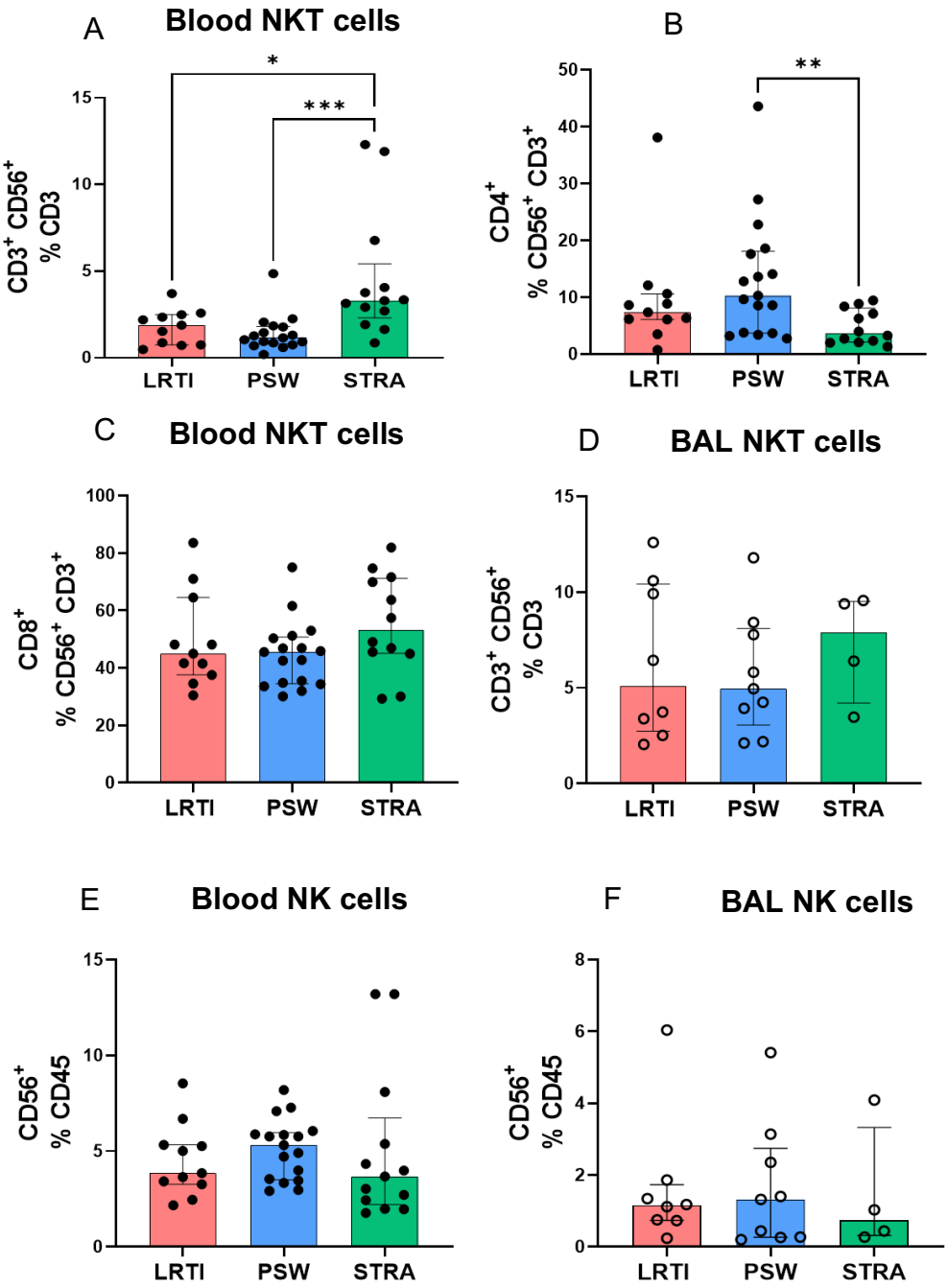


Fig 4.7. Peripheral NKT cells are increased in STRA children relative to PSW and LRTI

Proportion of blood **A)** $CD3^+$ $CD56^+$ cells as a percentage of $CD3^+$ T cells. **B)** $CD4^+$ and **C)** $CD8^+$ cells as a percentage of $CD3^+$ $CD56^+$ NKT cells. **D)** BAL $CD3^+$ $CD56^+$ cells as a percentage of $CD3^+$ T cells. Frequency of **E)** blood $CD56^+$ cells and **F)** BAL $CD56^+$ cells as a percentage of $CD45^+$ immune cells. Statistical significance was measured by Kruskal Wallis test + Dunn's multiple comparison test. Significance value presented * < 0.05, **<0.01, ***< 0.001. ****< 0.0001.

4.4.5 Distribution of B cells and association with IgE

More than two-thirds of asthmatics have an allergic phenotype which is associated with the presence of allergen specific-IgE[101]. B cells express immunoglobulins as a surface protein which are released when they differentiate into antibody-secreting plasma cells[102]. During an allergic reaction, secreted IgE binds to surface receptors on DCs and granulocytes to capture the allergens resulting in cell degranulation and release of pro-inflammatory mediators such T2 cytokines, which propagate the features of allergic airways disease[101,102]. Thus, characterising the distribution of B cell subsets and plasma cells is crucial to better understanding the immunology of allergic respiratory disease.

Total circulating $CD20^+$ B cells were comparable between the groups **(Fig. 4.8A)**, however, IgD^+ $CD27^-$ populations were increased in children with PSW and LRTI relative to STRA **(Fig. 4.8B)**. Typically, B cell populations vary with age with the majority of circulating B cells in children being CD27 negative[103] . Hence, this phenotype could be attributed to the difference in median age between the cohorts, as children with PSW and LRTI were younger than those with STRA **(Table 4.1).**

Conversely, STRA children demonstrated a notable rise in circulating $CD27^+$ IgD^- B cells **(Fig. 4.8C)**. The IgD^+ $CD27^-$ phenotype was associated with naive B cells whereas, the alternative $CD27^+$ IgD^- expression is used to define antigen-experienced memory B cells[104]. In the BAL, $CD20^+$ and IgD^+ $CD27^-$ B cell frequencies were similar between the subject groups **(Fig. 4.8D, E)**. Although $CD27^+$ IgD^- B cells were increased in the airways of STRA children

relative to LRTI, this is largely due to one outlier in a group of 4 patients and therefore not an accurate representation **(Fig. 4.8F)**.

During B cell differentiation, plasma cells are reported to downregulate CD20 protein expression[105], thus to quantify the proportion of plasma cells in the blood, $CD20^-$ $CD38^+$ $CD27^+$ expressing cells were examined and correlated to serum IgE levels. Overall, there was no difference in proportions of circulating $CD20^-$ $CD38^+$ $CD27^+$ cells between the cohorts **(Fig. 4.8G)**. There was no association between serum IgE levels and this subset in STRA and PSW children **(Fig. 4.8H, I)**. Together, these findings illustrate that STRA subjects had fewer circulating IgD^+ $CD27^-$ $CD20^+$ B cells but increased $CD27^+$ IgD^- $CD20^+$ cells which are associated with an effector phenotype, suggestive of an enhanced pro-inflammatory profile.

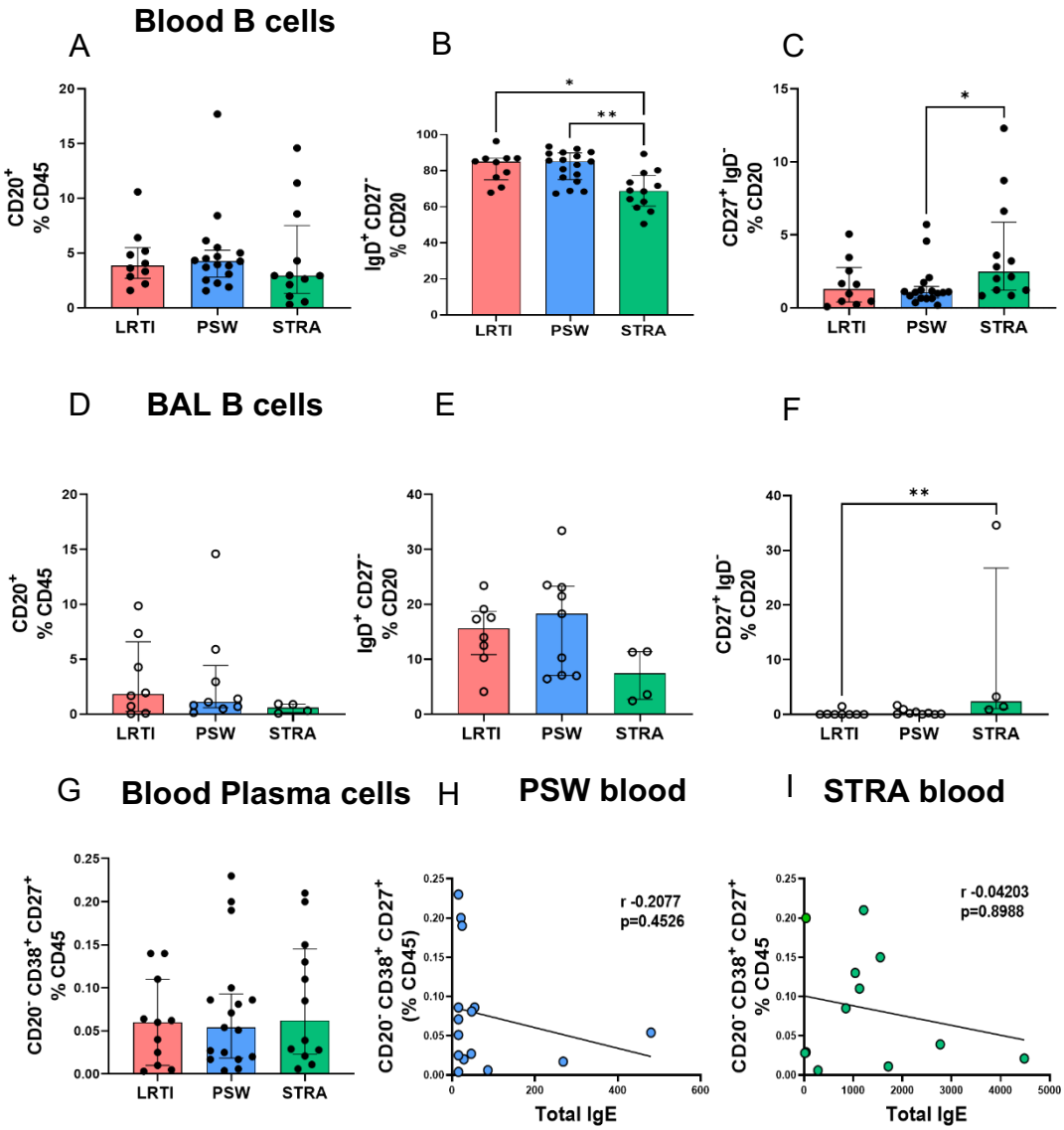


Fig 4.8. Circulating IgD$^+$ B cells are decreased in STRA patients
Proportion of peripheral **A)** CD20$^+$ cells as a percentage of CD45$^+$ immune cells, **B)** IgD$^+$ CD27$^-$ cells and **C)** CD27$^+$ IgD$^-$ cells as a frequency of CD20$^+$ cells. Proportion of BAL **D)** CD20$^+$ cells as a percentage of CD45$^+$ immune cells. **E)** IgD$^+$ CD27$^-$ cells and **F)** CD27$^+$ IgD$^-$ cells as a frequency of CD20$^+$ cells. **G)** Frequency of CD20$^-$ CD38$^+$ CD27$^+$ cells as a percentage of CD45$^+$ immune cells. Correlations between peripheral CD20$^-$ CD38$^+$ CD27$^+$ cells and total serum IgE in **G)** PSWs and **H)** STRAs. Statistical significance was measured by Kruskal Wallis test + Dunn's multiple comparison test. Correlations were conducted using Spearman test. Significance value presented * < 0.05, **<0.01, ***< 0.001. ****< 0.0001.

4.4.6 Quantification of eosinophils and correlation with clinical phenotypes

Since eosinophilia is a characteristic feature of allergic asthma and is associated with elevated IgE levels[101], the composition of circulating and airway eosinophils and their connection with serum IgE was investigated. Siglec-8$^+$ eosinophils were increased in the blood of paediatric STRA compared LRTI controls by flow analysis and differential cytospin counts **(Fig. 4.9A, B)**. In contrast, the proportions of BAL- Siglec-8$^+$ eosinophils were not substantially different between the subject groups. Although flow analysis indicated a pattern towards increasing eosinophils in PSW and STRA BAL samples **(Fig. 4.9C, D)**.

Correlation studies of Siglec-8$^+$ cell frequency and total IgE levels revealed a significant positive relationship between circulating eosinophils and serum IgE in PSW patients but not in LRTI or STRA **(Fig. 4.10A, B, C)**. Although there is a statistically significant association, the correlation graph does not appear to be meaningful, so this data needs to be interpreted with caution.

.

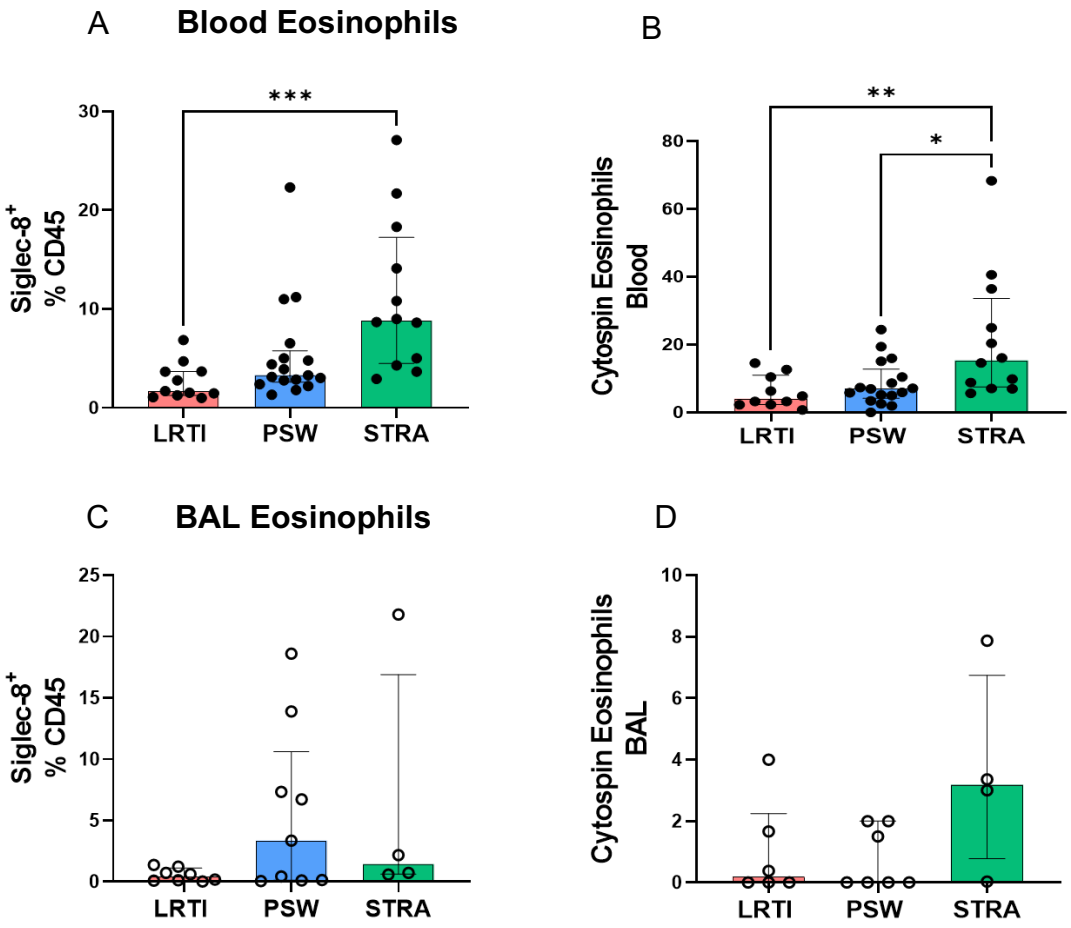


Fig 4.9. STRA children have increased frequency of blood eosinophils compared to LRTI

A) Proportion of circulating Siglec-8$^+$ cells as a percentage of CD45$^+$ immune cells, **B)** Differential cytospin count of blood eosinophils. **C)** Proportion of BAL Siglec-8$^+$ cells as a percentage of CD45$^+$ immune cells. **D)** Differential cytospin count of airway eosinophils. Statistical significance was measured by an unpaired, non-parametric Mann-Whitney test. Significance value presented * < 0.05, **<0.01, ***< 0.001. ****< 0.0001.

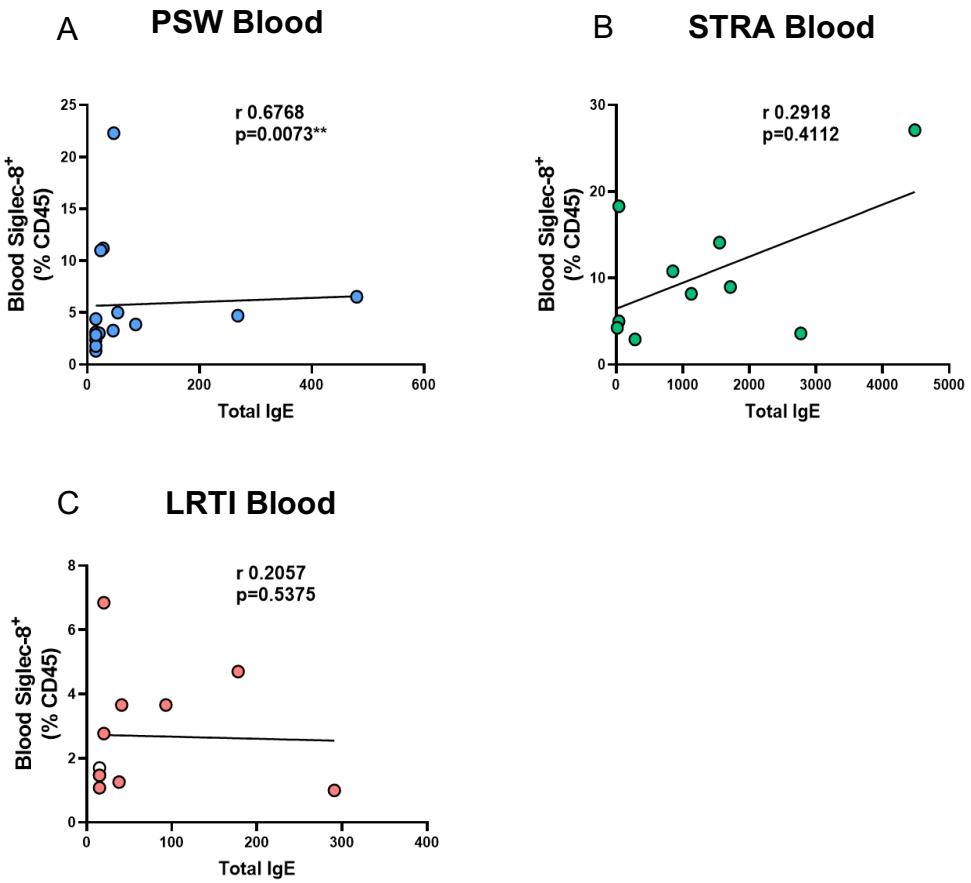


Fig 4.10. PSW patients exhibited a positive correlation between circulating eosinophils and serum IgE quantity

Correlation between circulating eosinophils and serum IgE levels in **A)** PSW, **B)** STRA and **C)** LRTI children. Statistical significance was measured by Kruskal Wallis test + Dunn's multiple comparison test. Correlations were conducted using Spearman test. Significance value presented * < 0.05, **<0.01, ***< 0.001. ****< 0.0001.

Atopy is considered a susceptibility factor for the development of asthma and is defined by an exaggerated secretion of IgE due to environmental allergens[101]. Consequently, the relationship between peripheral eosinophils, IgE levels and atopy were assessed in early-life wheeze and school-aged asthma. The serum IgE measurements and Siglec-8$^+$ cell frequencies of PSW and STRA patients were separated by clinical atopic status defined from reported allergies to outdoor and indoor allergens such as nuts, eggs, and house dust mite. The results demonstrated there was no significant distinction between atopic disposition and total IgE or eosinophils in the blood. Of note however, atopic individuals suggested an increasing frequency in Siglec-8$^+$ cells in PSWs and serum IgE level in STRA children **(Fig. 4.11A, B, C, D)**.

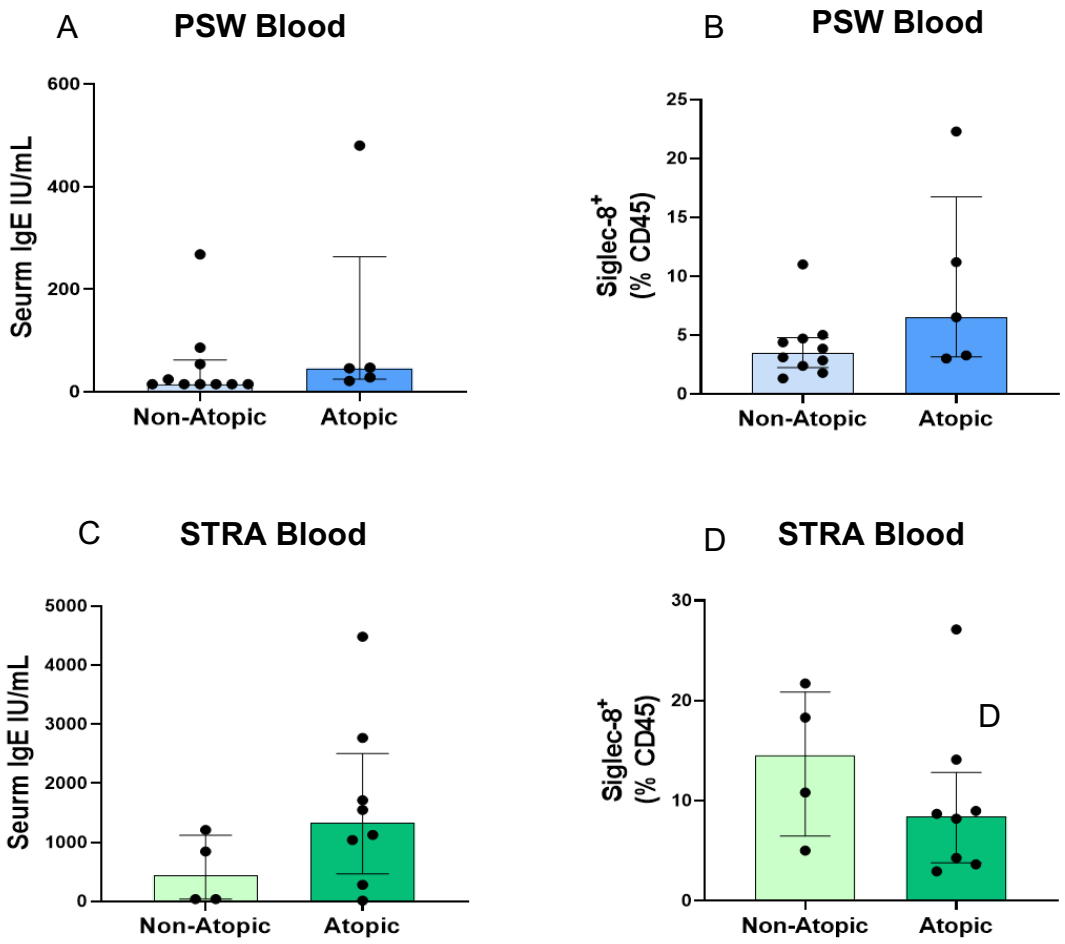


Fig 4.11. There is no difference in peripheral eosinophils or serum IgE levels in PSW or STRA subjects grouped by atopic disposition
PSW profile of **A)** Serum IgE levels and **D)** peripheral Siglec-8$^+$ cells grouped by atopic status. STRA profile of **E)** Serum IgE levels and **F)** circulating Siglec-8$^+$ cells grouped by atopic status. Statistical significance was measured by Kruskal Wallis test + Dunn's multiple comparison test. Correlations were conducted using Spearman test. Significance value presented * < 0.05, **<0.01, ***< 0.001. ****< 0.0001.

4.4.7 Frequency of neutrophils and association with infections

Based on the limited understanding of neutrophilic asthma, neutrophilia in children is not considered to be associated with disease severity but linked with airway microbiology and infection clearance[16,29]. Thus, the proportion of neutrophils in the lungs and periphery were determined by spectral cytometry and differential cytospin counts and correlated with the presence of airway infections. By flow analysis, $CD15^+$ blood neutrophils were not significantly different, but LRTI children had an increasing trend compared to PSW and STRA cohorts **(Fig. 4.12A)**. This was verified by differential cell counts which showed that both PSW and STRA children have reduced circulating neutrophils relative to LRTI **(Fig. 4.12B)**. There was no difference in BAL neutrophils between the study groups by flow or cytospin analysis **(Fig. 4.12C, D)**.

Correlations between the number of bacterial and viral infections and the frequency of neutrophils in each disease group across both tissues did not uncover any notable associations. However, when tested as a combined cohort, there was a significant correlation between BAL $CD15^+$ cells and number of viral infections and total number of viral and bacterial infections **(Fig. 4.12E, F, G)**. This may have been influenced by three PSW patients with elevated neutrophils and 2 to 4 viral infections (blue dots) and two LRTI children with 20% BAL neutrophils and 1-2 viral infections (red dots). When examined separately, PSWs with viral infections had a nonsignificant positive correlation with proportion of airway $CD15^+$ cells (virus $r = 0.5006$) (virus + bacteria $r = 0.6342$).

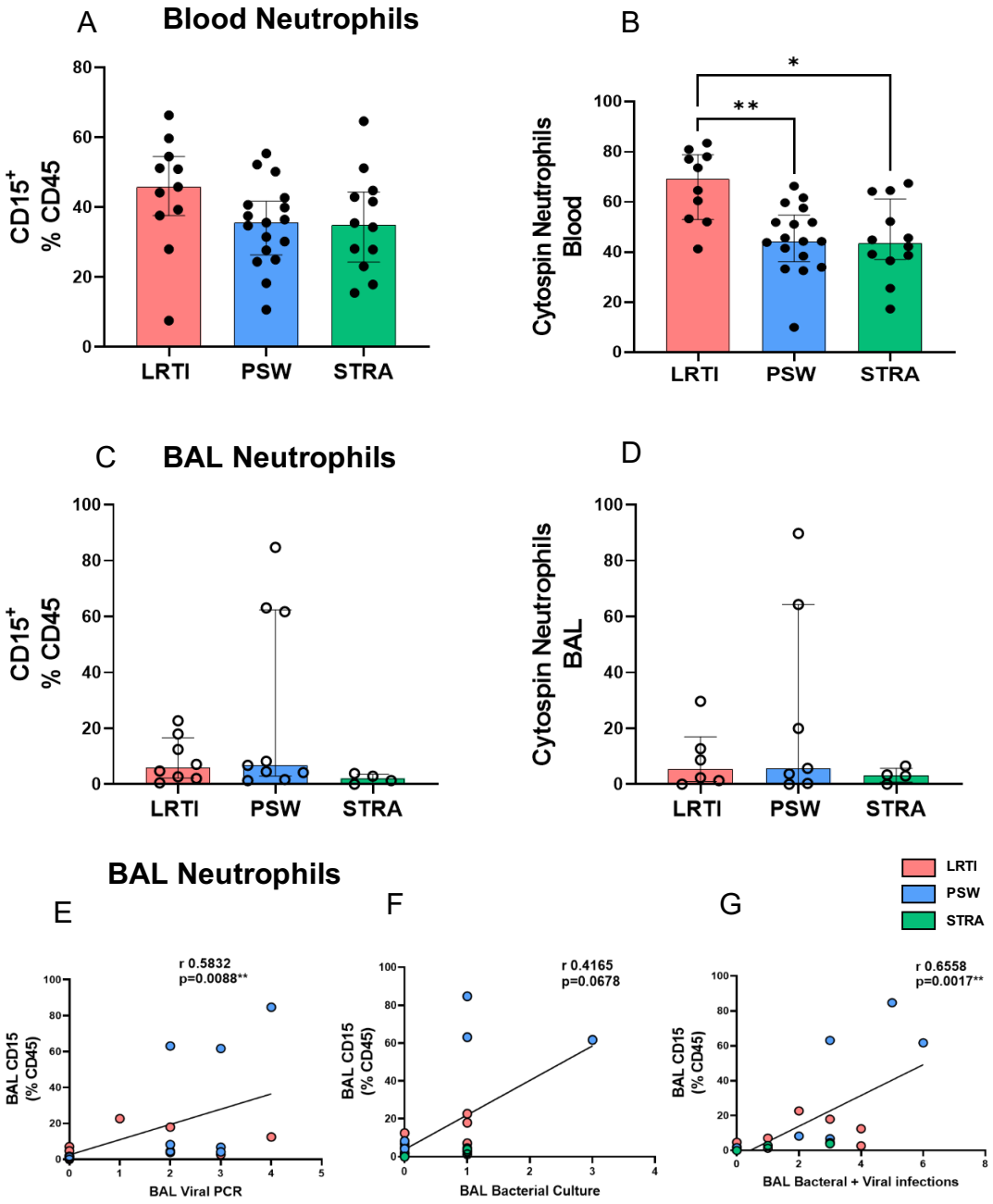


Fig 4.12. Peripheral neutrophils are lower in PSW and STRA children relative to LRTI

A) Proportion of circulating CD15⁺ cells as a percentage of CD45⁺ immune cells, **B)** Differential cytospin count of blood neutrophils. **C)** Proportion of BAL CD15⁺ cells as a percentage of CD45⁺ immune cells. **D)** Differential cytospin count of airway neutrophils. Correlation between BAL CD15⁺ cells and number of airway **E)** viral, **F)** bacterial culture or **G)** viral and bacterial infections in disease cohorts. Statistical significance was measured by Kruskal Wallis test + Dunn's multiple comparison test. Correlations were conducted using Spearman test. Significance value presented * < 0.05, **<0.01, ***< 0.001. ****< 0.0001.

4.4.8 Macrophage phenotypes and expression of co-stimulatory molecules

Airway macrophages are the predominant cell type in the lungs during homeostasis and provide host defence during lung injury and infection. It has been reported that inflammatory classical monocytes (CM) migrate from the blood into the lungs following tissue damage and thereupon differentiate into macrophage subsets[106]. The other major monocytes in the circulation comprise $CD14^+$ $CD16^+$ intermediate monocytes (IMs) which assist in antigen presentation and $CD16^+$ $CD14^-$ nonclassical monocytes (NCMs) which facilitate phagocytosis and anti-viral responses[107]. Numerous studies researching macrophage differentiation in the gastrointestinal tract have elucidated that peripheral $CD14^+$ CMs transition through IMs and $CD14^-$ state into macrophages, a process defined as the monocyte waterfall[106,108,109]. In allergic asthma, the dominant Type 2 cytokines promote a macrophage phenotype which exhibit anti-inflammatory and tissue repair mechanisms[110,111]. Thus, it is important to define macrophage and monocyte phenotypes and determine their association with infection. Analysis of $CD206^+$ macrophages in the BAL showed similar proportions between the different disease groups **(Fig. 4.13A)**. Gating the airway macrophages by CD11c and $CD14^{+/-}$ expression displayed an equal distribution between the subsets across the study cohorts **(Fig. 4.13B, C, D)**. PSW patients had a trend towards increasing $CD11c^+$ $CD14^-$ population which is indicative of large macrophages with less inflammatory capacity[111]. To examine the inflammatory phenotype of the two $CD206^+$ macrophage populations, $CD11c^+$ $CD14^{+/-}$ subsets were gated by scatter plot and the gMFIs of their activation markers

were quantified **(Fig. 4.13 E, F)**. Overall, the combined data showed no significant difference in the costimulatory signal expressed by the airway macrophage subsets of STRA, PSW and control patients.

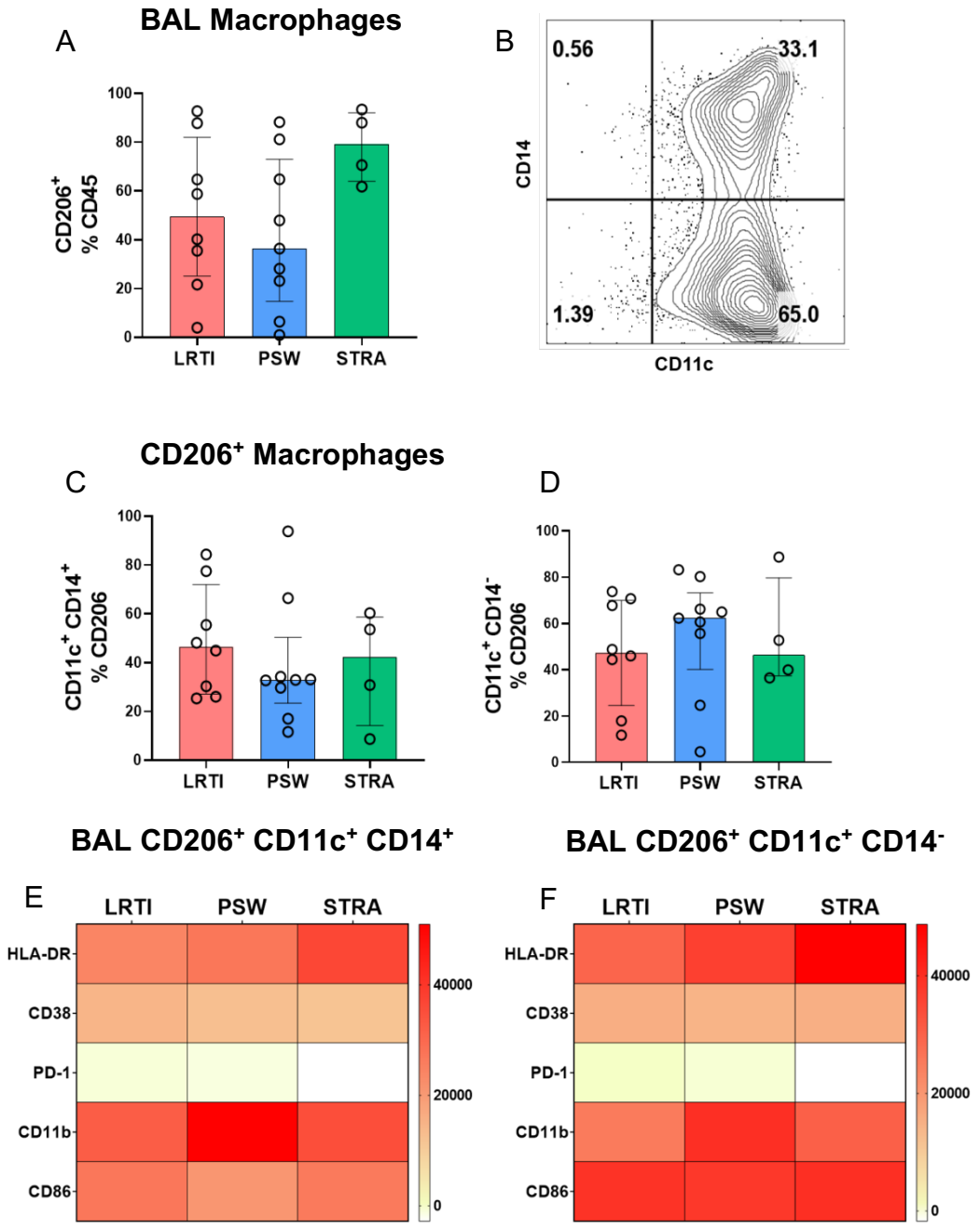


Fig 4.13. Airway macrophage frequencies are similar between children with PSW and STRA

Proportion of BAL **A)** $CD206^+$ cells as a percentage of $CD45^+$ immune cells. **B)** Scatter plot of CD11c and CD14 expression on $CD206^+$ macrophages, **C)** $CD11c^+$ $CD14^+$ cells and **D)** $CD11c^+$ $CD14^-$ cells as a percentage of $CD206^+$ cells. Heatmap of activation markers gMFI expressed by **E)** $CD11c^+$ $CD14^+$ and **F)** $CD11c^+$ $CD14^+$ $CD206^+$ macrophage subset. Statistical significance was measured by Kruskal Wallis test + Dunn's multiple comparison test. Significance value presented * < 0.05, **<0.01, ***< 0.001. ****< 0.0001.

4.4.9 Monocyte subsets and association with bacterial and viral infections

Looking at monocyte composition in the periphery, illustrated significant variation in $CD14^+$ CMs but no changes in IMs and NCMs between the patient groups. CMs were augmented in the blood of LRTI children compared to children with PSW, suggestive of their recurrent infections **(Fig. 4.14A, B, C)**. There were no differences in lung monocyte subsets **(Fig. 4.14D, E, F)**. The number of bacterial and viral infections in each disease group were tallied and correlated to the frequency of airway and peripheral $CD14^+$ monocytes. There was a notable positive association between blood $CD14^+$ $CD16^-$ cells and the number of bacterial infections in children with PSW **(Fig. 4.14G)**. This implied that as the number of airway infections increased, the proportion of inflammatory classical monocytes increased also to enhance the immune reaction.

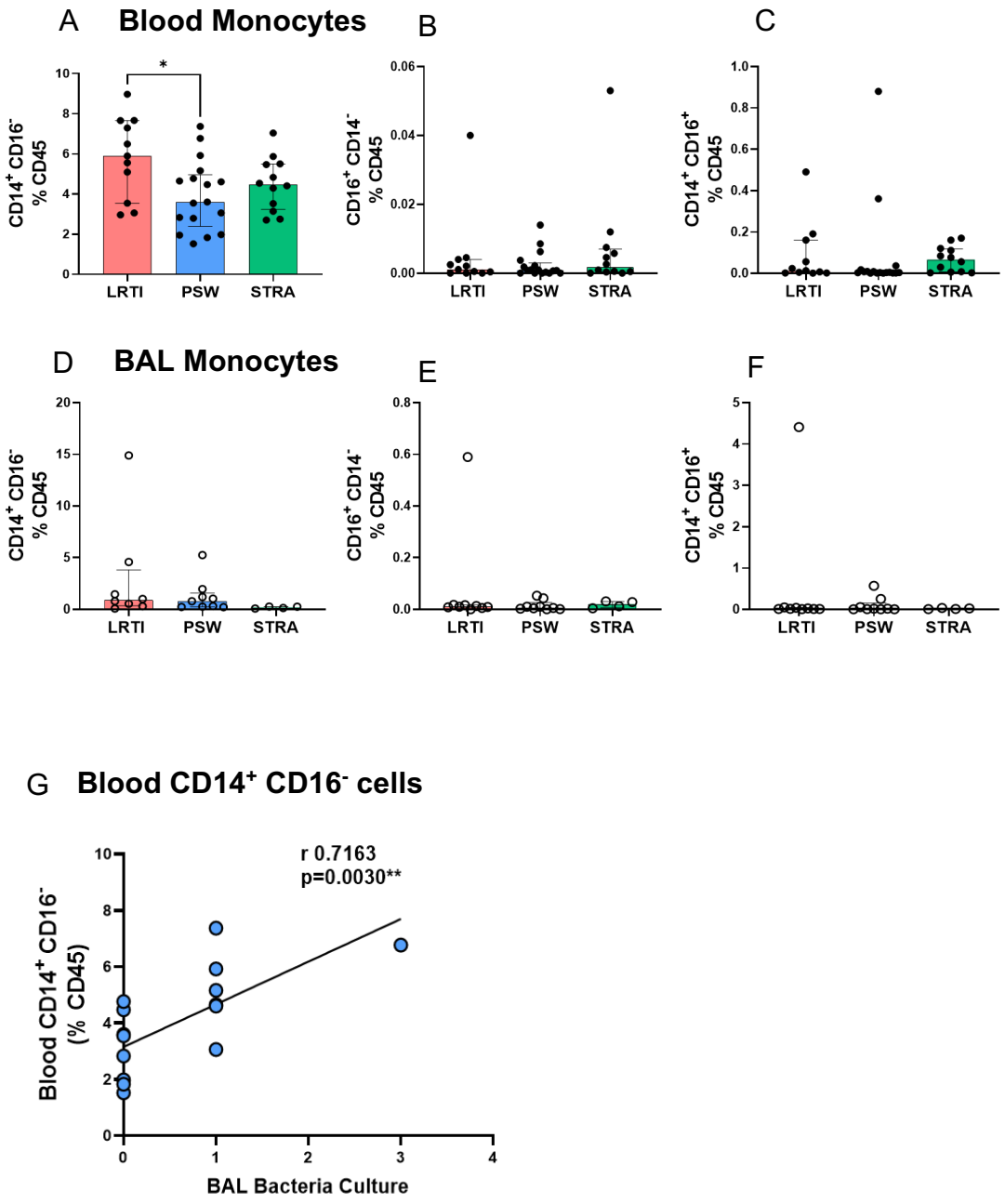


Fig 4.14. Classical monocytes are reduced in PSW blood compared to controls

Proportion of peripheral **A)** $CD14^+$ $CD16^-$ cells **B)** $CD16^+$ $CD14^-$ cells and **C)** $CD14^+$ $CD16^+$ cells as a percentage of $CD45^+$ immune cells. Frequency of airway **D)** $CD14^+$ $CD16^-$ cells **E)** $CD16^+$ $CD14^-$ cells and **F)** $CD14^+$ $CD16^+$ cells as a percentage of $CD45^+$ immune cells. **G)** Correlation between $CD14^+$ $CD16^-$ cells and number of airway bacterial infections in PSWs. Statistical significance was measured by Kruskal Wallis test + Dunn's multiple comparison test. Correlations were conducted using Spearman test. Significance value presented * < 0.05, **<0.01, ***< 0.001. ****< 0.0001.

4.4.10 Distribution of DC subsets and expression of co-stimulatory signals

It is acknowledged that DCs contribute to the induction of T2-dircted allergic asthma by migrating to the mesenchymal lymph nodes (MLN) to present antigens and therefore potentiate variable immune responses[25]. Studies have reported that the frequency of conventional DC1s and DC2s are altered in the peripheral blood and BAL of asthmatic patients and their expression of co-stimulatory molecules change in different tissue[112,113]. Thus, DCs were assessed using the Aurora panel markers CD1c, CD141 and CD123. Expression of CD86 and PD-1 were inspected using gMFI to determine inhibitory and stimulatory phenotypes of the DC subsets.

The proportion of DC subsets in STRA and PSW subjects' blood and BAL were assessed. The data showed a skew towards DC1 dominance in the blood and an abundance of DC2s in the BAL **(Fig. 4.15A, B)**. Further investigation of stimulatory and inhibitory molecules on airway $CD141^+$ DC1s revealed that there was no differential expression of CD86 and PD-1 gMFI **(Fig. 4.15C, D)**. While $CD1c^+$ DC2s showed no difference in CD86 expression **(Fig. 4.15E)**, STRA children had a substantial decrease in PD-1 gMFI **(Fig. 4.15F)**. There was no distinction in the gMFI of CD86 and PD-1 on peripheral DC subsets between the cohorts. In summary this data suggests that the airway DC composition is biased towards a DC2 phenotype and the $CD1c^+$ population in severe asthmatics exhibit less PD-1 molecule to promote further T2 T cell differentiation.

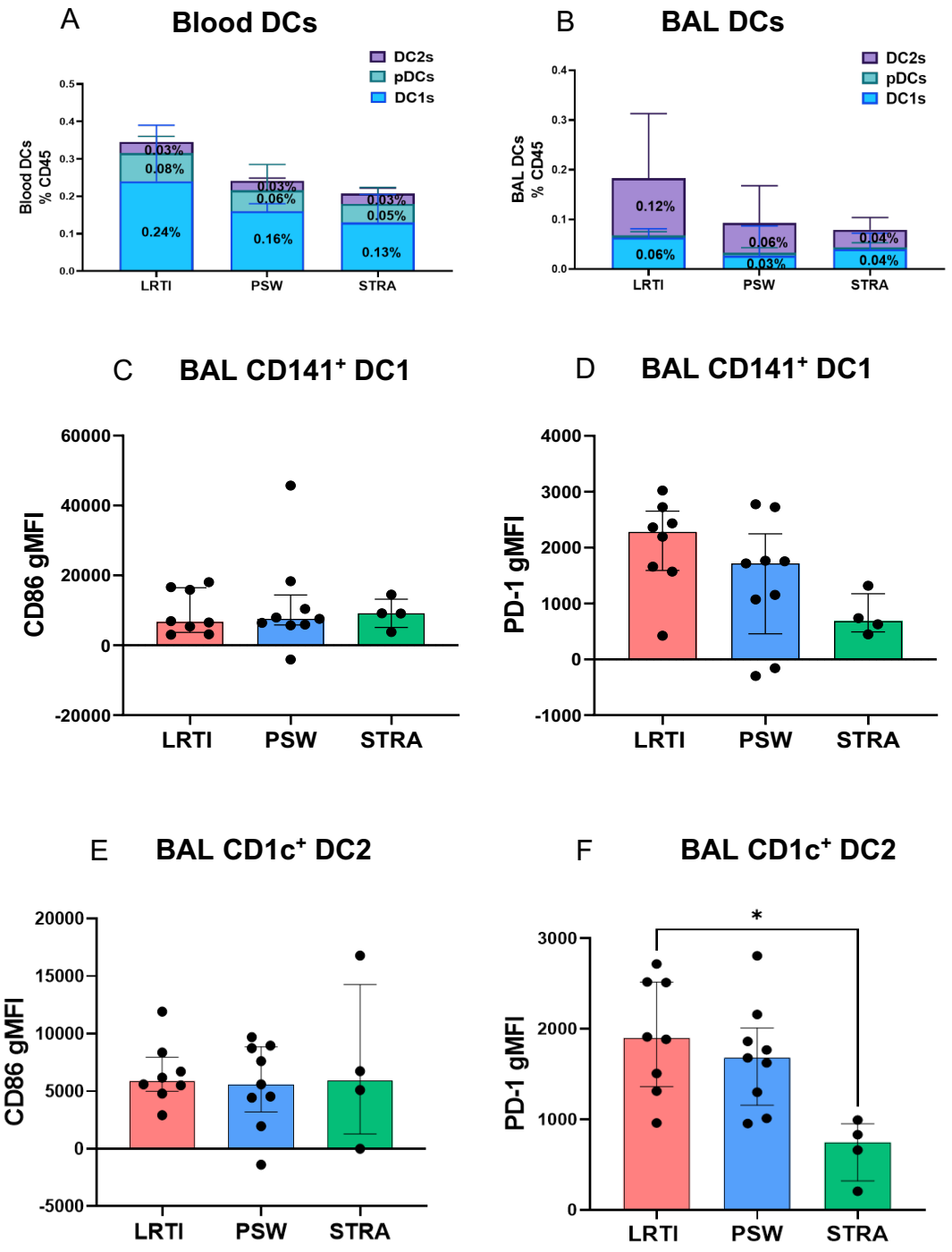


Fig 4.15. Airway CD1c$^+$ dendritic cells displayed decreased PD-1 expression in STRA children

Proportion of CD45$^+$ DC subsets in **A)** Blood and **B)**. gMFI of **C)** CD86 and **D)** PD-1 markers expressed by BAL CD141$^+$ cells. gMFI of **E)** CD86 and **F)** PD-1 markers expressed by BAL CD1c$^+$ cells**.** Statistical significance was measured by Kruskal Wallis test + Dunn's multiple comparison test. Significance value presented * < 0.05, **<0.01, ***< 0.001. ****< 0.0001.

4.4.11 Characterisation of rare lineage negative cells expressing CRTH2 and CD127

ILCs in cooperation with Th2 cells are a major source of T2 cytokine production in allergic asthma[114]. While ILC research has accelerated in recent years, the quantification of these rare cells is challenging, particularly in children. To overcome the limited cell recovery and restricted airway access, the aurora panel was implemented to enumerate key immune cells and exclusive lineage negative $CRTH2^+$ $CD127^+$ cells. To ensure accurate characterization, the lymphoid population was selected, and a list of lineage markers were sequentially removed by flow analysis **(Fig. 4.16)**. To compare to existing literature, lineage negative cells were analysed as a proportion of $CD45^+$ lymphoid cells **(Fig. 4.17A, B)** and the subsequent Lin^- $CRTH2^+$ $CD127^+$ cells were gated as a percentage of $CD45^+$ cells. Overall, the proportion of Lin^- $CRTH2^+$ $CD127^+$ ILCs were comparable between asthmatic and non-asthmatic children in the periphery **(Fig. 4.17C)**. Likewise, there was no distinctive expression observed in the airway between the disease groups **(Fig. 4.17D)**.

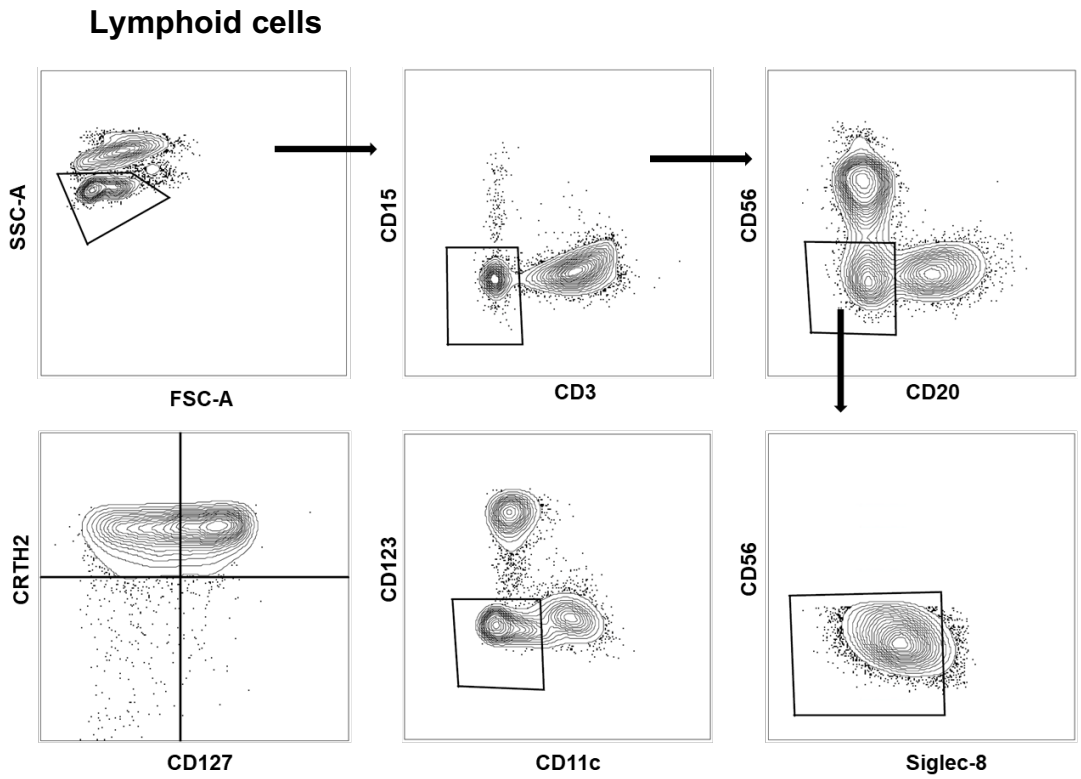


Fig 4.16. Gating strategy for Lineage negative ILCs using the Aurora panel Schematic of flow cytometry scatter plots showing ILC gating strategy. Singlets, live and $CD45^+$ cells were pre-set using the extended gating strategy above in **Fig 4.2.**

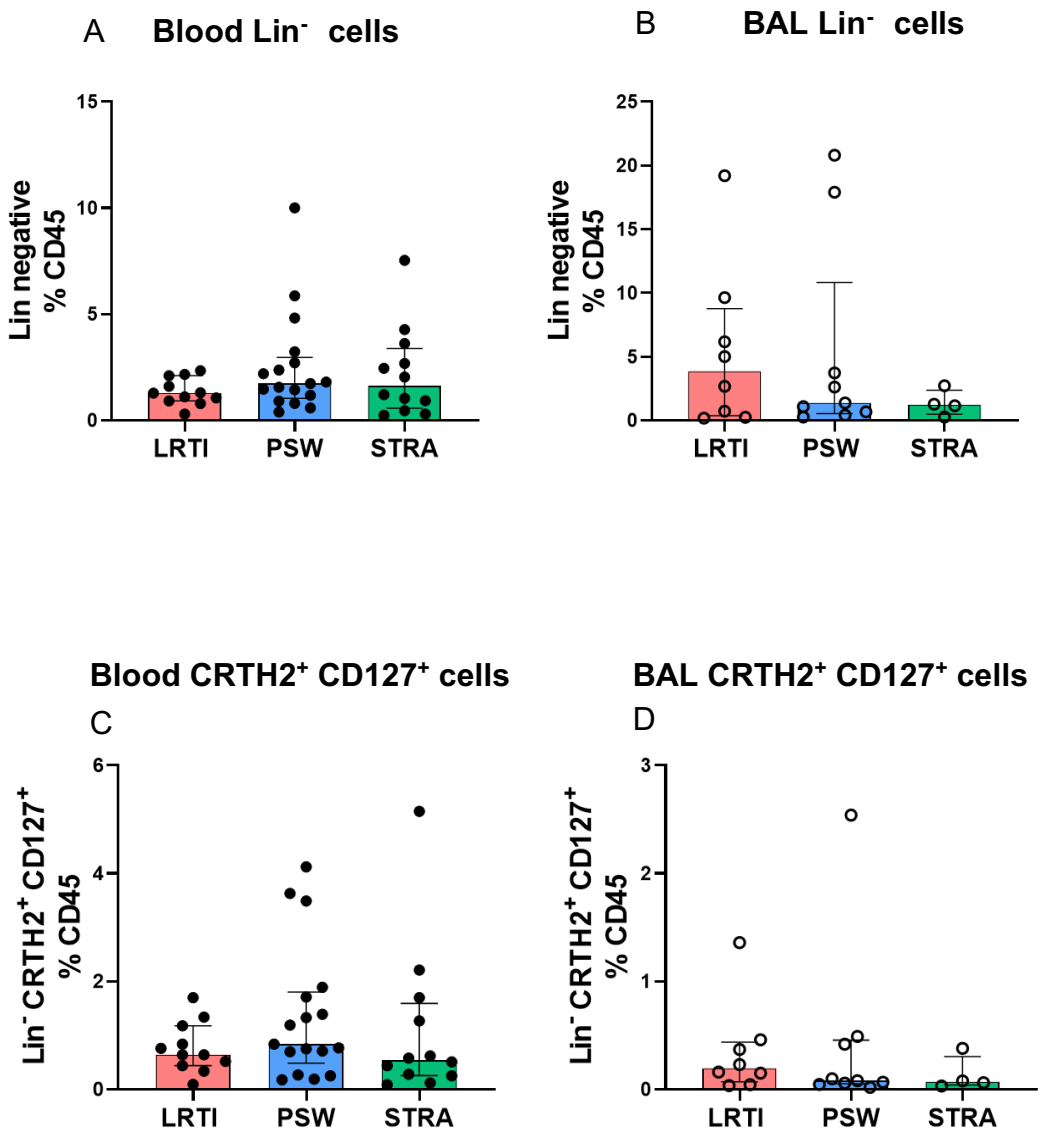


Fig 4.17. Circulating and airway CRTH2$^+$ CD127$^+$ ILC subsets are comparable between disease groups

Proportion of **A)** blood and **B)** BAL lymphoid cells that are negative for CD15, CD3, CD56, CD20 and Siglec-8 markers. Frequency of **C)** blood and **D)** BAL Lin$^-$ CRTH2$^+$ CD127$^+$ cells as a percentage of CD45$^+$ immune cells. Statistical significance was measured by Kruskal Wallis test + Dunn's multiple comparison test. Significance value presented * < 0.05, **<0.01, ***< 0.001. ****< 0.0001.

4.5 Discussion

The aim of this chapter was to characterise the cellular phenotype of peripheral and airway immune cells in preschool aged children with wheeze and school-aged children with severe asthma and uncover distinctive immuno-phenotypes. Therefore, blood and BAL samples were collected and analysed using a spectral cytometer integrated with a 34-colour panel. In chapter 3, the optimization of the flow panel and post-acquisition modifications were addressed. This chapter builds upon an established protocol to accurately phenotype the differential and activation status of lymphocyte, monocyte and granulocyte subsets within disease cohorts.

The use of nonatopic children with LRTIs exhibiting lower airway inflammation as a substitute for healthy control subjects is an important limitation acknowledged in this study. For ethical reasons, bronchoscopy can only be performed in patients undergoing elective procedures. This approach has been adopted by many previous paediatric studies[36,37].

To this end, each immune cell type was gated using the relevant surface markers and analysed as a proportion of a specific population of interest. It is worth noting however that a major limitation of this study is the low number of STRA BAL samples collected. Although these patients only progress to invasive procedures if they maintain poor asthma control despite maximal therapy[36], they can only undergo bronchoscopy during stable disease[115]. Due to this low number, some of the observed results such as the increased $CD27^+$ B cells in STRA airways is inconclusive due to one patient with an elevated frequency in a group of four.

Likewise, the proportion of the airway eosinophils (median 1.45%) and CRTH2^{+} CD127^{+} ILCs (0.071%) in this STRA cohort were inconsistent with published reports. Saglani and Lloyd lab have previously determined that STRA children exhibit increased airway eosinophilia (median 2.7%) compared to controls[8]. However, their study was based on 50 BAL samples obtained from a diverse demographic of 53 subjects of which 33 were young boys[8]. Furthermore, there is a gender bias in asthma susceptibility in early life, whereby young boys are more likely to develop asthma than girls, and there is a switch after puberty towards a female prevalence[116]. Taking this into consideration, this study is restricted to 6 boys and 6 girls with STRA, which is not an accurate representation of childhood asthma demographics and may limit the analysis and contribute to the discrepancy in ILCs.

Eosinophilic inflammation is considered a pathological hallmark of asthma in adults and children[117]. Thus, it is essential to quantify eosinophils in PSW for early detection of asthma progression. Existing literature has described that PSWs blood and BAL fluid eosinophil counts range between a median of 3.4 – 5.0% and 0.6 – 0.9% respectively. These medians vary with the type of trigger underlying the wheezing such as episodic viral or multiple trigger – induced wheezing[16]. As anticipated, PSWs did not present a notable rise in airway and circulating eosinophils, although they exhibited a positive association between blood eosinophils and serum IgE levels. This profile suggested that IgE production is associated with the recruitment of eosinophils or vice versa in PSW patients.

Indeed, Siglec-8^{+} eosinophils were raised in the peripheral blood of STRA children relative to LRTI, indicating disease exacerbations[101]. There was no

relationship between atopic status and serum IgE or Siglec-8^{+} eosinophils in the periphery. Published data have reported median blood eosinophils of 7.5% in children with STRA[33]. This proportion is relatively close to this study's median peripheral eosinophils of 8.83% in children with STRA. Moreover, previous studies indicate that the frequency of circulating eosinophils are associated with allergen sensitization[15,118]. As the STRA cohort in this study had more individuals with atopy, it was speculated that this may influence peripheral eosinophil frequency. However, there was a nonsignificant increase in atopic STRA patients' blood eosinophils (median 8.44%) compared to atopic PSWs (median 6.53%). This is likely because STRA children are sensitised to more allergens and are more severely sensitised, as their sensitisation status increases with age and allergen exposure. These outcomes highlight the heterogenous nature of paediatric asthma and underlines the need for extensive phenotyping and specialised technology to determine an effective personalised therapy.

The STRA children in this study did not exhibit considerable airway inflammation as total airway leukocytes showed a decreasing trend. A plausible explanation for this observation could be that the high doses of ICS they receive (1000mcg median) suppressed airway inflammation by inhibiting the vascular migration of leukocytes[119]. Alternatively, studies have shown that the systemic bioavailability of ICS are lower in subjects with asthma compared to healthy controls. As these drugs function locally in the lung, a reduced amount reaches the lung periphery[120]. However, a limited number of STRA BAL samples restricts the capacity to envision this.

ILC frequencies in this study were not consistent with published literature. Saglani and Lloyd lab have demonstrated that Lin^- $CRTH2^+$ $CD127^+$ ILCs are increased in BAL compared to blood in STRA children with median frequencies of 0.2% and 0.05% respectively and compared to BAL LRTI controls[36]. In contrast, this study showed that Lin^- $CRTH2^+$ $CD127^+$ ILCs were more prevalent in circulation (median 0.545%) than in the airways (median 0.07%) of children with STRA. A potential explanation for this outcome could be that most human ILC studies are conducted using peripheral blood mononuclear cells (PBMCs) isolation which eliminate granulocytes. Given that the aim of this study was to phenotype most major immune cells, whole blood was utilized which may alter the proportion of ILCs obtained. The influence of including all cell types in ILC analysis is not well known and could be further investigated by comparing the number obtained by the different processing methods. Alternatively, this flow panel lacks transcription factors to accurately characterise ILC subsets which may hinder the results. This element is covered in the final discussion chapter 6.

Compared to adult studies, healthy controls with a mean age of 48 have demonstrated 0.02% ILC2s in PBMCs[121], whereas healthy controls with a mean age of 27 exhibited a mean of 1% ILC2s in PBMCs with some subjects having more pronounced composition 2 – 4%[122]. This implied that ILCs may vary with age, as they are more abundant in young adults but decrease in older adults.

Although there was no difference observed in Lin^- $CRTH2^+$ $CD127^+$ ILCs between the disease cohorts in both blood and BAL, a subset of children with PSW had a rising trend in blood and BAL Lin^- $CRTH2^+$ $CD127^+$ cells suggesting

the involvement of ILC2s in early-life wheezing that could potentially progress to asthma. ILC2s have been reported to be detectable in the peripheral blood of PSWs, with a mean frequency of 0.056% of PBMCs and decline after recovery from exacerbations[123].

The finding that circulating $CD45RA^+$ $CD4^+$ T cells were increased in PSW and LRTI children relative to STRA suggested that naïve T cells decrease with age. In children, T cell homeostasis is influenced by growth and increasing blood volume. Furthermore after the first year of life, thymus production reaches a maximum and declines and stabilises[96]. Published data showed that $CD45RA^+$ $CD4^+$ T cell decreased from birth to 6 months by 9.4% and from 6 to 12 months by 5.7%[124]. $CD45RA^+$ T cells have been reported to decrease from an average of 53% in 20-40-year olds to an average of 45% in over 40-year olds. Longitudinal analysis of this cohort confirmed that 0.3% $CD45RA^+$ $CD4^+$ T cell were lost each year[125]. Given that our STRA cohort is much older than the wheezers and disease control group it is probable that age is a contributing factor for the observed decline in peripheral $CD45RA^+$ $CD4^+$ T cells.

Children with PSW exhibited a $CD4^+$ $CD25^+$ $CD127^-$ T cell phenotype representative of an acute phase. Circulating $CD4^+$ $CD25^+$ $CD127^-$ cells were augmented in STRA and LRTI children compared to PSW. This cellular phenotype is attributed to Tregs which perform immunosuppressive activities that inhibit effector functions. Furthermore, the $CD4^+$ $CD25^+$ $CD127^-$ T cell subset express the highest level of Foxp3 with a frequency of 84.92 ± 4.14% in adult blood[97]. In autoimmune disorders, a decrease in peripheral Tregs is associated with disease exacerbations, resulting in persistent proliferation of autoreactive lymphocytes and secretion of multiple inflammatory mediators

which harm organs[97]. Childhood studies examining the proportions of CD4 Tregs in asthma have shown that Tregs decline with disease severity but increase during the remission phase[126,127]. In a cohort of 150 asthmatic children with an average age of 5.6 years the $CD4^+$ $CD25^+$ $Foxp3^+$ T cells in their peripheral blood increased from 1.2% during the acute phase to 2.0% during remission and all asthmatics were significantly lower compared to disease controls (2.2%)[126]. In another study of asthmatic children with a median age of 8, the proportion of blood and BAL $CD4^+$ $CD25^{hi}$ T cells were 1.9% and 6.5% respectively[127]. Moreover, 4 weeks of ICS administration significantly increased $CD4^+$ $CD25^{hi}$ T cells in the blood and predominantly in the BAL fluid of asthmatic children[127].

Tregs are well documented in mouse studies to inhibit allergic airways disease[128], however T cell activation is hindered by ICS[62]. As the subjects with STRA in this study received higher doses of ICS therapy, it may explain the discrepancy in unchanged total T cells but altered T cell subsets such as increased peripheral $CD4^+$ $CD25^+$ $CD127^-$ T cells and $CD8^+$ $CXCR5^+$ $PD\text{-}1^+$ T cells. Further investigation of activation markers revealed that CD38 fluorescence intensity was increased on $CD4^+$ $CD25^+$ $CD127^-$ T cells in children with LRTI and PSW but not STRA children. Importantly, patient studies show that $CD38^+$ Tregs overexpress immune-inhibitory signals relative to $CD38^-$ Tregs[129], suggesting that in patients with asthma, the Tregs may not be highly suppressive. While there is a lower percentage of $CD4^+$ $CD25^+$ $CD127^-$ Tregs in children with PSW, the population maintains an activated $CD38^+$ phenotype, indicating an increased potential to block the proliferation of effector cells. The opposite is true for allergic asthma, whereby Tregs have

been described to have limited suppressive function[128]. The corresponding $CD4^+$ subsets in the airways were not statistically different between the disease groups, indicating that BAL $CD4^+$ T cells were phenotypically similar.

As previously discussed, circulating $CD8^+$ $CXCR5^+$ $PD1^+$ T cells were elevated in STRA patients. CXCR5 expression promotes colocalization of T and B cells into the germinal centre of lymph nodes, allowing for cell interactions and antigen recognition[130]. These CD8 follicular T cells also contribute to B cell antibody production by stimulating B cell class switching[131]. Given that the peripheral IgD^-CD27^+ $CD20^+$ B cell subset was markedly increased in STRA subjects, it is conceivable that the increased CD8+ CXCR5+ PD1+ T cell profile may contribute to the elevated effector B cell phenotype.

Interestingly, LRTI subjects exhibited significantly increased $CD8^+$ $CD25^+$ $CD127^-$ T cells which have a regulatory function and can inhibit $CD8^+$ T cell responses via IL-10 cytokine secretion[98]. The suppressive potential of this specialised CD8 subset may rationalise the nonsignificant increase of total $CD8^+$ and $CD69^+$ $CD8^+$ T cells in LRTI individuals.

Increased total NKT cells in STRA patients could be implicated in disease pathogenesis as NKT cells recognize protein antigens and induce AHR independently of conventional $CD4^+$ TH2 cells[99, 132]. Examination of exclusive NKT subset frequencies in the circulation based on CD4 and CD8 expression highlighted that, children with PSW displayed a pro-inflammatory profile, as $CD4^+$ $CD3^+$ $CD56^+$ NKT cells rapidly release TH2 cytokines IL-4 and IL-13. Heightened cytokine production by NKT cells contribute to subsequent adaptive responses executed by DCs and B cells[99]. Interestingly, the

abundance of circulating $CD8^+$ $CD3^+$ $CD56^+$ NKT cells suggests that patients were also experiencing immunosuppressive NKT responses concurrently[133].

There was no substantial recruitment of neutrophils into the airways of STRA patients, however some children with PSW had a greater proportion. Lower airway microbiota research in PSWs has demonstrated that BAL neutrophils are elevated in wheezers with positive BAL bacterial cultures but there is no association between airway neutrophils and the presence of viral infections[15,16]. In this study, the PSW cohort showed a nonsignificant positive correlation between the number of viral infections and proportion of airway $CD15^+$ cells. When the data was combined with LRTI and STRA children, a stronger association was seen, with a correlation between BAL $CD15^+$ cells and number of viral infections and total number of viral and bacterial infections. This outcome was attributed to PSW and LRTI children as only one STRA child had a viral infection.

Furthermore, differential cytospin counts revealed that peripheral neutrophils were significantly increased in children with LRTI compared to both PSW and STRAs. LRTIs such as respiratory syncytial virus and adenovirus are common in PSWs and healthy infants leading to hospitalization[5,134]. As neutrophilia is associated with clearance of bacterial and viral pathogens, the elevated abundance in LRTI infants is reasonable[31].

Monocytes were augmented in the periphery of patients with a history of recurrent infections. This increase may be linked to monocyte migration through the blood to reach inflamed tissue[135] or priming for phagocytosis activity[107]. Furthermore, the positive correlation between proportion of CMs

and the number of bacterial pathogens in PSW, implies they were responding to the recurrent infections reported in these patients such as rhinovirus and Moraxella[15,16].

Like monocytes, DCs circulate in the blood and ultimately relocate to tissue sites to initiate immune responses[136]. DCs are rare cells, representing less than 1% of circulating or tissue immune cells[137]. These antigen-presenting cells were characterised using the aurora panel markers as non-lymphoid, non-granulocyte, and non-monocyte cells expressing CD141 or CD1c surface markers. Analysis of DCs conveyed that the airways of these children were dominated by DC2 phenotype whereas the blood was primarily composed of DC1s. Furthermore, the decreased expression of PD-1 inhibitory molecule on BAL DC2s conveyed that STRA children had a T2 DC phenotype which are involved in TH2 skewing[25].

4.6 Conclusion

In summary, this chapter explored major immune cell phenotypes in preschool wheeze and severe asthma. Furthermore, exclusive cell types across disease groups were investigated such as NKT cells, DCs and ILCs. The results underlined multiple immune phenotypic differences between PSWs and LRTI such as peripheral $CD4^+$ $CD25^+$ $CD127^-$ T cells, $CD15^+$ neutrophils and $CD14^+$ $CD16^-$ classical monocytes were decreased in PSWs compared to children with LRTIs. In addition, PSWs exhibited reduced airway $CD8^+$ $CD25^+$ $CD127^-$ T cells and a positive correlation between serum IgE levels and blood eosinophils suggesting severe exacerbations. This supports the hypothesis

that PSW children have a distinct airway and blood immune cell profile compared to non-wheeze disease controls.

Chapter 5. Unbiased analysis of airway and peripheral immune cells

5.1 Introduction

In chapter three, a 34-multicolour panel combined with an AF removal workflow was devised to efficiently phenotype major immune subsets in peripheral blood and BAL samples. Then in chapter four, the panel was implemented to identify differential immune profiles of children with airways disease using a conventional analysis approach, particularly PSW and STRA compared to LRTI controls. This chapter focuses on the use of unbiased analysis algorithms to visualise high-parameter data and accelerate immune profiling.

Current advances in multiparameter single cell flow cytometers have been beneficial in our understanding of the heterogenous nature of the human immune system at high resolution. However, the utility of such multi-dimensional data is hindered by biased deductions and a limitation in visualising the full depth of datasets in a relevant approach. In routine flow cytometry, cell subsets are ascertained by sequentially manual gating on two-dimensional scatter plots[138]. This method makes the analysis subjective and time-consuming, particularly if dealing with a 34-colour panel. Naturally, researchers have developed computational tools that can conduct unbiased automated analysis to characterise cell populations whilst simultaneously generating visualisation aids to reduce dimensionality[139].

In this chapter, a CyTOF workflow[38] incorporated with the FlowSOM algorithm is utilized to facilitate unsupervised clustering of immune cells. FlowSOM is software which objectively clusters cells using selected markers and can reveal subsets that could be overlooked in manual gating during flow cytometry analysis[139]. This algorithm employs a consensus hierarchical

clustering method to generate high quality schematics in the form of self-organizing maps (SOM) which cluster cell populations based on their similarity. In the CyTOF pipeline, a second layer of clustering is conducted to generate metaclusters which encompass the lower-level SOM clusters and represent the predicted cell types in the dataset[140].

To define the cellular phenotype and relationship to diagnosis, the immune cell clusters identified by unbiased analysis were manually gated in the patient flow samples. By using clustering heatmaps and histograms of markers expressed in each cluster, the distinct immune cells were determined by gating on positive and negatively expressed markers.

5.2 Hypothesis

Unbiased analysis of high-dimensional spectral flow cytometric data can uncover distinct immune clusters between paediatric airways disease cohorts

5.3 Aims

1. Conduct unsupervised clustering of paediatric blood and Bal samples
2. Define the cellular phenotype of immune cell clusters identified by unbiased analysis

5.4 Results

5.4.1 Experimental workflow of unsupervised clustering and data analysis

The experimental pipeline for unsupervised clustering consisted of acquiring samples on the Aurora spectral cytometer using a 34-colour panel **(Fig. 5.1A)**, followed by an AF removal process as explained in chapter 3. Next, the desired population in the sample flow file was gated using Flowjo by selecting cells that were singlets, live and $CD45^+$ **(Fig. 5.1B)**. Flow files containing total $CD45^+$ events were exported to R studio to perform unbiased clustering analysis using FlowSOM and CyTOF workflow packages to generate heatmaps[38,139] **(Fig. 5.1C)**. Then subjective gating was applied to the sample flow files to visualise any unique immune populations identified by unbiased clustering **(Fig. 5.1D)**. Thirty-five FCS files of the 40 samples analysed in chapter 4 were imported to R studio. This was due to errors during flow acquisition, whereby identical channels were not selected and therefore could not be merged in the automated analysis.

As might be expected the number $CD45^+$ events in blood and Bal flow files varied between donors. Although this was not explicitly linked to disease group, bar plots of blood samples showed an increase in $CD45^+$ events in several STRA samples **(Fig. 5.1E)**, as previously shown by manual gating **(Fig. 4.1B)**. Grouping individual BAL $CD45^+$ events revealed that the airway cellularity was mostly comparable between the subject groups **(Fig. 5.1F)**.

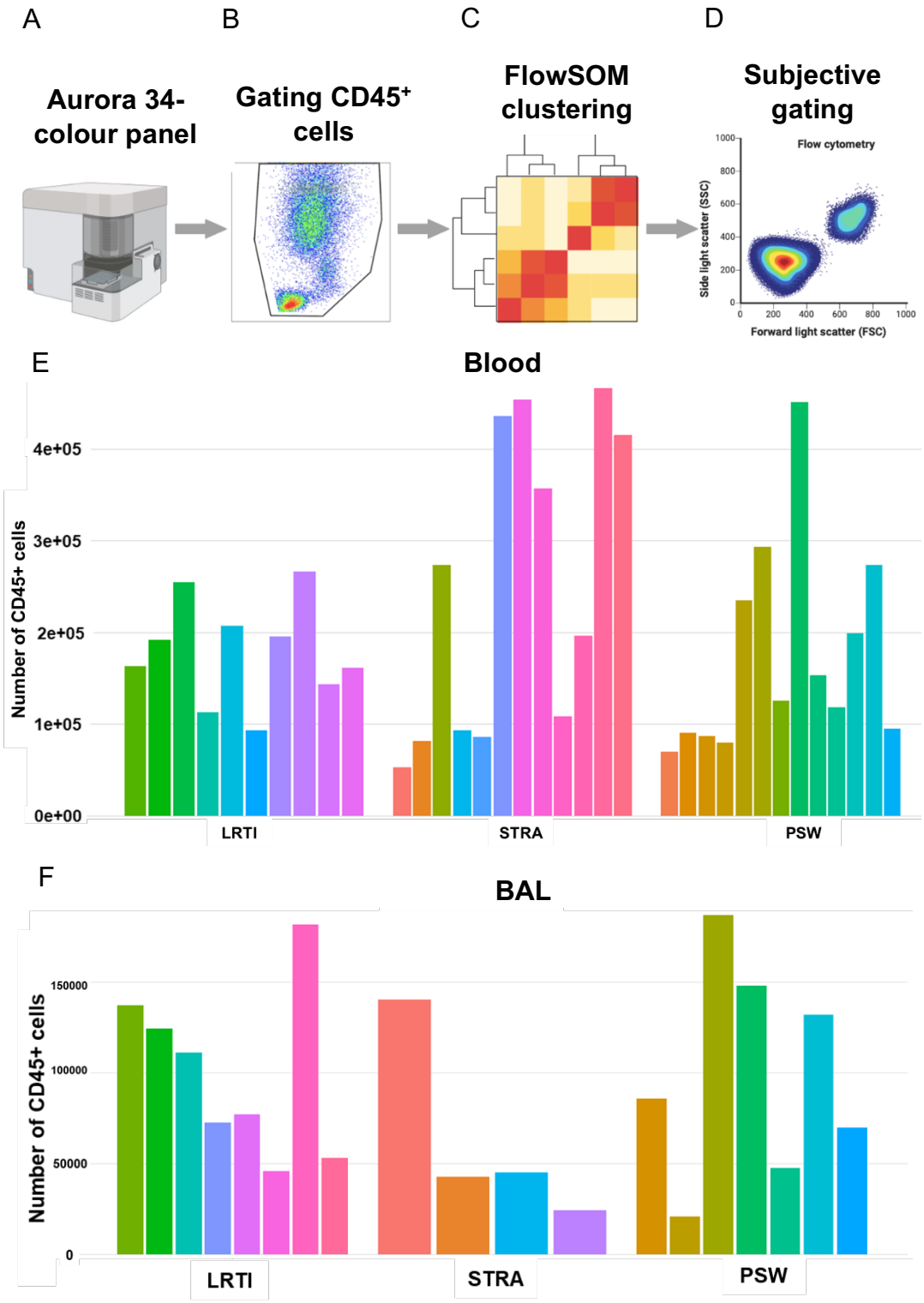


Fig 5.1. Summary of experimental pipeline for data acquisition and unbiased analysis

Illustration of the unbiased analysis workflow consisting of **A)** acquisition on the Aurora 34-colour panel, **B)** manually gating viable CD45$^+$ events, **C)** FlowSOM clustering algorithm and **D)** dimensionality-reduction algorithm. Number of CD45$^+$ cells per donor imported into R studio in **E)** Blood and **F)** BAL samples grouped by disease type.

5.4.2 Unsupervised clustering of blood immune cells revealed 10 unique populations

Peripheral $CD45^+$ cells were categorized by high resolution FlowSOM clustering and low-resolution metaclustering algorithms using all the markers available on the panel. Live-dead, CD45 and CD206 markers were excluded to eliminate repetitive grouping and non-existent cells. The panel contained differential markers that are characteristic of immune cell lineages such as CD15, activation markers (CD69, CD27) and inhibitory markers (PD1). The FlowSOM clustering of SOMs is embedded in consensus clustering which is presented as an elbow plot of metaclusters. This plot illustrates the natural number of cell types in the data, which equate to the value of k, where there is no substantial increase in stability thus simplifying the dataset[38]. Within each metacluster, there are 10 clusters to identify differential sub-populations.

FlowSOM objective analysis was performed by using 100 clusters and 10 metaclusters. The number of cell types were first over-clustered using maxK =14 to avoid the risk of missing rare populations **(Fig. 5.2A)**. The intrinsic number of distinct circulating immune cell clusters in blood were ascertained to be 10, illustrated by the elbow plots showing that the plot plateaus at k = 10. **(Fig. 5.2B)**.

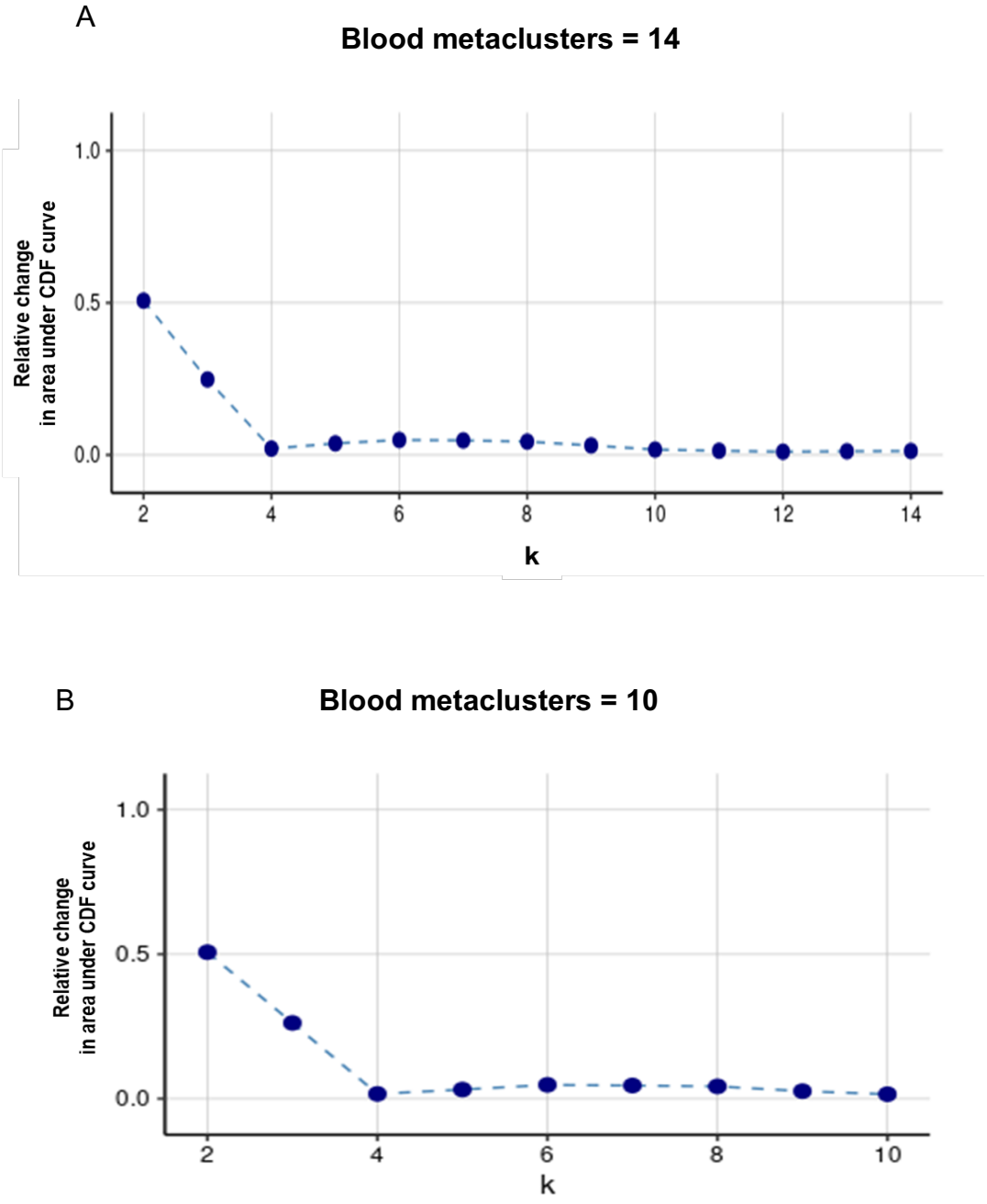


Fig 5.2. The number of unique metaclusters in blood paediatric samples

Elbow plot showing the natural number of metaclusters in blood using a maximum of **A)** fourteen and **B)** ten clusters (maxK).

5.4.3 Phenotyping of blood leukocyte clusters using differential marker expressions

Next, a heatmap of median marker intensities was constructed to determine the cellular phenotypes of each cell type encompassed in the blood metaclusters **(Fig. 5.3)**. Of note, each metacluster contains 10 sub-clusters which were assigned by the FlowSOM analysis. This means that the expression of markers observed at the metaclusters level can be split further into subtypes when assessed at the higher level of clusters. This is explored later by examining the heatmaps of the n=100 clusters.

In the heatmap of blood metaclusters, cluster 1 appeared to express $CD15^+$ $CD16^+$ $CD11b^+$ $CD86^+$ surface proteins, whilst cluster 2 denoted a $CD14^+$ $CD16^+$ $HLA\text{-}DR^+$ $CD11c^+$ $CD11b^+$ $CD86^+$ $CD38^+$ expression profile. Cluster 3 was enriched with a combination of $CD1c^+$ $CD141^+$ $CD11b^+$ $CD69^+$ $CD127^+$ $CD28^+$ markers. Cluster 4 encompassed $CD16^+$ $CD123^+$ $CD11b^+$ $CD38^+$ proteins whereas cluster 5 exhibited $CD20^+$ IgD^+ $HLA\text{-}DR^+$ $CD45RA^+$ $PD1^+$ phenotype. Cluster 6, 7 and 9 appeared to contain subsets of $CD3^+$ cells. Cluster 6 displayed $CD4^+$ $TCR\alpha\beta^+$ $CD27^+$ $CD28^+$ markers whereas cluster 9 demonstrated a $CD4^+$ $TCR\alpha\beta^+$ $CD28^+$ $CD25^+$ $CD127^+$ surface profile. In contract, cluster 7 was attributed to a $CD8^+$ $TCR\alpha\beta^+$ $CD45RA^+$ $CD161^+$ $PD1^+$ subset. Furthermore, cluster 8 was enriched with $CD15^+$ $CD103^+$ $CD11b^+$ $CD11c^+$ and cluster 10 illustrated a $CD16^+$ $CD45RA^+$ $HLA\text{-}DR^+$ cellular phenotype.

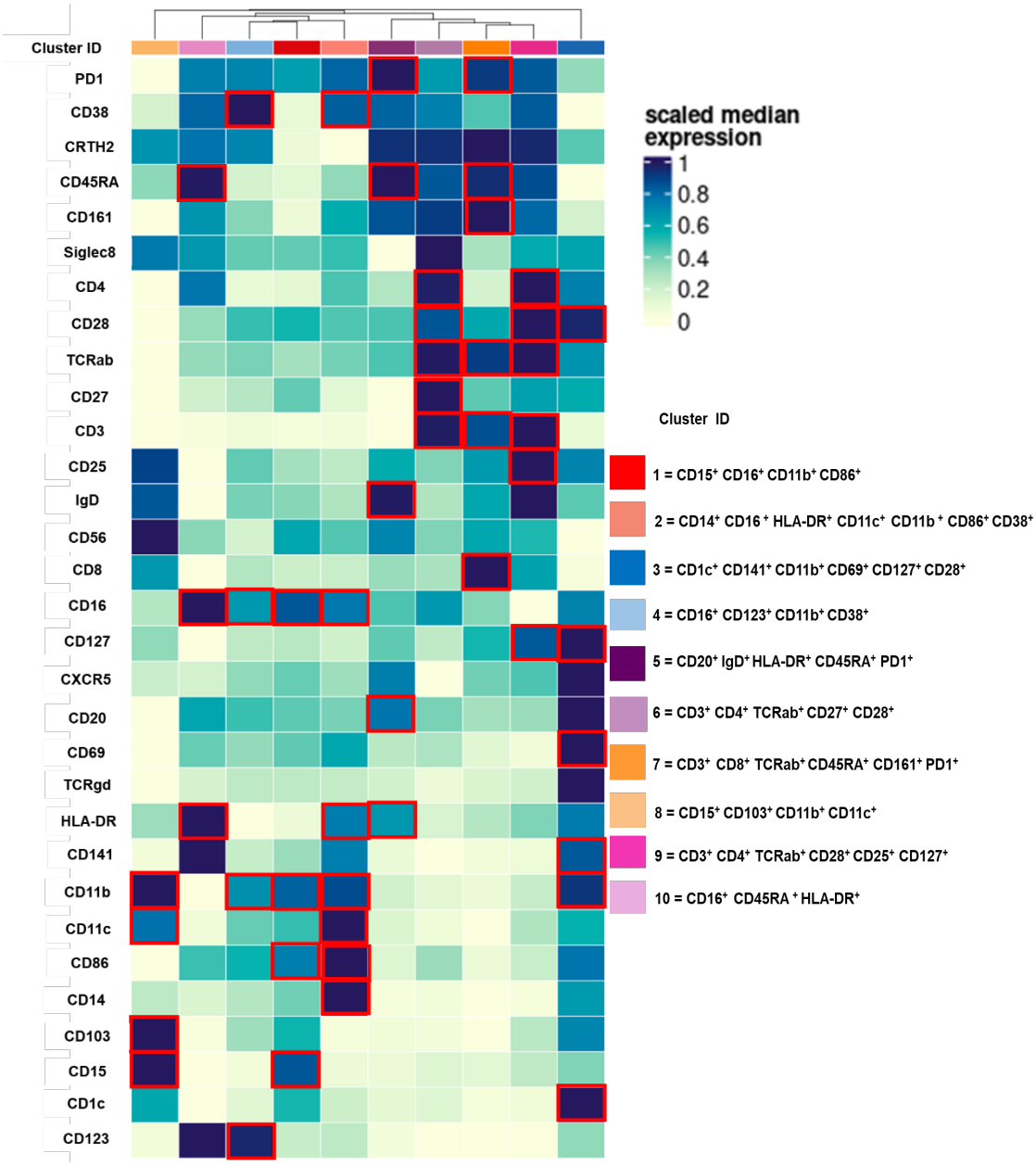


Fig 5.3. Heatmap of blood immune cell metaclusters defined by marker expressions

Heatmap of median marker intensities was constructed by hierarchical clustering using all markers in the panel except CD45, CD206 and live-dead. Red boxes outline the augmented markers within each cluster.

5.4.4 Automated clustering uncovered sixteen peripheral populations that were differentially expressed in PSWs compared to children with LRTI and STRA

To determine any differential populations between the wheeze and non-wheezers, the proportion of each cluster in the blood samples were quantified. Multiple comparison tests were conducted between the means of PSW and LRTI immune populations. The six clusters that were significantly increased ($p<0.05$) in the peripheral blood of PSWs compared to LRTI children were C12, C14, C54, C83, C92 and C93 **(Fig. 5.4A)**. In contrast, three clusters were markedly reduced in PSWs relative to LRTIs which were C49, C58 and C74 **(Fig. 5.4B)**.

Similarly, multiple comparison tests between the means of PSW and STRA cell populations confirmed that seven peripheral immune clusters were differently expressed. Clusters 4, 23, 46, 83 and 93 were notably increased in PSWs **(Fig. 5.5A)** whereas clusters 62 and 77 were decreased relative to STRA children **(Fig. 5.5B)**.

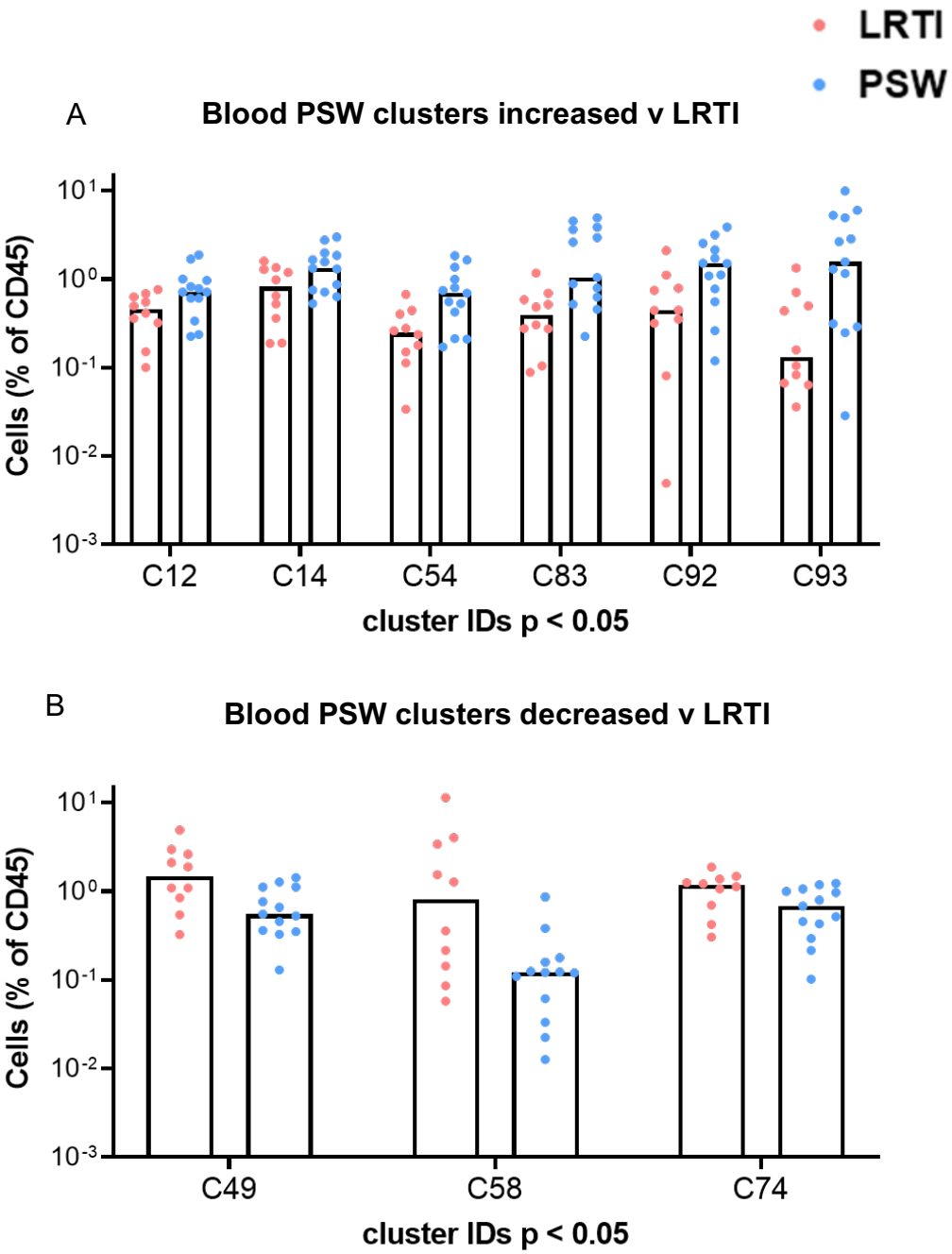


Fig 5.4. The proportion of significantly different immune cell clusters in PSW blood compared to LRTIs

Frequency of peripheral $CD45^+$ immune cell clusters that are **A)** increased in PSWs compared to LRTI and **B)** decreased in PSWs compared to LRTI controls. Statistical significance was measured by an unpaired non-parametric Mann-Whitney U Test.

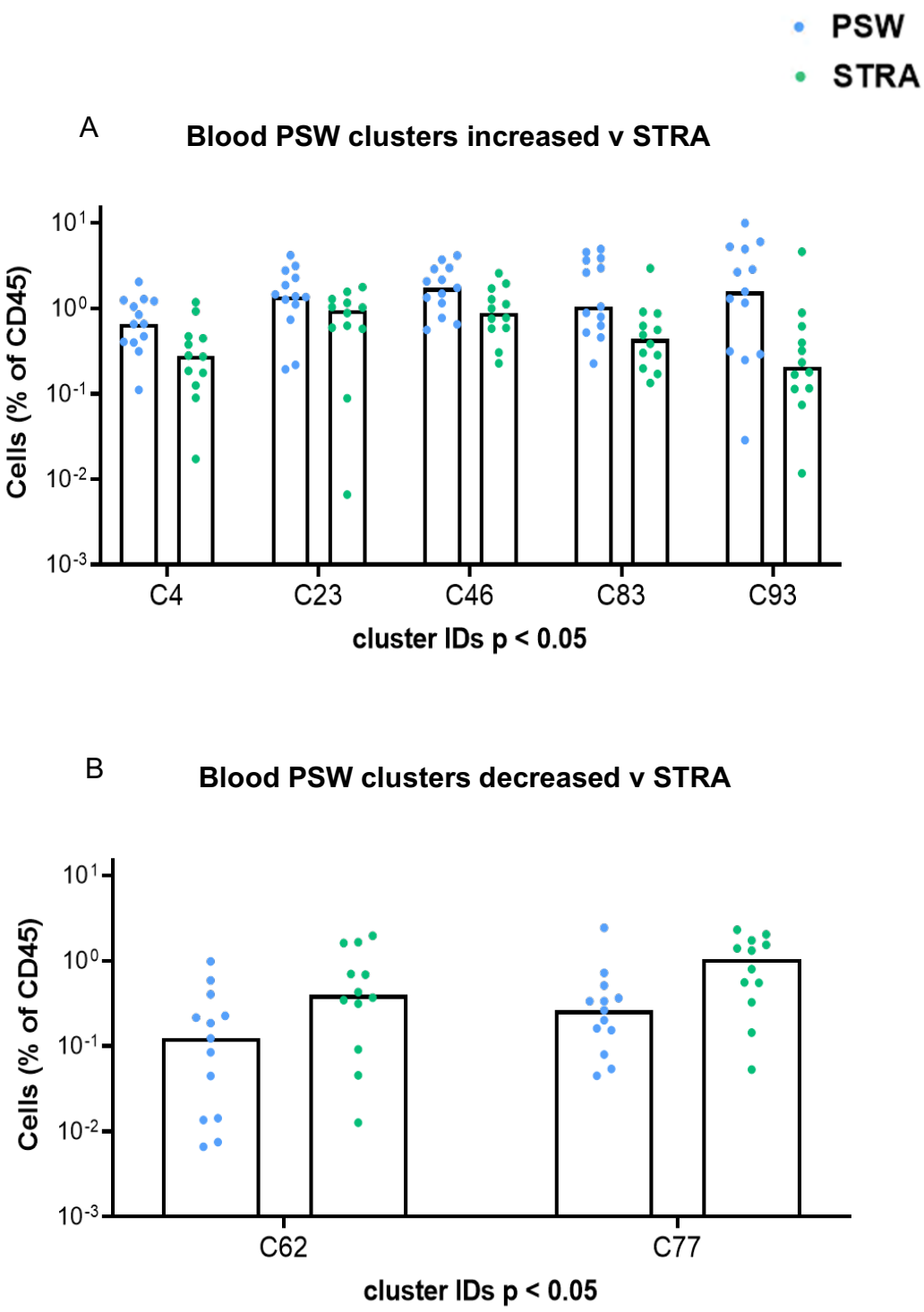


Fig 5.5. The frequency of markedly different leukocyte clusters in PSW blood compared to STRAs

Frequency of peripheral $CD45^+$ immune cell clusters that are **A)** increased in PSWs compared to STRAs and **B)** decreased in PSWs compared to STRAs. Statistical significance was measured by an unpaired non-parametric Mann-Whitney U Test.

5.4.5 Unbiased analysis discovered three circulating immune populations that were differentially expressed in children with STRAs compared to LRTI disease controls

Likewise, unbiased analysis found three unique peripheral immune cell subsets that were significantly altered between STRA and LRTI conditions. Multiple comparison tests between the means of both disease groups confirmed that C100 was notably elevated in STRA children **(Fig. 5.6A)**, whereas C33 and C46 were reduced relative to infection controls **(Fig. 5.6B)**. Interestingly C46 was also decreased in the severe asthmatic children compared to the PSW cohort which indicated a distinct STRA phenotype.

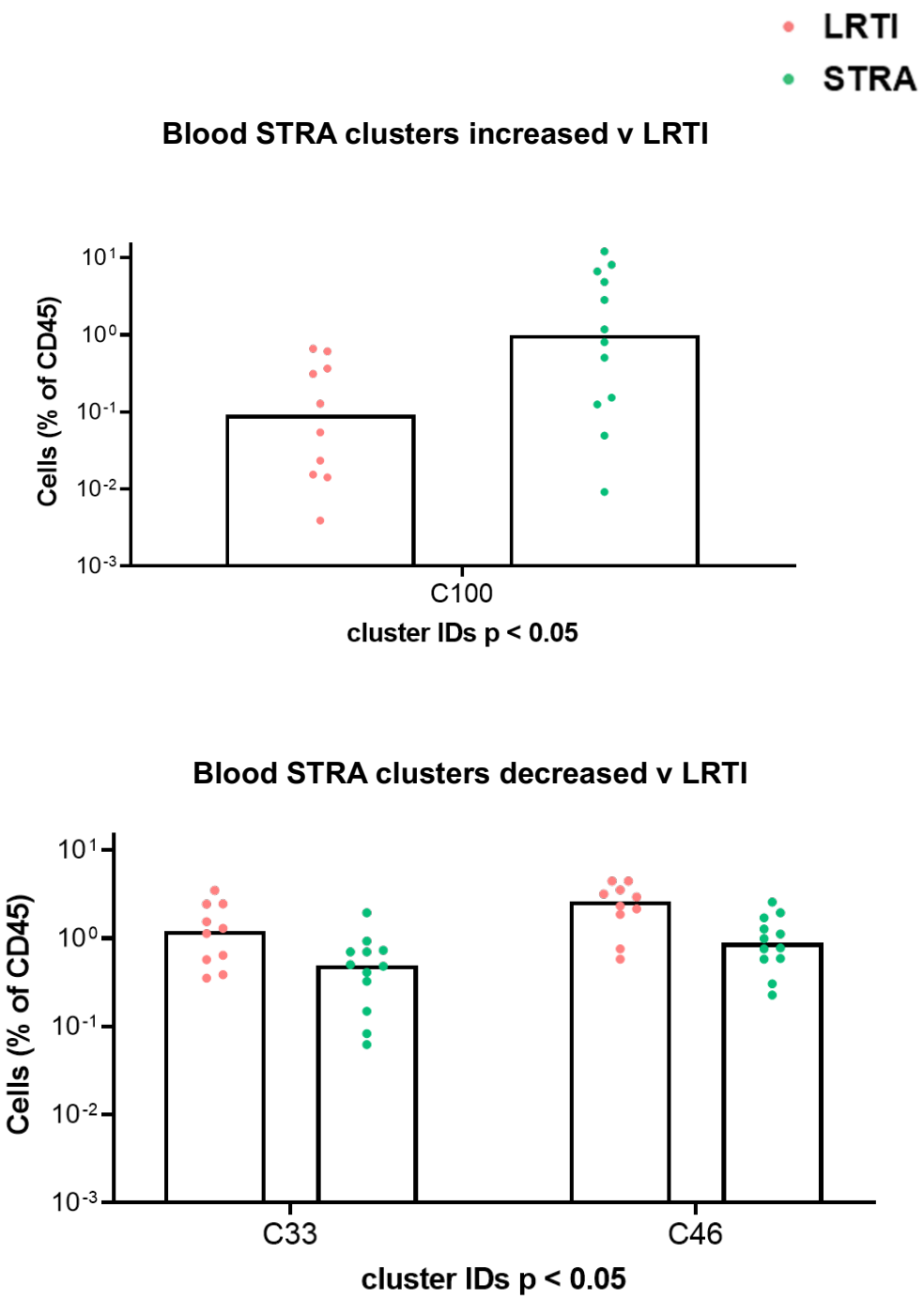


Fig 5.6. The frequency of markedly different immune cell clusters in STRA blood compared to LRTIs

Frequency of peripheral CD45^{+} immune cell clusters that are **A)** increased in STRA compared to LRTI and **B)** decreased in STRA compared to LRTI. Statistical significance was measured by an unpaired non-parametric Mann-Whitney U Test.

5.4.6 Phenotyping of blood leukocyte clusters using differential marker expressions

A heatmap of median marker intensities was constructed using all applicable markers within the panel to assign phenotypes to each population cluster **(Fig. 5.7)**. The immune phenotypes and disease types of the significantly altered clusters in blood are summarized in **Table 5.1**. Of the clusters that were elevated in PSWs compared to LRTIs; cluster 12 was $CD15^+$ $CD16^+$, $CD11b^+$, and cluster 14 was $CD16^+$ $CD14^+$ $CD11b^+$. Cluster 54 expressed a $CD15^{low}$ $CD11b^{low}$ profile. Cluster 83 had a $CD16^+$ $HLA\text{-}DR^+$ $CD45RA^+$ immune profile. While cluster 92 and 93 were both $CD20^+$ and $HLA\text{-}DR^+$, C92 exhibited an IgD^+, $CD45RA^+$ phenotype whereas C93 was IgD^- but $CD45RA^+$.

Next the marker expressions of peripheral blood cell clusters that were reduced in PSWs compared to LRTIs were ascribed. Cluster 49 showed $CD3^+$, $TCR\alpha\beta^+$, $CD4^+$, $CD27^+$, $CD28^+$ expression. Cluster 58 had a $CD3^+$, $CD4^+$, $TCR\alpha\beta^+$, $CD25^+$, $CD27^+$, $CD28^+$ phenotype. Cluster 74 displayed $CD56^+$, $CD161^+$, $CD38^+$, surface expression.

Subsequently, the expression of immune cell types that were elevated in PSWs compared to STRAs were assessed. Cluster 4 displayed $CD14^+$ $CD16^+$, $CD11b^+$, and $CD86^+$ phenotype. Cluster 23 demonstrated a $CD15^+$ $CD103^+$ $CD86^+$ $CD11b^+$ expression profile. Cluster 46 showed a $CD16^+$, $CD11b^{low}$, $CD86^{low}$ profile.

In contrast, the two populations that were reduced in PSW blood compared to STRAs were defined as cluster 62 with a $CD141^+$, $CD11c^+$, $HLA\text{-}DR^+$

phenotype and cluster 77 which portrayed a $CD3^+$, $TCR\alpha\beta^+$, $CD8^+$, $CD161^+$, $PD1^+$ characteristic.

Finally, the immune cluster 100 that was distinctly increased in the periphery of STRA children compared to LRTIs portrayed a $CD3^+$, $TCR\alpha\beta^+$, $CD8^+$, $CD27^+$ $CD25^+$, $CD45RA^+$ surface expression profile.

Although clusters 12 and 14 were numbered closely, the immune population in cluster 12 displayed a $CD15^+$ $CD16^+$ profile, whilst cluster 14 uniquely exhibited CD14 but lacked CD15 expression.

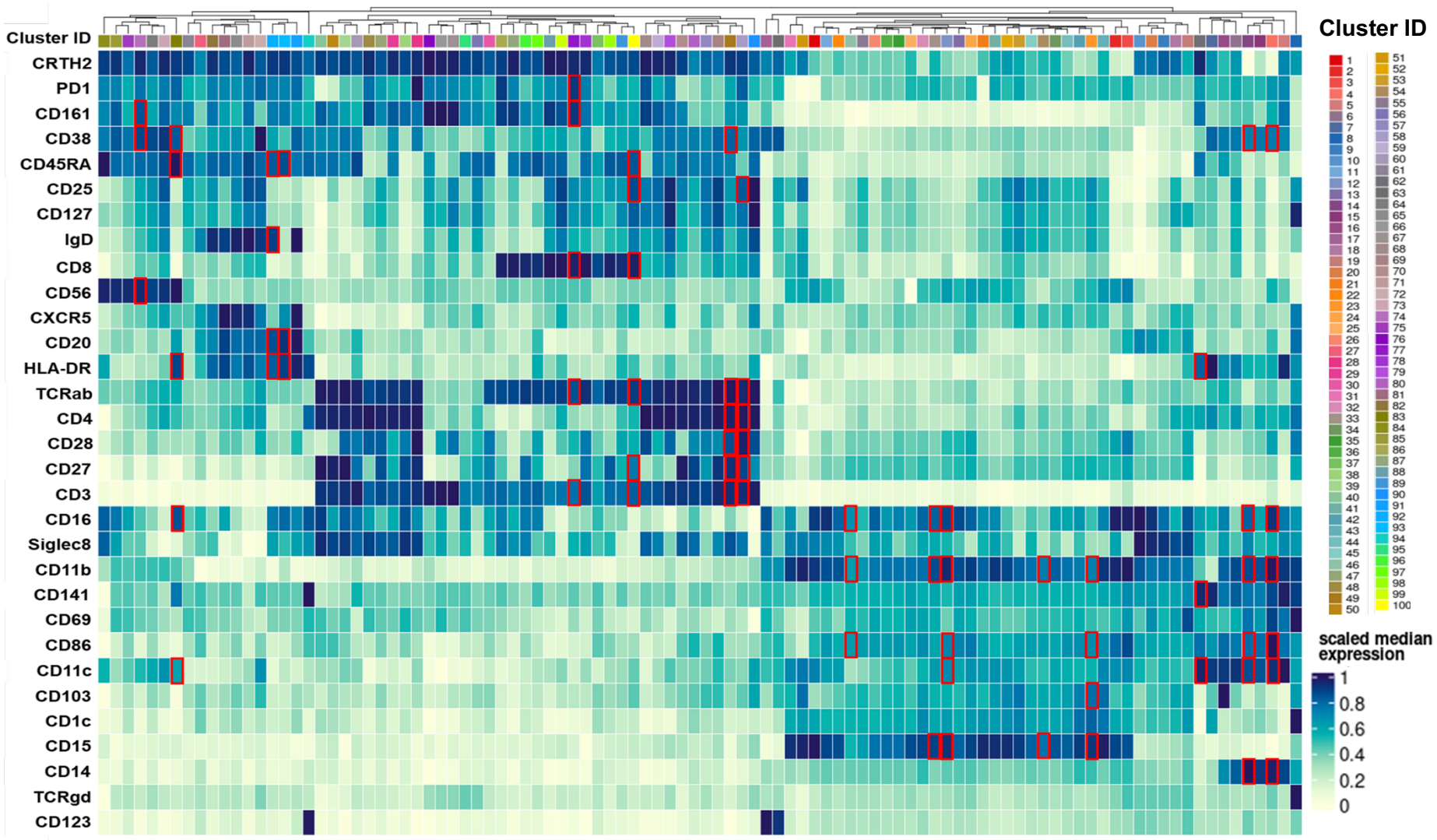

Cluster ID
CRTH2
PD1
CD161
CD38
CD45RA
CD25
CD127
IgD
CD8
CD56
CXCR5
CD20
HLA-DR
TCRab
CD4
CD28
CD27
CD3
CD16
Siglec8
CD11b
CD141
CD69
CD86
CD11c
CD103
CD1c
CD15
CD14
TCRgd
CD123
Cluster ID
1 2 3 4 5 6 7 8 9 10 11 12 13 14 15 16 17 18 19 20 21 22 23 24 25 26 27 28 29 30 31 32 33 34 35 36 37 38 39 40 41 42 43 44 45 46 47 48 49 50
51 52 53 54 55 56 57 58 59 60 61 62 63 64 65 66 67 68 69 70 71 72 73 74 75 76 77 78 79 80 81 82 83 84 85 86 87 88 89 90 91 92 93 94 95 96 97 98 99 100
scaled median expression
1
0.8
0.6
0.4
0.2
0

Fig 5.7. Heatmap illustration of blood immune cell clusters outlined by marker expressions

Heatmap of median marker intensities was constructed by hierarchical clustering using all markers in the panel except CD45, CD206 and live-dead. Red boxes outline the augmented markers within each cluster.

Blood cluster ID	Disease type	Expression profile	p-value
C4	PSW > STRA	$CD16^{+}$ $CD14^{+}$ $CD11b^{+}$ $CD38^{+}$ $CD11c^{high}$ $CD86^{high}$	0.011394
C12	PSW > LRTI	$CD15^{+}$ $CD16^{+}$ $CD11b^{+}$ $CD86^{low}$ $CD11c^{low}$	0.035844
C14	PSW > LRTI	$CD16^{+}$ $CD14^{+}$ $CD11b^{+}$ $CD38^{+}$ $CD11c^{+}$ $CD86^{+}$	0.042158
C23	PSW > STRA	$CD15^{+}$ $CD103^{+}$ $CD86^{+}$ $CD11b^{+}$	0.039795
C33	STRA < LRTI	$CD15^{+}$ $CD16^{+}$ $CD11b^{+}$	0.042570
C46	PSW > STRA LRTI > STRA	$CD16^{low}$ $CD11b^{low}$ $CD86^{low}$ HLA-DR^{-} $CD45RA^{-}$	0.034513 0.011153
C49	PSW < LRTI	$CD3^{+}$ $TCRab^{+}$ $CD4^{+}$ $CD28^{+}$ $CD27^{+}$ $CD38^{+}$	0.035844
C54	PSW > LRTI	$CD15^{+}$ $CD11b^{+}$	0.008024
C58	PSW < LRTI	$CD3^{+}$ $TCRab^{+}$ $CD4^{+}$ $CD28^{+}$ $CD27^{+}$ $CD25^{+}$	0.017775
C62	PSW < STRA	$CD141^{high}$ $CD11c^{high}$ HLA-DR^{+}	0.034513
C74	PSW < LRTI	$CD56^{+}$ $CD161^{+}$ $CD38^{+}$	0.035844
C77	PSW < STRA	$CD3^{+}$ $TCRab^{+}$ $CD8^{+}$ $CD161^{+}$ $PD1^{+}$	0.034513
C83	PSW > LRTI PSW > STRA	$CD16^{+}$ HLA-DR^{+} $CD11c^{low}$ $CD45RA^{+}$ $CD38^{+}$ $CD86^{-}$	0.005180 0.007980
C92	PSW > LRTI	$CD20^{+}$ HLA-DR^{+} IgD^{+} $CD45RA^{+}$	0.025518
C93	PSW > LRTI PSW > STRA	$CD20^{+}$ HLA-DR^{+} $CD45RA^{+}$	0.009888 0.009556
C100	STRA > LRTI	$CD3^{+}$ $TCRab^{+}$ $CD8^{+}$ $CD25^{+}$ $CD27^{+}$ $CD45RA^{+}$	0.024916

Table 5.1. The cell phenotypes and disease types of the significantly altered clusters in blood unbiased analysis

Peripheral immune cell clusters altered between the paediatric clinical diagnoses. Populations were established by FlowSOM clustering and those with p-values below 0.05 are shown.

5.4.7 Subjective gating of peripheral immune cell clusters identified by unbiased analysis

As numerous peripheral immune populations were determined by unsupervised analysis to be differentially expressed between the paediatric patients, subjective gating was implemented to examine these populations that may have been overlooked by traditional gating. Several altered populations with the lowest p-value with the potential of observing a significant variance were investigated.

The immune populations 46, 83 and 77 were selected in peripheral blood samples. FlowSOM analysis showed that cluster 46 was exclusively decreased in STRA compared to PSW ($p = 0.034513$) and LRTI ($p = 0.011153$) **(Table. 5.1)** and expressed the markers CD16, CD11b and CD86 **(Fig. 5.7)**.

Initially, immune cells were gated by removing debris, doublets and dead cells. This was followed by gating on $CD45^+$ $CD15^-$ $CD3^-$ cells to exclude abundant cell types that were unrelated to the population of interest **(Fig. 5.8)**. Based on the heatmap of marker densities, cluster 46 was characterised by gating on $CD16^+$ HLA-DR^- $CD86^+$ $CD45RA^-$ $CD11b^+$ cells. Contrary to unbiased analysis, subjective gating illustrated that cluster 46 was substantially elevated in STRA blood samples compared to LRTI **(Fig. 5.9A)**, whereas PSWs possessed a similar distribution to STRA children **(Fig. 5.9B)**. This outcome may have been influenced by the biased gating boundaries positioned by eye, the lack of information on the hierarchy of markers and perhaps the limited exclusion of lineage markers.

Additionally, cluster 83 which was exclusive increased in PSW blood compared to STRA and LRTI patients in unsupervised analysis, exhibited a unique $CD16^+$ immune profile. To distinguish from cluster 46, immune cells in cluster 83 were defined by $CD16^+$ $HLA\text{-}DR^+$ $CD45RA^+$ $CD38^+$ $CD86^-$ expression. Assessment of this population as a percentage of $CD45^+$ cells, showed that the distributions were comparable between PSW and non-wheezers **(Fig. 5.9C, D)**. However, there were some patients with a pronounced frequency in the PSW and STRA cohort. Based on the expression of these proteins, cluster 46 and 83 indicated a monocyte phenotype.

Finally, the circulating immune cell cluster 77 was defined by the expression of $CD8^+$ $CD161^+$ and $PD1^+$ which suggested a $CD8^+$ T cell profile. This population was initial gated using $CD45^+$, $CD3^+$ and $TCR\alpha\beta^+$ expression based on the heatmap and histogram outline **(Fig. 5.7, 5.10A)**. Whilst unbiased analysis reported that cluster 77 was increased in STRA blood relative to PSW ($p = 0.034513$), supervised gating showed that the proportion of circulating $CD8^+$ $CD161^+$ and $PD1^+$ cells were similar between STRA and PSW subjects **(Fig. 5.10B)**.

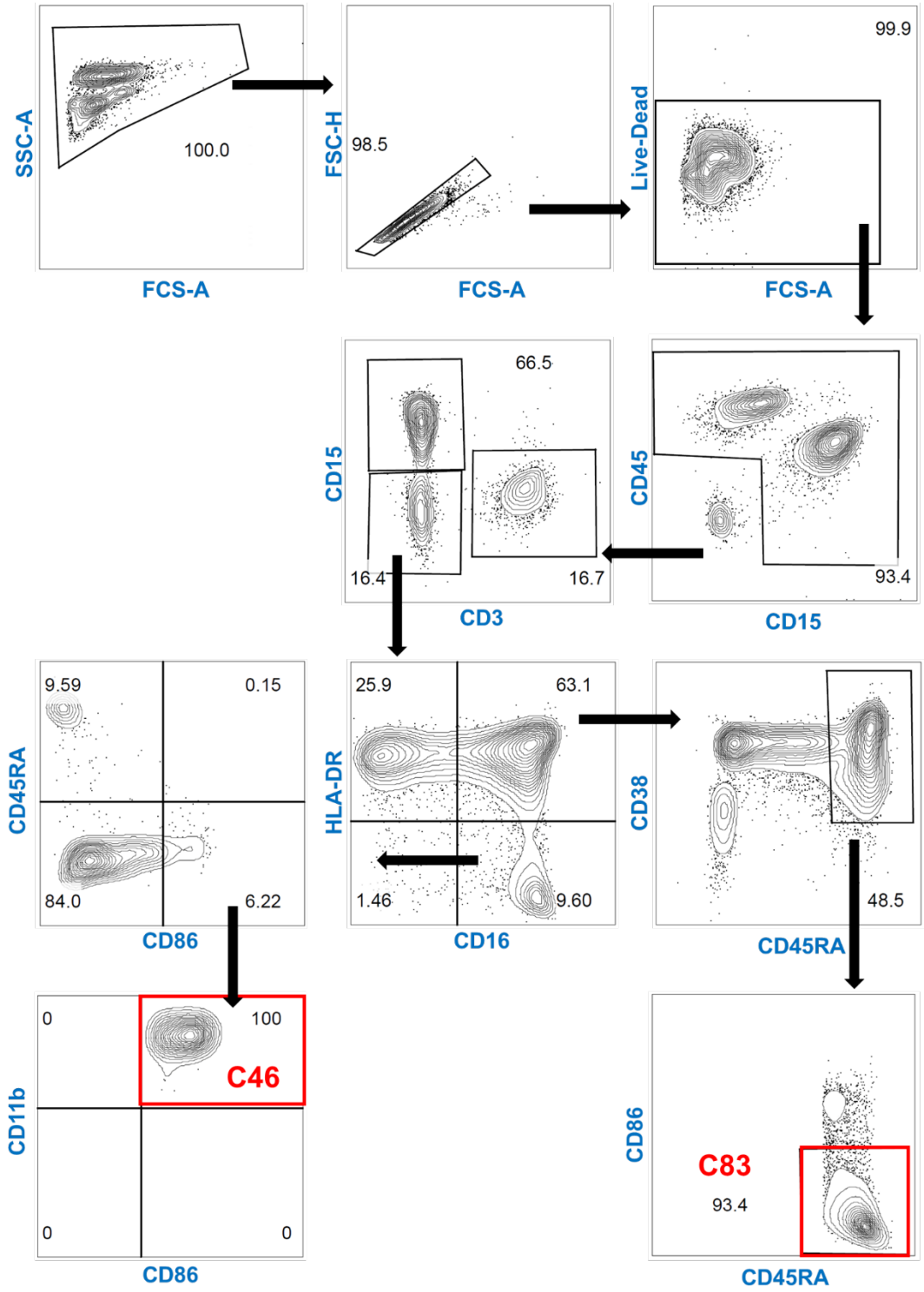


Fig 5.8. Gating strategy for peripheral immune cell clusters 83 and 46

Schematic of flow cytometry scatter plots showing immune cell gating strategy using LRTI sample. All cells were selected using forward and side scatter. Doublets were removed by gating for single cells using FSC-A versus FSC-H. Live cells were selected as Live-Dead blue negative cells. Viable immune cells were defined as CD45 positive.

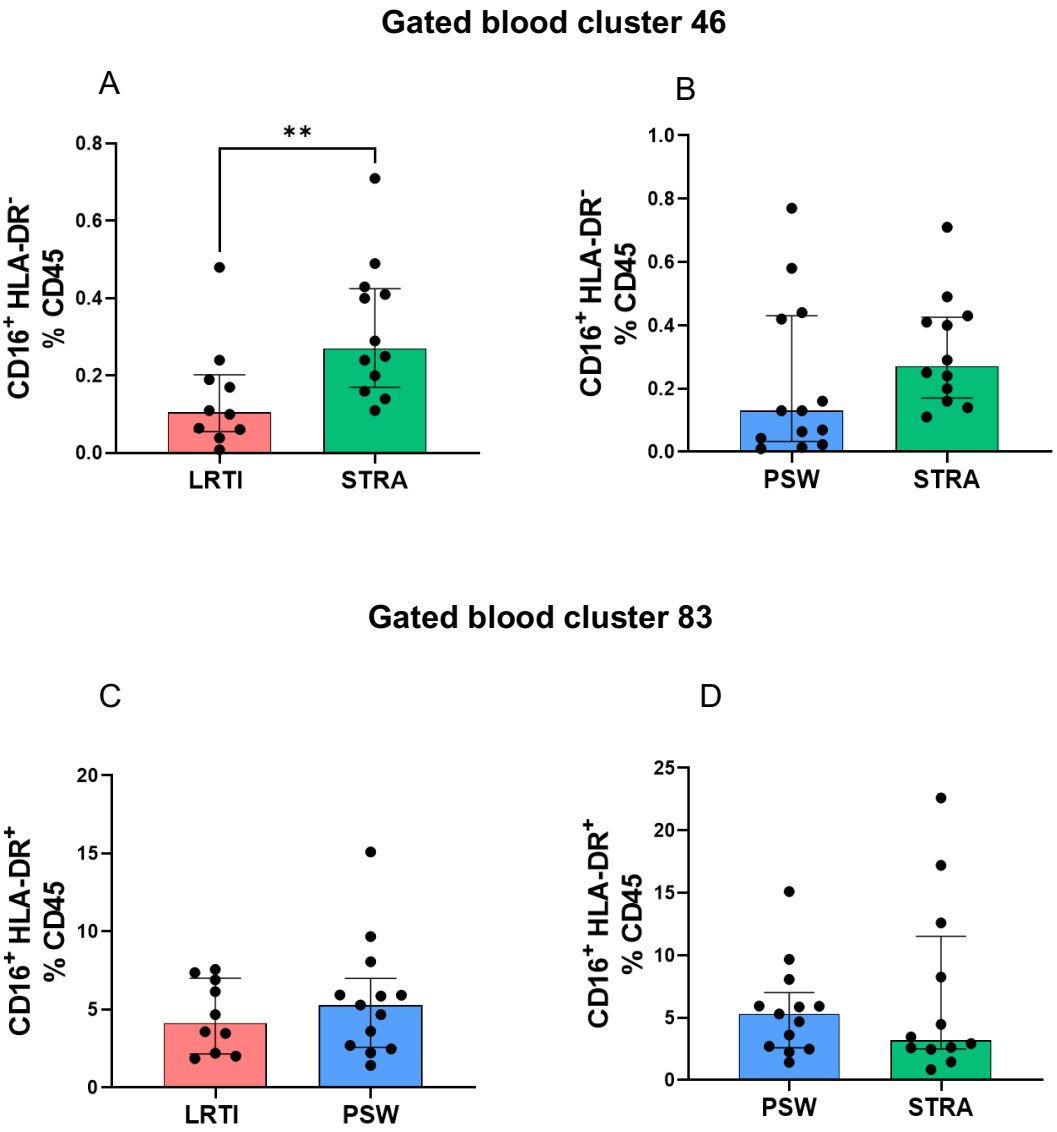


Fig 5.9. The frequency of altered immune cell populations in PSW and STRA blood

Frequency of circulating $CD16^+$ $HLA\text{-}DR^-$ immune cells in **A)** STRA compared to LRTI and **B)** STRA compared to PSW as a proportion of $CD45^+$ cells. Proportion of circulating $CD16^+$ $HLA\text{-}DR^+$ immune cells in **C)** PSW compared to LRTI and **D)** PSW compared to STRA as a percentage of $CD45^+$ cells. Statistical significance was measured by an unpaired non-parametric Mann-Whitney U Test.

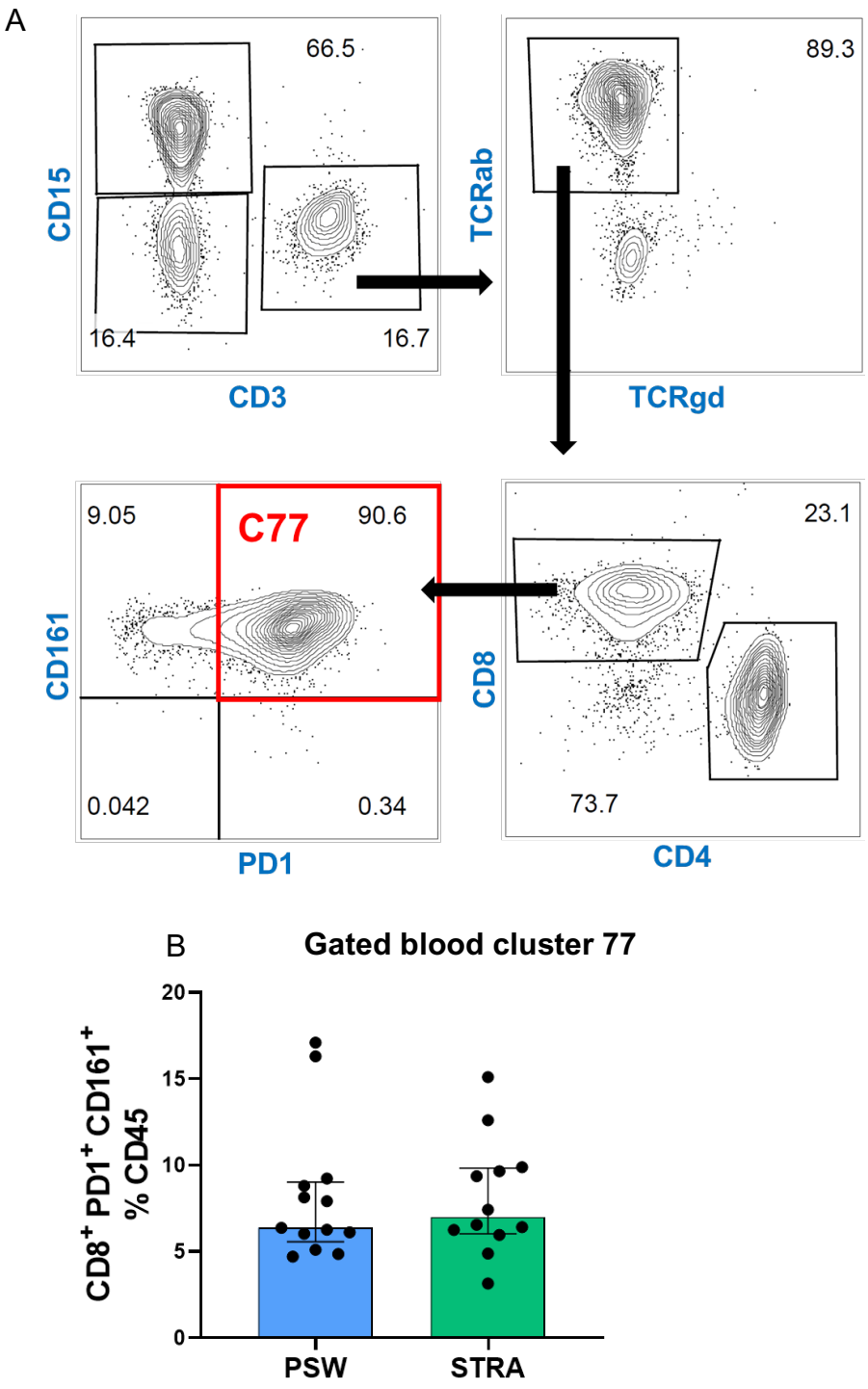


Fig 5.10. Gating strategy and proportion of peripheral immune cell cluster 77

A) Schematic of flow cytometry scatter plots showing immune cell gating strategy using LRTI sample. All cells were selected using forward and side scatter. Doublets were removed by gating for single cells using FSC-A versus FSC-H. Live cells were selected as Live-Dead blue negative cells. Viable immune cells were defined as CD45 positive. **B)** Frequency of circulating $CD8^+$ $PD1^+$ $CD161^+$ immune cells in PSW compared to STRA as a proportion of $CD45^+$ cells.

5.4.8 Unsupervised analysis of BAL immune cells identified 10 different populations

Analogous to blood samples, BAL $CD45^+$ cells were analysed by high-level FlowSOM clustering and low-resolution metaclustering algorithms using all markers on the panel including CD206 for the identification of macrophages. Live-dead and CD45 markers were eliminated from the analysis to avoid clustering predetermined features. FlowSOM analysis was conducted using 100 clusters and 10 metaclusters. The number of cell types were first over-clustered using k =14 which showed that the diversity of the immune cell populations plateaus at k = 10 **(Fig. 5.11A)**. Thus, BAL $CD45^+$ cells were re-clustered using k = 10 **(Fig. 5.11B)**.

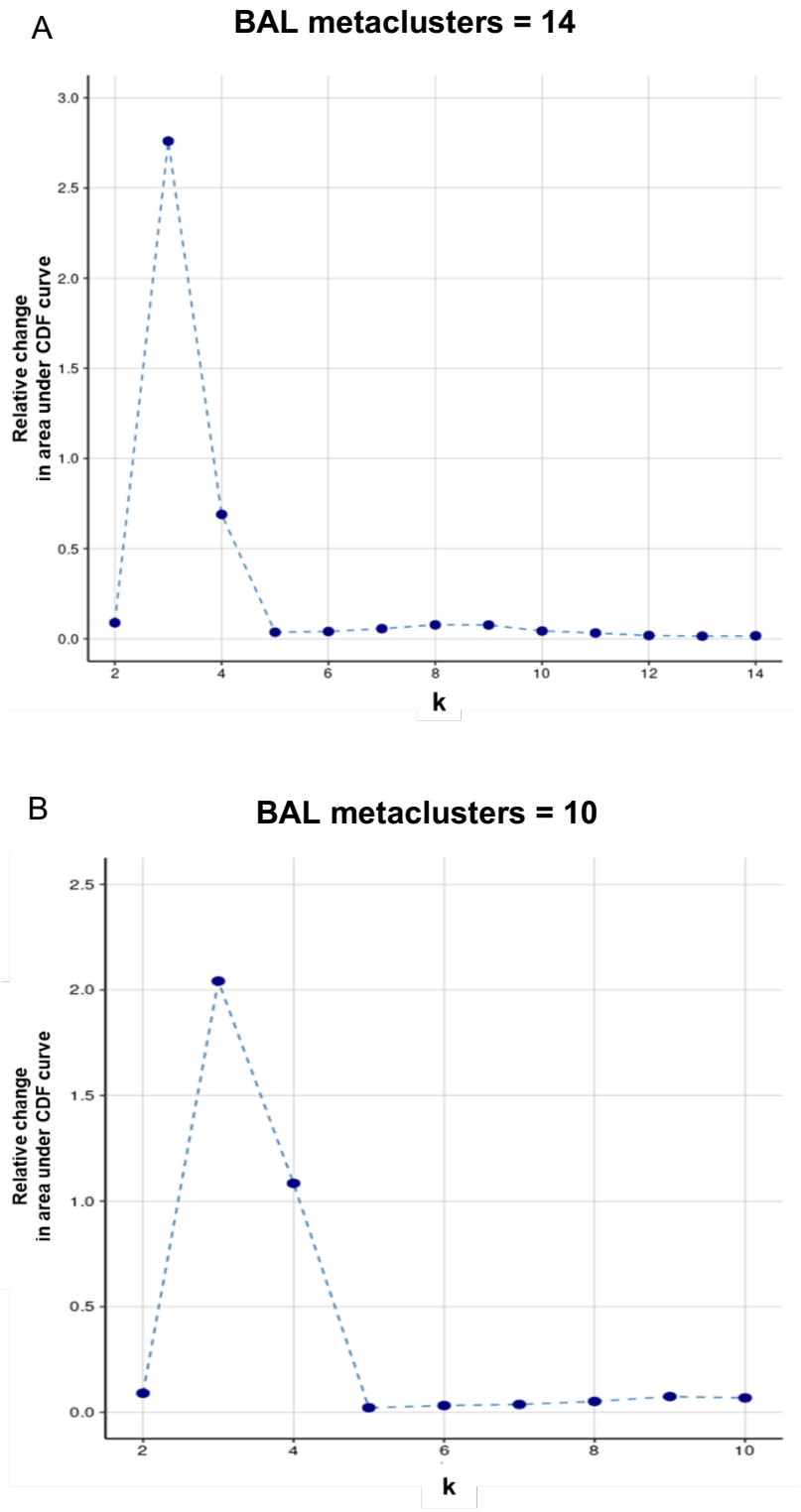


Fig 5.11. The number of unique metaclusters in BAL paediatric samples

Elbow plot showing the natural number of metaclusters in BAL using a maximum of **A)** fourteen and **B)** ten clusters (maxK)

5.4.9 Phenotyping of BAL leukocyte clusters using differential marker expressions

To phenotype the 10 immune cell types identified in BAL samples by FlowSOM analysis, a heatmap was generated showcasing the median marker expressions for each cluster **(Fig. 5.12A)**. The heatmap displayed four distinct populations (cluster 1, 2, 6, 7) expressing $CD206^+$ marker with divergent CD16 and CD14 co-expression. Cluster 3, 4 and 5 were enriched with the proteins $CD20^+$, $CD15^+$, and $CD4^+$ $CD69^+$ $CD103^+$ sequentially. The remaining population clusters 8, 9 and 10 defined by the unbiased analysis contained $CD14^+$, $CD8^+$ and $CD56^+$ cells respectively. To note, there was some spillover of CD206 into other clusters such as cluster 5 which encompassed a $CD3^+$ $TCR\alpha\beta^+$ $CD4^+$ $CD69^+$ $CD103^+$ cell type. This was attributed to the high AF signature of $CD206^+$ cells, signifying that AF removal is not as effective in BAL samples.

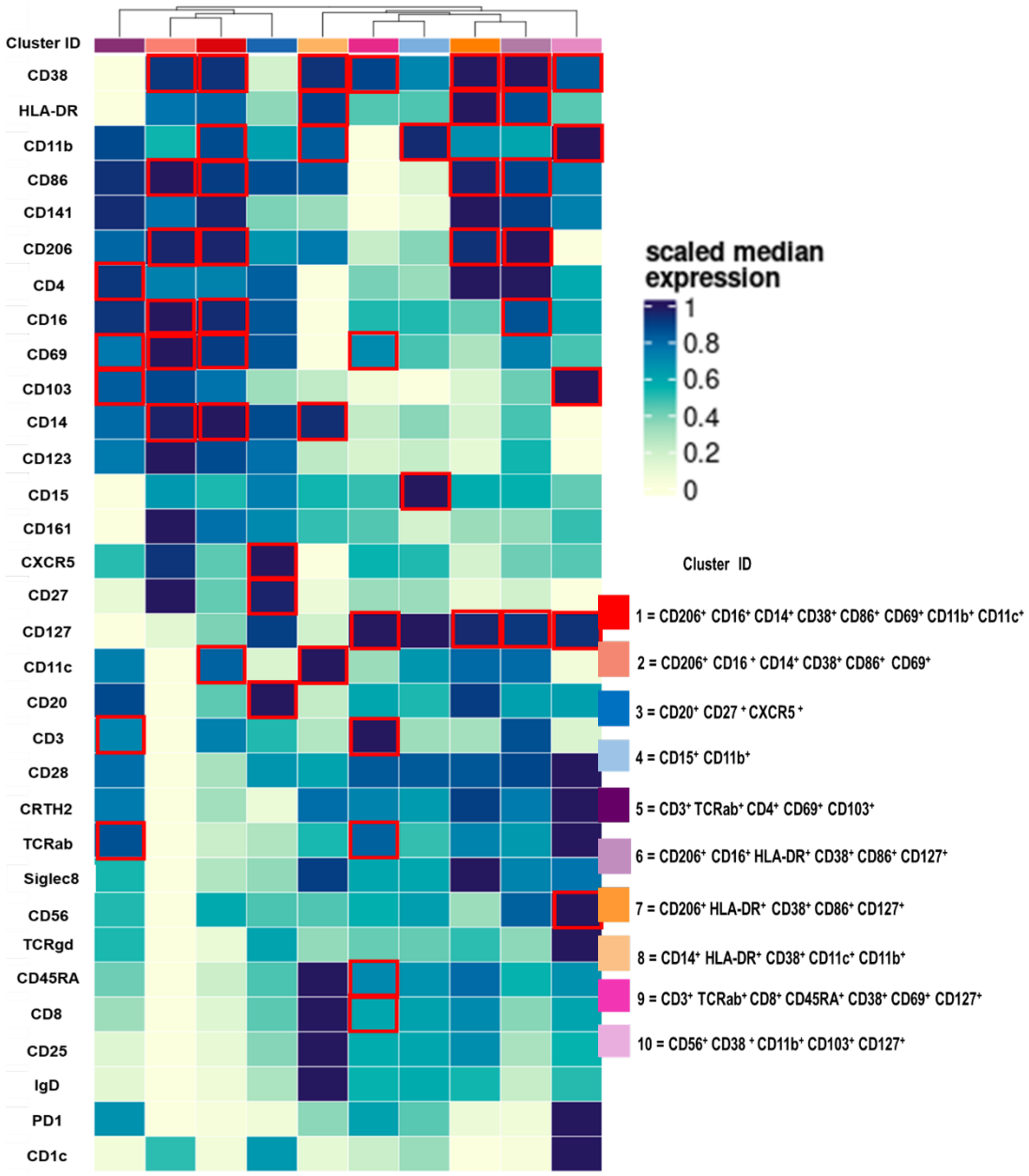


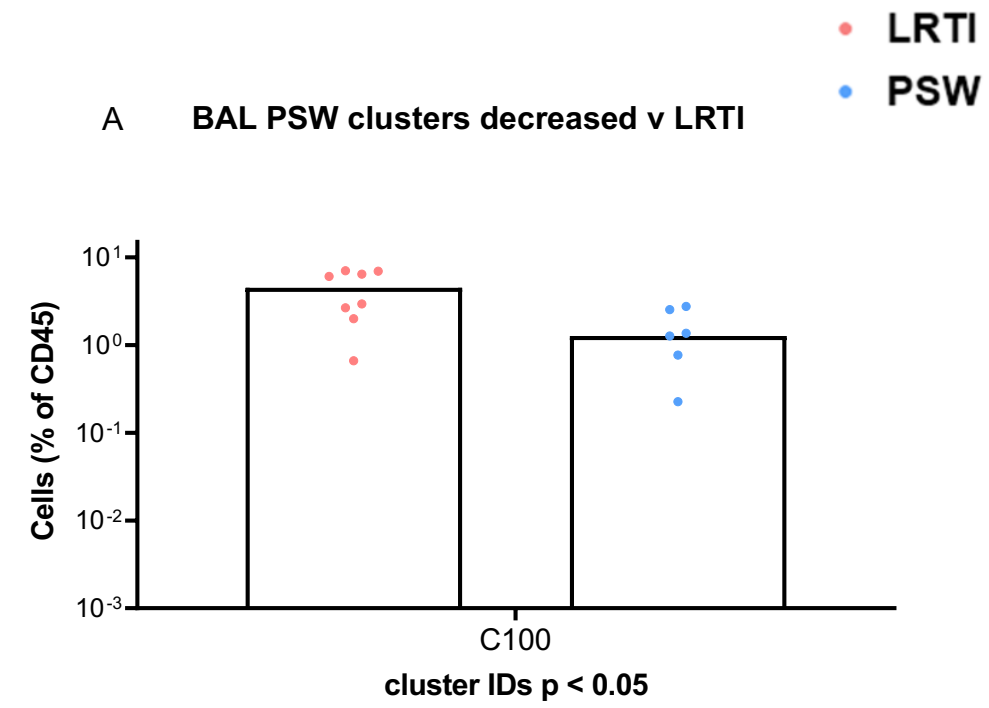
Fig 5.12. Heatmap of BAL immune cell metaclusters defined by marker expressions

Heatmap of median marker intensities was constructed by hierarchical clustering using all markers in the panel except CD45 and live-dead. Red boxes outline the augmented markers within each cluster.

5.4.10 Objective analysis detected four airway immune populations that were differentially expressed in PSWs compared to non-wheeze children

To evaluate the differential abundance of BAL immune cell clusters, multiple comparison analysis was performed between the means of the three disease groups. Notably, there were no considerably expanded populations in PSW airways compared to STRA or LRTIs. Whereas one PSW immune cell clusters designated as C100 was substantially reduced compared to LRTIs **(Fig. 5.13A)**. Additionally, the BAL leukocyte clusters C55, C61 and C85 were decreased in PSWs relative to STRAs **(Fig. 5.13B)**.

Inversely, impartial analysis of STRA BAL immune cell populations deduced that C54 was augmented relative to LRTI **(Fig. 5.14A)**, whereas C100 was notably reduced **(Fig. 5.14B)**.



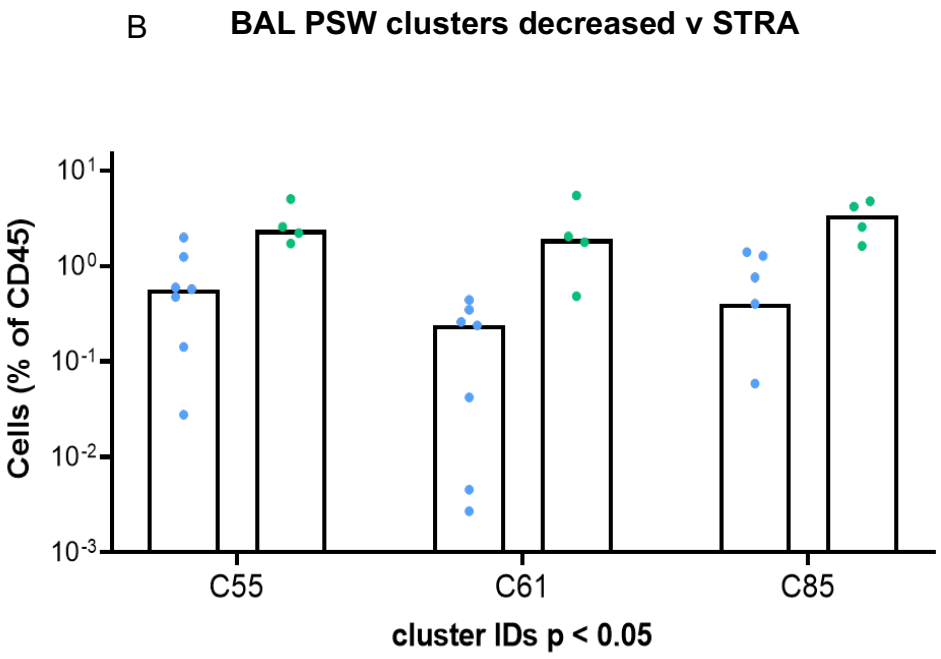


Fig 5.13. The proportion of notably different immune cell types in PSW BAL compared to LRTI and STRAs

Frequency of airway CD45^{+} immune cell clusters that are **A)** decreased in PSWs compared to LRTI and **B)** decreased in PSWs compared to STRA. Statistical significance was measured by an unpaired non-parametric Mann-Whitney U Test.

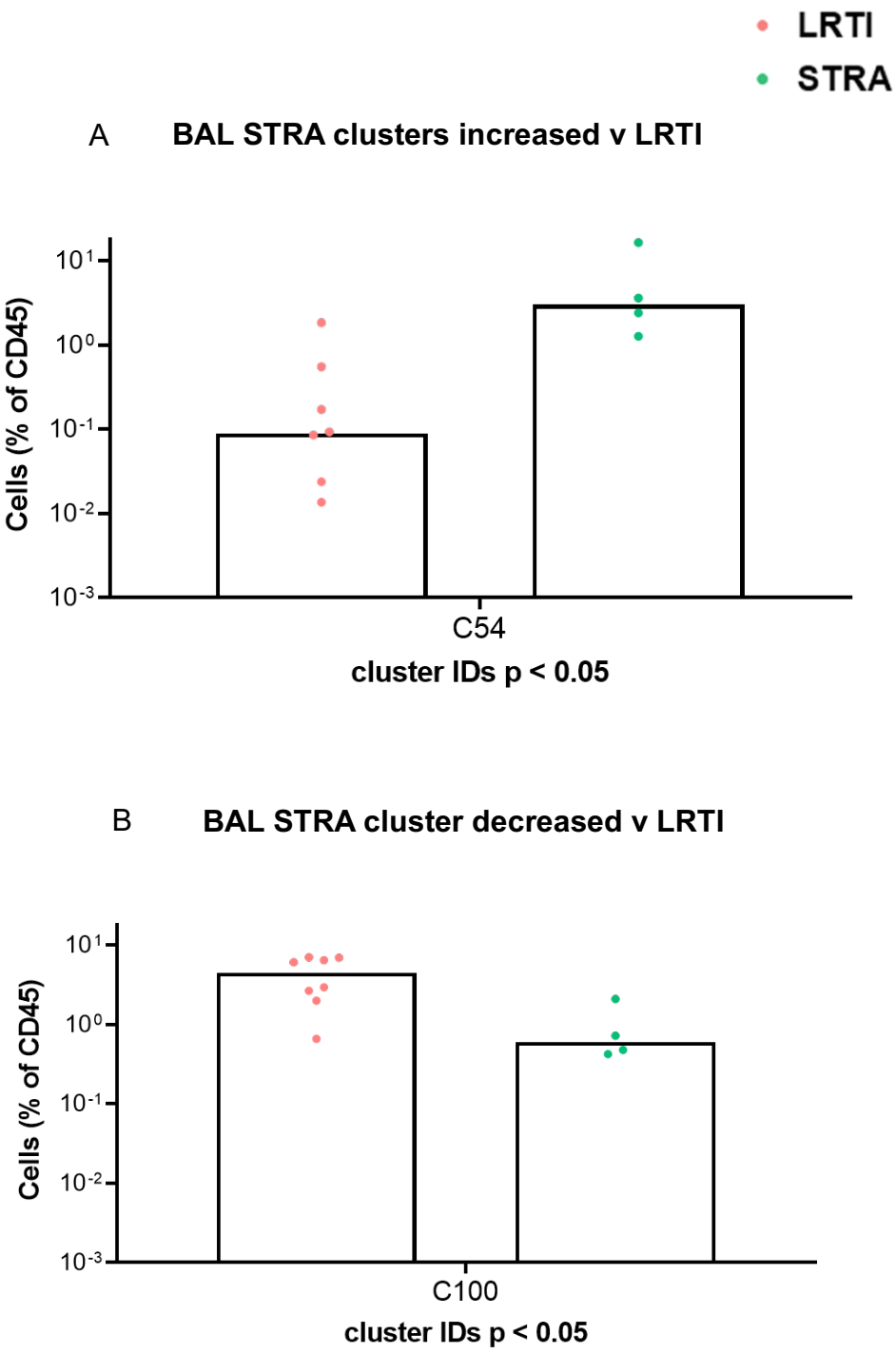


Fig 5.14. The frequency of altered immune cell populations in STRA BAL compared to LRTIs

Frequency of airway CD45^{+} immune cell clusters that are **A)** increased in STRAs compared to LRTI and **B)** decreased in STRAs compared to LRTI controls. Statistical significance was measured by an unpaired non-parametric Mann-Whitney U Test.

5.4.11 Phenotyping of BAL leukocyte clusters using differential marker expressions

To define the airway immune cell types generated by the FlowSOM analysis, a heatmap of median marker intensities was created **(Fig. 5.15)**. The five significantly altered BAL cell clusters were characterised by their protein expression profiles which were outlined in red boxes on the heatmap and tabulated **(Table 5.2)**.

Of the notable airway populations, cluster 100 was reduced in PSW ($p = 0.020513$) and STRA ($p = 0.028283$) compared to LRTIs, indicating a unique feature. Cluster 100 had a $CD3^+$, $TCR\alpha\beta^+$, $CD8^+$, $CD103^+$, $CD69^+$ immune profile. In contrast, the three BAL populations that were markedly reduced in PSWs relative to STRA were designated as cluster 55, 61 and 85. Cluster 55 showed a $CD206^+$, $CD16^+$, $CD127^+$ phenotype and cluster 61 displayed a $CD206^+$, $CD16^+$, $HLA\text{-}DR^+$, $CD69^+$, $CD28^+$ cellular phenotype. Whilst, cluster 85 exhibited $CD206^+$, $CD16^+$, $HLA\text{-}DR^+$, $CD127^+$ expression.

In addition, one immune subset that was elevated in STRA patients compared to LRTI which was denoted as cluster 54 portrayed a $CD206^+$, $CD16^+$, $CD86^+$, $HLA\text{-}DR^+$ surface profile.

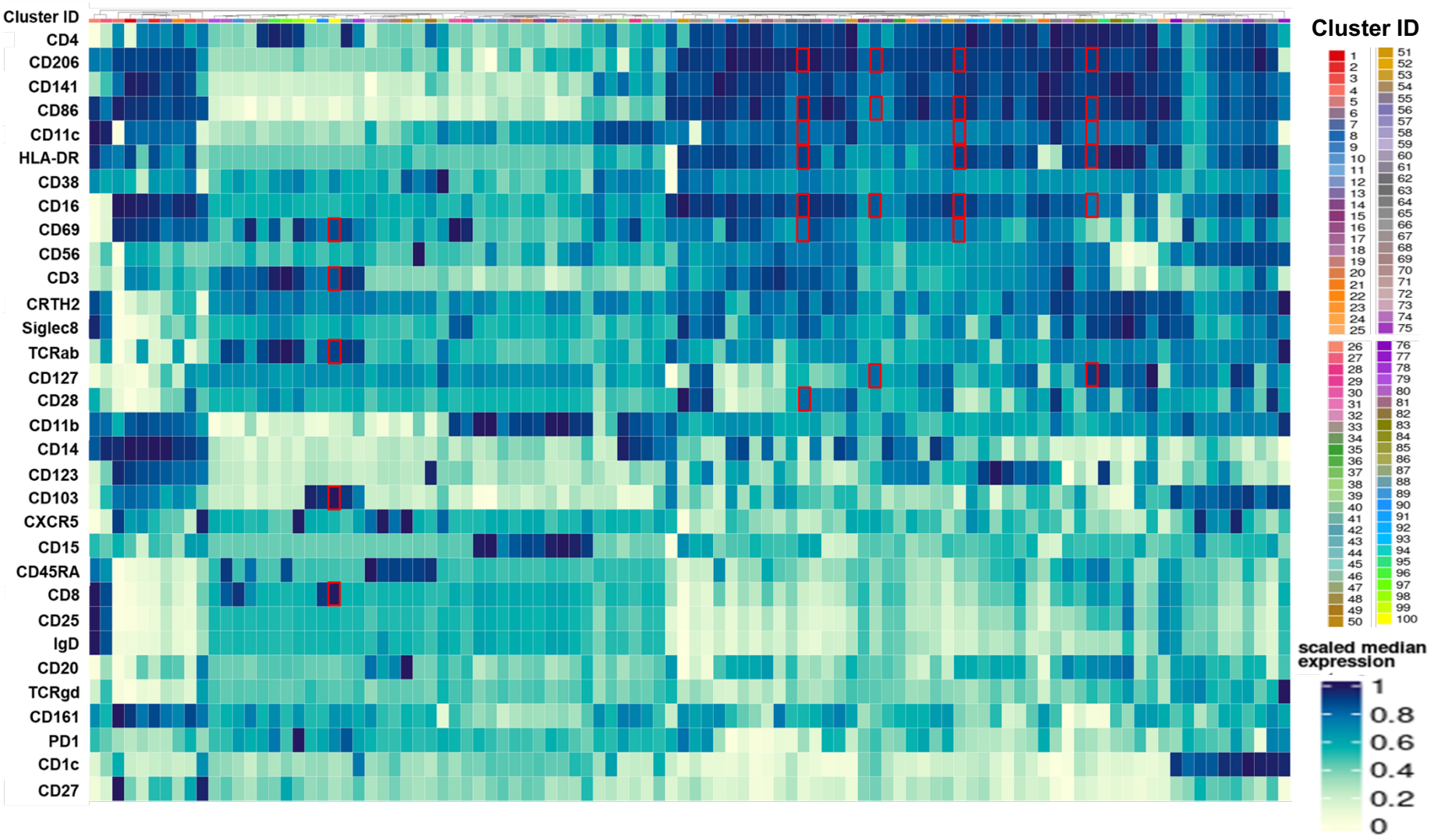

Cluster ID
CD4
CD206
CD141
CD86
CD11c
HLA-DR
CD38
CD16
CD69
CD56
CD3
CRTH2
Siglec8
TCRab
CD127
CD28
CD11b
CD14
CD123
CD103
CXCR5
CD15
CD45RA
CD8
CD25
IgD
CD20
TCRgd
CD161
PD1
CD1c
CD27
Cluster ID
1 2 3 4 5 6 7 8 9 10 11 12 13 14 15 16 17 18 19 20 21 22 23 24 25
51 52 53 54 55 56 57 58 59 60 61 62 63 64 65 66 67 68 69 70 71 72 73 74 75
26 27 28 29 30 31 32 33 34 35 36 37 38 39 40 41 42 43 44 45 46 47 48 49 50
76 77 78 79 80 81 82 83 84 85 86 87 88 89 90 91 92 93 94 95 96 97 98 99 100
scaled median expression
1
0.8
0.6
0.4
0.2
0

Fig 5.15. Heatmap illustration of BAL immune cell clusters outlined by marker expressions

Heatmap of median marker intensities was constructed by hierarchical clustering using all markers in the panel except CD45 and live-dead. Red boxes outline the augmented markers within each cluster.

BAL cluster ID	Disease type	Expression profile	p-value
C54	STRA > LRTI	$CD206^+$ $CD16^+$ $CD86^+$ $CD11c^+$ HLA-DR^+ $CD69^+$	0.008081
C55	PSW < STRA	$CD206^+$ $CD16^+$ $CD86^+$ $CD127^+$	0.012121
C61	PSW < STRA	$CD206^+$ $CD16^+$ $CD86^+$ $CD11c^+$ HLA-DR^+ $CD69^+$ $CD28^+$	0.006061
C85	PSW < STRA	$CD206^+$ $CD16^+$ $CD86^+$ $CD11c^+$ HLA-DR^+ $CD127^+$	0.006061
C100	PSW < LRTI STRA < LRTI	$CD3^+$ $TCRab^+$ $CD8^+$ $CD69^+$ $CD103^+$	0.020513 0.028283

Table 5.2. The cell phenotypes and disease types of the significantly altered clusters in BAL unbiased analysis

Airway immune cell clusters altered between the paediatric clinical diagnoses. Populations were established by FlowSOM clustering and those with p-values below 0.05 are shown.

5.4.12 Supervised gating of airway immune cell clusters identified by unbiased analysis

Similar to the blood analysis, multiple differentially altered BAL cell populations ascertained by impartial clustering were subjectively gated using conventional flow cytometry to determine if they are real immune populations.

Given their significantly low p-values, the three airway populations focused on were cluster 61, 85 and 100. FlowSOM clustering revealed that cluster 100 was distinctly reduced in the airways of PSW ($p = 0.020513$) and STRA ($p = 0.020513$) children relative to LRTIs. To manually gate these population, the highly expressed markers illustrated on the heatmap **(Fig. 5.15)** and table (**Table 5.2)** were examined.

BAL cluster 100 was defined as $CD3^+$ $TCR\alpha\beta^+$ $CD8^+$ $CD69^+$ $CD103^+$ cells. To delineate leukocytes, debris, doublets and dead cells were first removed, followed by gating on $CD45^+$ cells. CD206-negative cells were selected to eliminate the airway macrophage[141]. To concentrate on cluster 100, $CD3^+$ $CD15^-$ cells were gated, followed by $TCR\alpha\beta^+$ and $CD8^+$ cells. Finally, dual expression of $CD69^+$ and $CD103^+$ cells were identified **(Fig 5.16)**. Subjective analysis confirmed that airway $CD8^+$ $CD69^+$ $CD103^+$ cells as a proportion of $CD45^+$ were decreased in PSW and STRA compared to LRTI **(Fig 5.17A, B)**. However as previously stated, STRA BAL samples are limited to 4 patients which should be taken into consideration in these results.

Moreover, the CD8 population in cluster 100 appeared to express CD161 and PD1 which were measured by gMFI to evaluate the difference between the disease cohorts. The results showed that there was no significant difference in the gMFI of CD161 and PD1 on BAL $CD8^+$ cells in PSW **(Fig 5.17C, D)**. or STRA **(Fig 5.17E, F)** compared to infection controls.

Next the immune populations in cluster 61 and 85 were gated based on their marker expressions to compare with the phenotypes obtained by unbiased analysis. As noted earlier, FlowSOM clustering demonstrate that immune clusters 61 ($p = 0.006061$) and 85 ($p = 0.006061$) were reduced in PSW relative to STRA patients (**Table 5.2).** Both airway populations displayed $CD206^+$, $CD16^+$, $HLA\text{-}DR^+$, $CD86^+$, $CD11c^+$ surface proteins but differed by CD127 and CD69 expression which were utilized to characterise the subsets by manual gating **(Fig 5.18)**. Cluster 61 exhibited $CD69^+$ $CD127^-$ phenotype whereas cluster 85 possessed a $CD127^+$ $CD69^-$ profile. To assess the distribution of these immune population between the disease types, the gated cells were assessed as a proportion of $CD45^+$ cells. Contrary to impartial clustering, the data showed that these $CD206^+$ subsets were comparable between PSW and STRA **(Fig 5.19A, B)**. However, these observations are restricted by the number of STRA BAL samples, as an outlier can influence the results.

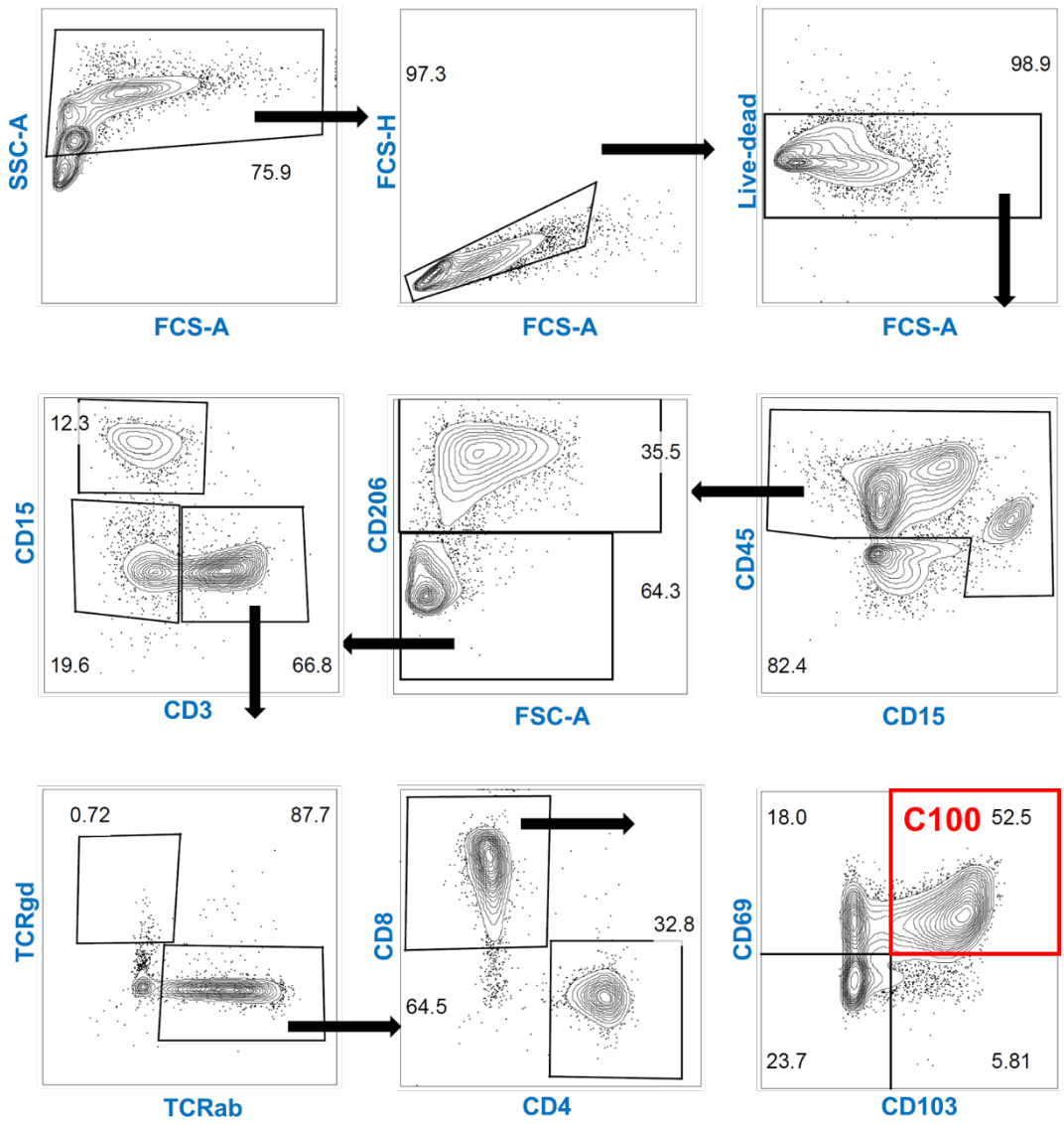


Fig 5.16. Gating strategy for BAL immune cell cluster 100
Schematic of flow cytometry scatter plots showing immune cell gating strategy using LRTI sample. All cells were selected using forward and side scatter. Doublets were removed by gating for single cells using FSC-A versus FSC-H. Live cells were selected as Live-Dead blue negative cells. Viable immune cells were defined as CD45 positive.

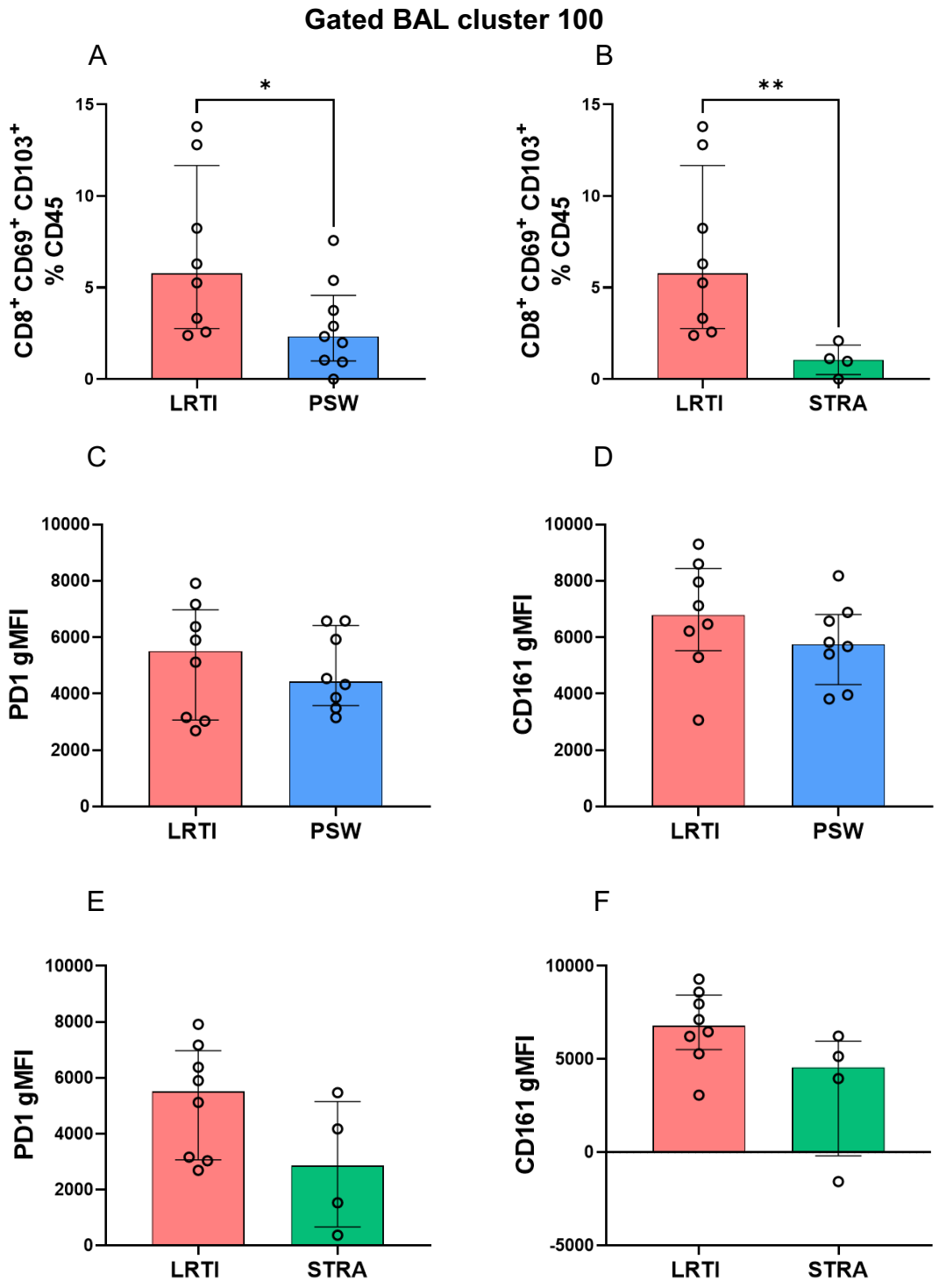


Fig 5.17. The proportion of differential immune cell populations in PSW and STRA BAL compared to LRTIs

Frequency of airway CD45$^+$ immune cell clusters that are **A)** decreased in PSW and **B)** decreased in STRAs compared to LRTI controls. Comparisons of CD8$^+$ CD69$^+$ CD103$^+$ cells gMFI of **C)** PD1 and **D)** CD161 in PSW BAL compared to LRTI and **E)** PD1 and **F)** CD161 in STRA compared to LRTI. Statistical significance was measured by an unpaired non-parametric Mann-Whitney U Test.

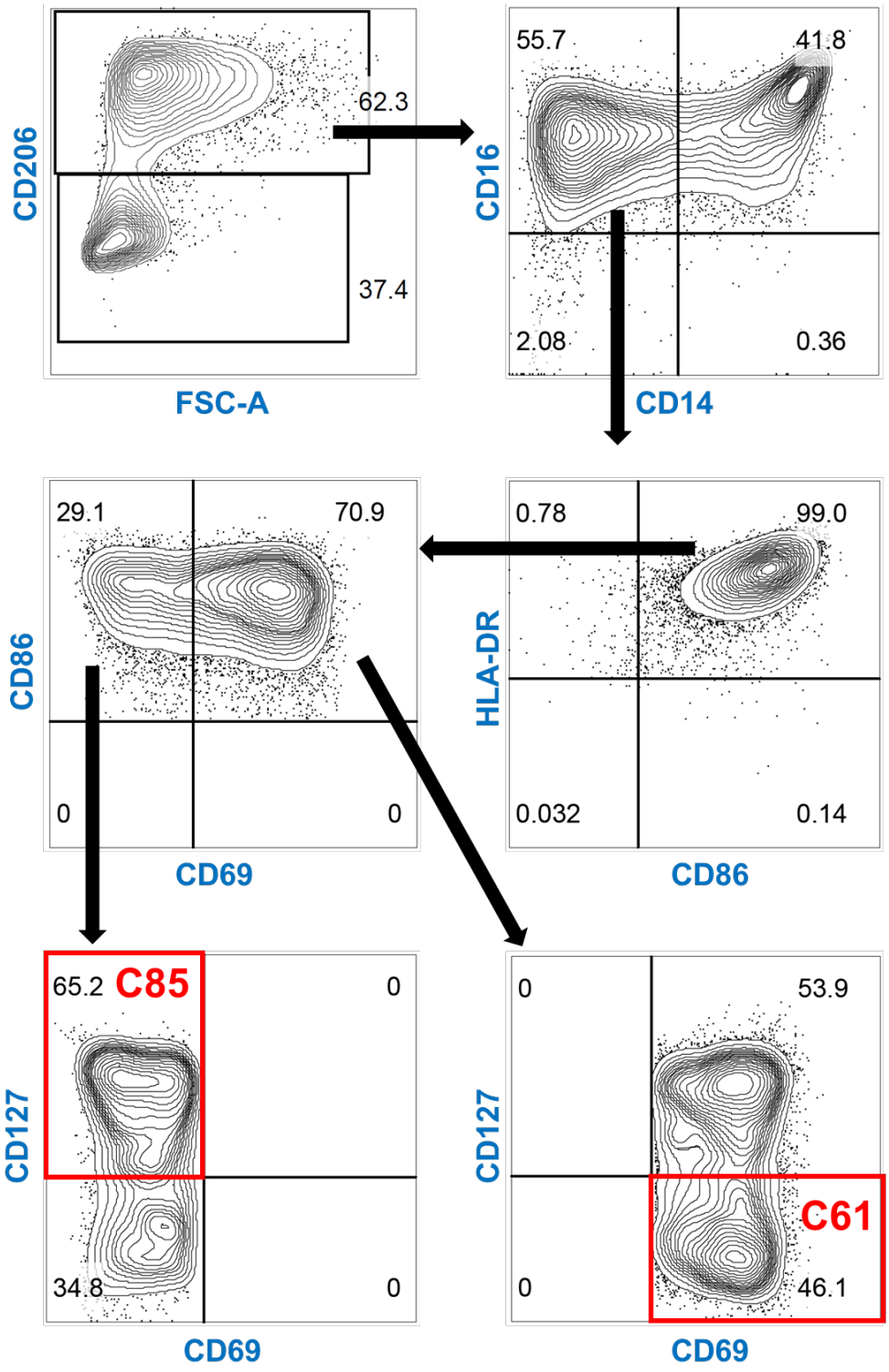


Fig 5.18. Gating strategy for BAL immune cell clusters 61 and 85
Schematic of flow cytometry scatter plots showing immune cell gating strategy using STRA sample. All cells were selected using forward and side scatter. Doublets were removed by gating for single cells using FSC-A versus FSC-H. Live cells were selected as Live-Dead blue negative cells. Viable immune cells were defined as CD45 positive.

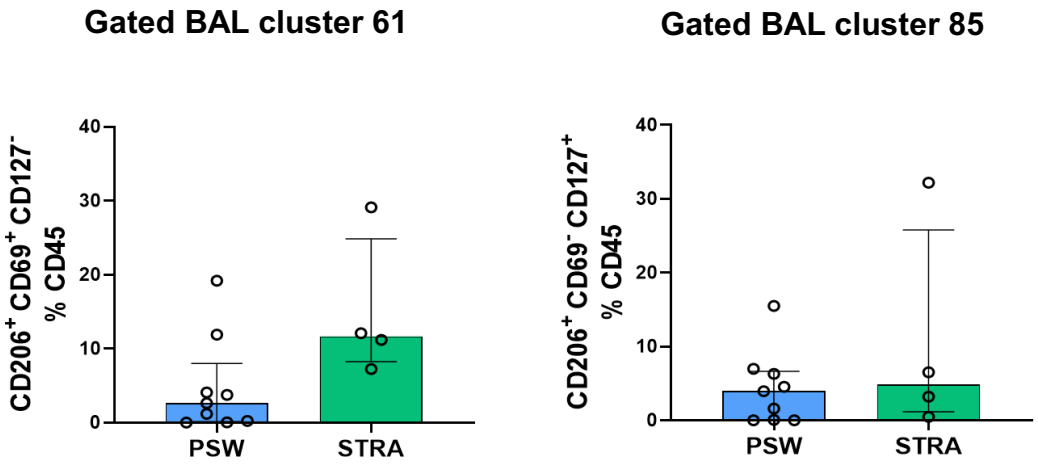


Fig 5.19. Comparisons of gated BAL immune cell clusters between PSW and STRA BAL

Frequency of airway $CD206^+$ immune cells that are **A)** $CD69^+$ $CD127^-$ and **B)** $CD69^-$ $CD127^+$ between PSW and STRA patients. Statistical significance was measured by an unpaired non-parametric Mann-Whitney U Test.

5.5 Discussion

In summary, this chapter highlighted that unbiased clustering can determine distinct immune clusters between paediatric airways disease cohorts. Unsupervised analysis demonstrated that PSWs exhibit several unique immune cell phenotypes in their airways and circulation compared to non-wheezers.

In the periphery for example, the immune cell clusters 46 and 83 which were significantly increased in PSW and LRTI compared to STRA were defined by $CD16^+$ expression with differential levels of molecules associated with antigen presentation and co-stimulation[142]. However, subjective gating of these subsets revealed that the population in cluster 46 described as $CD16^+$ HLA-DR^- $CD86^+$ $CD45RA^-$ was elevated in STRA relative to LRTI patients, whereas the proportion of population cluster 83 designated as $CD16^+$ HLA-DR^+ $CD86^-$ $CD45RA^+$ was comparable between PSW and non-wheezers. According to published literature, leukocytes that express CD16 but lack CD14 are described as nonclassical monocytes[106] and the presence of CD45RA surface expression is associated with activated monocytes, particularly in the blood[64]. Peripheral non-classical monocytes have been reported to monitor the luminal side of the vascular endothelium during steady state and inflammation to remove dead cells and debris[143]. In COPD for example, patients with severe disease had increased circulating non-classical monocytes compared to individuals with moderate COPD or healthy controls[144].

Furthermore, the peripheral immune population designated cluster 77 was substantially elevated in STRA blood compared to PSW in unbiased analysis and was manually identified by conventional gating using the markers $CD3^+$ $TCR\alpha\beta^+$ $CD8^+$ $CD161^+$ $PD1^+$. However, subjective gating showed similar frequencies between the

cohorts. $CD8^+$ $CD161^+$ T cells with low levels of PD1, a marker of T cell exhaustion, have been described as highly cytotoxic against infectious microbes[83].

Research on $CD161^+$ cells in adult asthma have shown that asthmatic patients have a higher circulating proportion compared to healthy subjects[145]. Furthermore, another study examining the frequency T cells subsets with CD161 expression established that adults with allergic rhinitis had a substantially higher proportion of peripheral $CD8^+$ $CD161^+$ T cells[146].

Unbiased analysis of BAL samples uncovered five differential immune populations between the disease types. The three immune populations with the most significant p-value were investigated by subjective gating to delineate any distinct difference between the patient groups.

Both airway population clusters 61 and 85 exhibited $CD206^+$, $CD16^+$, $HLA\text{-}DR^+$, $CD86^+$, $CD11c^+$ proteins, but differed by CD69 and CD127 expression. Although automated analysis found these subsets were decreased in PSW airways compared to STRA children, manual gating did not show any substantial variance. However, as previously noted these results are restricted by the small number of STRA BAL samples and can be influenced by an outlier.

CD206 is a cell surface protein that serves as a useful marker for the identification of macrophages[147] and CD69 which is expressed on macrophages, is a marker of early activation[148]. During inflammation peripheral monocytes relocate to the airway lumen to differentiate into macrophages that perform pro-inflammatory responses[106] thus, these population clusters were characterised as macrophages. Moreover, CD127 is expressed on monocytes and macrophages during inflammation[149]. In the BAL fluid of COVID-19 patients, cells of monocyte and macrophage lineage makeup 64% of

CD127$^+$ cells and were associated with a trademark of human inflammatory conditions in infected tissue[149].

Finally, the BAL immune cluster 100 was defined as CD3$^+$, TCRαβ$^+$, CD8$^+$, CD103$^+$, CD69$^+$ cells that were decreased in PSW and STRA compared to LRTIs. This phenotype was also observed by subjective analysis, thus highlighting that impartial analysis can elucidate exclusive subsets that might be missed during sequential gating of two parameters at a time. Furthermore, existing literature have defined this cell surface phenotype as CD8$^+$ TRM T cells[150] which are found in the lung parenchyma and carry out protective functions against viruses[151]. In RSV condition, the presence of RSV-specific CD8$^+$ TRMS have been correlated with decreased severity and healthy adults challenged with experimental RSV exhibit reduced viral load[152].

Although, unbiased analysis offers many advantages such as probing large datasets and accelerating the duration of phenotyping cell types, it does have some limitations. The flow files used in this unbiased workflow were acquired on the Aurora spectral cytometer using a 34-colour panel. This 5-laser instrument contains 64 fluorescent detector channels which generates extensively large flow files due to the multiple parameters associated with each file. Furthermore, the aurora provides three scatter channels and an AF channel which are all embedded into the flow files[40,41]. This high-dimensionality coupled with the growing list of patient samples necessitates a large computer power that can effectively perform the workflow.

Data quality is an essential criterion for performing automated analysis. To ensure flow files are of high quality, each sample must be manually assessed by gating live, single CD45$^+$ cells. This strategy eliminates artefacts and any samples with residual AF can be inspected. Although a rigours AF extraction workflow was employed, there was still

some spillover of AF from CD206^{+} macrophages in the heatmap of BAL clusters. In addition, FlowSOM clustering is influenced by compensation, AF, event sampling settings and the clustering markers selected.

Another limitation of unbiased analysis is the reproducibility of clustering algorithms, especially when working with continuous patient samples which requires updating datasets and figures. Although the same seed number can be applied, the order of clusters changes after each run which leads to reassessing and annotating the heatmap configuration. Due to these variations, multiple attempts may be needed to ascertain the ideal configurations that provide the most suitable presentations for each dataset. Moreover, FlowSOM is very sensitive to differences between samples analysed together and can assign a cluster to a population that is abundant in one or two patients which was noticeable in the numerous CD206^{+} BAL populations.

5.6 Conclusion

Taken together, this chapter demonstrates that unbiased clustering can discover distinct immune populations between paediatric airways disease cohorts and accelerate immune phenotyping. Objective clustering is comparable to subjective analysis but surpasses in multi-patient studies and provides high quality information on differential cell frequencies across donors.

Chapter 6. Final discussion

6.1 General discussion

Environmental and genetic interactions are driving factors in childhood asthma development and persistence. It is postulated that these interactions initially take place in the womb and early life and shape the immune system. Persistent low lung function trajectory is a pathological feature of asthma which is displayed by age 6 and continues into adulthood. This poor lung performance is triggered by many factors including viral infections and allergic sensitization which leads to increased airway smooth muscle mass that is observed in infants with sever wheeze[32]. Furthermore, airway smooth muscle remodelling is associated with airway obstruction and inflammation characterised by the recruitment of inflammatory cells and secretion of cytokines[153]. Thus, growing evidence indicate that early-life therapeutic interventions could offer the best opportunity to alter asthma trajectory.

Moreover, it has been established that PSWs are often overprescribed corticosteroid medication prior to asthma diagnosis[14]. Given that asthma is distinguished by numerous immunological sub-phenotypes, better characterisation of immune cell phenotypes in early-life is required to establish effective therapies. The focus of this thesis was to phenotype airway and peripheral cell types that are involved in the inflammatory process of wheeze and atopic asthma. By addressing the research aims, insight was obtained on differential immune phenotypes between wheeze and non-wheezers and concepts were outlined for further investigation which are discussed in this chapter.

6.2 Spectral cytometry can be used to accurately identify 33 immunological surface markers simultaneously

A novel spectral cytometry technique was developed to study restricted airway and peripheral samples in children with PSW and STRA. To achieve this, a 34-colour panel was optimized to examine the phenotypes of lymphocytes, monocytes and granulocytes and outline the differential distributions between disease groups. In work described in chapter 3, the data showed that most of the antibody markers were distinguishable at 1 in 100 dilutions. However, several markers required higher concentrations including CD69, CD127 and CD141. This outcome was attributed to the characteristics of the expression density of the protein or the frequency of the cell type. As CD69 and CD127 are activation markers associated with differentiated cells[47,154], naturally their staining index will result in low intensity in the periphery. Additionally, if there is a low frequency of specific positive cells, titrations will be difficult to evaluate therefore there is a need for higher concentration of antibody such as CD141 antibody which is ascribed to DCs[137]

Overall, using subdivided FM-panel (fluorescence-minus) controls as a practical alternative to 33 single stain FMOs were adequate in setting population gating boundaries. However, AF extraction was major limitation of this spectral cytometry approach. Although an extensive AF removal workflow was developed, unmixing of CD206 and CD16 markers were imperfect as they are expressed on highly autofluorescent macrophages which appeared to spread across channels in manual gating and unbiased analysis. While the batch unmixing protocol using a median unstained control was adequate for this limited study, overtime the sample variance of large clinical studies will increase inaccuracies. Future work that should be conducted

to address this would be to combine samples from both disease and healthy patients for unstained and FM-panel controls.

A notable limitation of the 34-colour panel is the lack of transcription factors (TFs) and cytokines. Previous studies using conventional flow cytometry have utilized the expression of GATA-3 TF and the cytokines IL-13 and IL-4 to determine the presence of inflammatory ILC2s and Th2 cells in asthma pathogenesis[37,155]. In this thesis, ILC2s were phenotyped by gating a lymphoid population and sequentially removing cell lineage markers and eventually gating $CRTH2^+$ and $CD127^+$ cells. However, as ILC1s share the expression of CD127, research shows that GATA3 is essential for the development of ILC2s which distinguish them from ILC1s[114].

Thus, the ILC data presented in this thesis is potentially inaccurate and a better panel tailored to ILC2s would be more accurate. However, adding intracellular markers to the panel would present different challenges that would increase the complexity of the antibody-fluorophore combinations and the spectral unmixing protocol. As intracellular staining involves additional fixation and permeabilization steps this would further increase AF signatures[156].

6.3 Preschool wheeze children have a distinct immune cell profile compared to non-wheezers

As discussed in chapter 4, the aim of this study was to phenotype the cellular profile of the lower airway and peripheral immune cells in PSWs compared to age-matched non-wheeze disease controls. School-aged STRA children were also included to understand the immunology of paediatric asthma phenotypes compared to early life. The results showed that PSWs had several different immune phenotypes compared

to children with LRTI and STRA. Circulating $CD4^+$ $CD25^+$ $CD127^-$ T cells, $CD15^+$ neutrophils and $CD14^+$ $CD16^-$ classical monocytes were decreased in PSWs compared to children with LRTIs. Additionally, PSWs displayed reduced airway $CD8^+$ $CD25^+$ $CD127^-$ T cells and a positive association between serum IgE levels and blood eosinophils indicating heightened exacerbations. Conversely, STRA children exhibited decreased peripheral $CD4^+$ $CD45RA^+$ T cells, $CD3^+$ $CD4^+$ $CD56^+$ NKT cells but elevated $CD4^+$ $CD25^+$ $CD127^-$ T cells compared to PSWs. The decline in naïve $CD4^+$ $CD45RA^+$ T cells in STRA blood was also significant compared to LRTIs. Ageing was considered to be a contributing factor to this decrease as the thymus production of naïve T cells culminates in year one of life[96]. Given that the median age of STRA children is 5-times and 3-times greater than that of PSW and LRTIs subjects respectively, the age disparity underscored a major drawback of the study.

Furthermore, another key limiting factor in this study was the small number of BAL STRA samples. Due to ethical regulations, children with STRA can only undergo bronchoscopy during steady disease state, thus restricting the number of BAL samples collected over time. Ultimately a sample size of 4 is inadequate to establish accurate conclusions.

Interestingly, several PSW patients displayed a pronounced Lin^- $CRTH2^+$ $CD127^+$ ILC population in their blood which emphasised a potential sub-phenotype. While ILC2s have been described to be elevated in the blood of PSWs during exacerbations[123], their relevance in PSW airways remains an open question. Hence, future work should investigate ILC2 sub-phenotypes in a greater number of BAL samples from PSW patients.

6.4 Automated analysis can detect distinct immune cell clusters overlooked by manual gating

Unsupervised clustering analysis was implemented to uncover any unique airway or peripheral sub-phenotypes that may have been missed by conventional two-dimensional flow analysis. Multiple differentially expressed immune populations were identified in blood and BAL. To determine if the immune subsets identified by unbiased analysis were real populations, manual gating was performed using the high and low expressed markers generated by clustering heatmaps. Three immune cluster populations from blood and BAL samples with the most significantly low p-values were examined by flow cytometry. While these immune cell clusters were detectable by subjective gating, only the BAL population denoted as cluster 100 was significantly different between the disease groups (%CD45). Cluster 100 was described as $CD3^+$, $TCR\alpha\beta^+$, $CD8^+$, $CD103^+$, $CD69^+$ cells that were decreased in PSW and STRA compared to LRTIs. This confirmed that unsupervised analysis can elucidate exclusive subsets that might be missed during conventional sequential gating method. This cell type was related to $CD8^+$ TRM T cells[150] which exist in the lungs and perform protective functions against viruses[151].

In chapter 4 which covered cellular phenotyping of immune subsets in blood and BAL samples, this airway $CD8^+$, $CD103^+$, $CD69^+$ T cell subset was examined but no difference was observed between the cohorts (%CD8). This difference could be that in chapter 4 the gating strategy was specific to identify all T cell subsets whereby $CD45RA^+$ and $CD25^+$ cells were first gated out before focusing on $CD103^+$, $CD69^+$ T cell and may have influenced the remaining proportions. As noted in chapter 5, the hierarchy of makers used to generate the clusters is unknown in unbiased analysis.

In addition, automated clustering algorithms are sensitive to high AF expression and cannot accurately separate the AF spread of problematic markers, such as CD206 and CD16 expressed by macrophages from unrelated population clusters. An alternative solution to conduct objective analysis on spectral flow data would be to import flow files containing only a specific population, where each cell type is isolated using lineage-specific markers such as CD3 and CD15. This approach avoids analysing macrophages alongside less AF populations, however the immune populations cannot be compared in the analysis.

6.5 Conclusion

Collectively, the work presented in this thesis has demonstrated that high parameter immune cell phenotyping can identify unique immunological profiles in PSW children compared to non-wheeze disease controls and automated analysis can uncover unique immune cell subsets that were overlooked in standard flow gating. This thesis provides a basis to further pursue the understanding of the pathophysiology and immunology of early-life wheeze and the development of school-aged asthma phenotypes.

7. References

1. Bissonnette EY, Lauzon-Joset JF, Debley JS, Ziegler SF. Cross-Talk Between Alveolar Macrophages and Lung Epithelial Cells is Essential to Maintain Lung Homeostasis. *Front Immunol*. 2020;11(October):1-12. doi:10.3389/fimmu.2020.583042

2. Miller AJ, Spence JR. In vitro models to study human lung development, disease and homeostasis. *Physiology*. 2017;32(3):246-260. doi:10.1152/physiol.00041.2016

3. Mendez R, Banerjee S, Bhattacharya SK, Banerjee S. Lung inflammation and disease: A perspective on microbial homeostasis and metabolism. *IUBMB Life*. 2019;71(2):152-165. doi:10.1002/iub.1969

4. Quinton LJ, Walkey AJ, Mizgerd JP. Integrative physiology of pneumonia. *Physiol Rev*. 2018;98(3):1417-1464. doi:10.1152/PHYSREV.00032.2017

5. Reddel HK, Bacharier LB, Bateman ED, et al. Global Initiative for Asthma Strategy 2021: executive summary and rationale for key changes. *Eur Respir J*. 2022;59(1). doi:10.1183/13993003.02730-2021

6. Delimpoura V, Bostantzoglou C, Liu N, Nenna R. Novel therapies for severe asthma in children and adults. *Breathe*. 2018;14(1):59-62. doi:10.1183/20734735.018917

7. Côté A, Godbout K, Boulet LP. The management of severe asthma in 2020. *Biochem Pharmacol*. 2020;179:114112. doi:10.1016/j.bcp.2020.114112

8. Bossley CJ, Fleming L, Gupta A, et al. Pediatric severe asthma is characterized by eosinophilia and remodeling without TH2 cytokines. *J Allergy*

Clin Immunol. 2012;129(4):1-23. doi:10.1016/j.jaci.2012.01.059

9. Kuruvilla ME, Lee FEH, Lee GB. Understanding Asthma Phenotypes, Endotypes, and Mechanisms of Disease. *Clin Rev Allergy Immunol*. 2019;56(2):219-233. doi:10.1007/s12016-018-8712-1

10. Global Initiative for Asthma. Global Initiative for Asthma: Global strategy for asthma management and prevention (Updated 2020). *Rev Fr d'Allergologie d'Immunologie Clin*. 2020;36(6):685-704. doi:10.1016/S0335-7457(96)80056-6

11. Del Giacco SR, Bakirtas A, Bel E, et al. Allergy in severe asthma. *Allergy Eur J Allergy Clin Immunol*. 2017;72(2):207-220. doi:10.1111/all.13072

12. Scotney E, Saglani S. Diagnosis and Management of Problematic Severe Asthma. *Acta Med Acad*. 2020;49(2):117-129. doi:10.5644/ama2006-124.291

13. Lloyd CM, Saglani S. Opening the Window of Immune Opportunity: Treating Childhood Asthma. *Trends Immunol*. 2019;40(9):786-798. doi:10.1016/j.it.2019.07.004

14. Bloom CI, Franklin C, Bush A, Saglani S, Quint JK. Burden of preschool wheeze and progression to asthma in the UK: Population-based cohort 2007 to 2017. *J Allergy Clin Immunol*. Published online 2021. doi:10.1016/j.jaci.2020.12.643

15. Robinson PFM, Fontanella S, Ananth S, et al. Recurrent Severe Preschool Wheeze: From Prespecified Diagnostic Labels to Underlying Endotypes. *Am J Respir Crit Care Med*. 2021;204(5):523-535. doi:10.1164/rccm.202009-3696oc

16. Robinson PFM, Pattaroni C, Cook J, et al. Lower airway microbiota associates with inflammatory phenotype in severe preschool wheeze. *J Allergy Clin*

Immunol. 2019;143(4):1607-1610.e3. doi:10.1016/j.jaci.2018.12.985

17. Bonner K, Scotney E, Saglani S. Factors and mechanisms contributing to the development of preschool wheezing disorders. *Expert Rev Respir Med*. 2021;15(6):745-760. doi:10.1080/17476348.2021.1913057

18. Scotney E, Burchett S, Goddard T, Saglani S. Pediatric problematic severe asthma: Recent advances in management. *Pediatr Allergy Immunol*. Published online 2021. doi:10.1111/pai.13543

19. Hedlin G, Bush A, Lødrup Carlsen K, et al. Problematic severe asthma in children, not one problem but many: A GA 2LEN initiative. *Eur Respir J*. 2010;36(1):196-201. doi:10.1183/09031936.00104809

20. Haktanir Abul M, Phipatanakul W. Severe asthma in children: Evaluation and management. *Allergol Int*. 2019;68(2):150-157. doi:10.1016/j.alit.2018.11.007

21. Vu LD, Siefker D, Jones TL, et al. Elevated levels of type 2 respiratory innate lymphoid cells in human infants with severe respiratory syncytial virus bronchiolitis. *Am J Respir Crit Care Med*. 2019;200(11):1414-1423. doi:10.1164/rccm.201812-2366OC

22. Akdis CA, Arkwright PD, Brüggen MC, et al. Type 2 immunity in the skin and lungs. *Allergy Eur J Allergy Clin Immunol*. 2020;75(7):1582-1605. doi:10.1111/all.14318

23. Lloyd CM, Saglani S. Epithelial cytokines and pulmonary allergic inflammation. *Curr Opin Immunol*. 2015;34:52-58. doi:10.1016/j.coi.2015.02.001

24. Palikhe NS, Laratta C, Nahirney D, et al. Elevated levels of circulating CD4+CRTh2+ T cells characterize severe asthma. *Clin Exp Allergy*.

2016;46(6):825-836. doi:10.1111/cea.12741

25. Vroman H, Hendriks RW, Kool M. Dendritic cell subsets in asthma: Impaired Tolerance or exaggerated inflammation? *Front Immunol*. 2017;8(AUG):941. doi:10.3389/fimmu.2017.00941

26. Hayashi Y, Ishii Y, Hata-Suzuki M, et al. Comparative analysis of circulating dendritic cell subsets in patients with atopic diseases and sarcoidosis. *Respir Res*. 2013;14(1):1. doi:10.1186/1465-9921-14-29

27. Dua B, Watson RM, Gauvreau GM, O'Byrne PM. Myeloid and plasmacytoid dendritic cells in induced sputum after allergen inhalation in subjects with asthma. *J Allergy Clin Immunol*. 2010;126(1):133-139. doi:10.1016/j.jaci.2010.04.006

28. El-Gammal A, Oliveria JP, Howie K, et al. Allergen-induced changes in bone marrow and airway dendritic cells in subjects with asthma. *Am J Respir Crit Care Med*. 2016;194(2):169-177. doi:10.1164/rccm.201508-1623OC

29. Crisford H, Sapey E, Rogers GB, et al. Neutrophils in asthma: The good, the bad and the bacteria. *Thorax*. 2021;76(8):835-844. doi:10.1136/thoraxjnl-2020-215986

30. Lloyd CM, Saglani S. Development of allergic immunity in early life. *Immunol Rev*. 2017;278(1):101-115. doi:10.1111/imr.12562

31. Johansson C, Kirsebom FCM. Neutrophils in respiratory viral infections. *Mucosal Immunol*. 2021;14(4):815-827. doi:10.1038/s41385-021-00397-4

32. Pijnenburg MW, Fleming L. Advances in understanding and reducing the burden of severe asthma in children. *Lancet Respir Med*. 2020;8(10):1032-

1044. doi:10.1016/S2213-2600(20)30399-4

33. Andersson CK, Adams A, Nagakumar P, et al. Intraepithelial neutrophils in pediatric severe asthma are associated with better lung function. *J Allergy Clin Immunol*. 2017;139(6):1819-1829.e11. doi:10.1016/j.jaci.2016.09.022

34. Akdis CA, Arkwright PD, Brüggen MC, et al. Type 2 immunity in the skin and lungs. *Allergy Eur J Allergy Clin Immunol*. 2020;75(7):1582-1605. doi:10.1111/all.14318

35. Simoni Y, Fehlings M, Kløverpris HN, et al. Human Innate Lymphoid Cell Subsets Possess Tissue-Type Based Heterogeneity in Phenotype and Frequency. *Immunity*. 2017;46(1):148-161. doi:10.1016/j.immuni.2016.11.005

36. Nagakumar P, Denney L, Fleming L, Bush A, Lloyd CM, Saglani S. Type 2 innate lymphoid cells in induced sputum from children with severe asthma. *J Allergy Clin Immunol*. 2016;137(2):624-626.e6. doi:10.1016/j.jaci.2015.06.038

37. Nagakumar P, Puttur F, Gregory LG, et al. Pulmonary type-2 innate lymphoid cells in paediatric severe asthma: phenotype and response to steroids. *Eur Respir J*. 2019;54(2). doi:10.1183/13993003.01809-2018

38. Nowicka M, Krieg C, Weber LM, et al. CyTOF workflow: Differential discovery in high-throughput high-dimensional cytometry datasets. *F1000Research*. 2017;6:748. doi:10.12688/f1000research.11622.1

39. Gentleman RC, Carey VJ, Bates DM, et al. Bioconductor: open software development for computational biology and bioinformatics. *Genome Biol*. 2004;5(10).

40. Ferrer-Font L, Pellefigues C, Mayer JU, Small SJ, Jaimes MC, Price KM.

Panel Design and Optimization for High-Dimensional Immunophenotyping Assays Using Spectral Flow Cytometry. *Curr Protoc Cytom*. 2020;92(1). doi:10.1002/cpcy.70

41. Ferrer-Font L, Small SJ, Lewer B, et al. Panel Optimization for High-Dimensional Immunophenotyping Assays Using Full-Spectrum Flow Cytometry. *Curr Protoc*. 2021;1(9). doi:10.1002/cpz1.222

42. Li F, Yang M, Wang L, et al. Autofluorescence contributes to false-positive intracellular Foxp3 staining in macrophages: A lesson learned from flow cytometry. *J Immunol Methods*. 2012;386(1-2):101-107. doi:10.1016/j.jim.2012.08.014

43. Adewoyin AS, Nwogoh B. Peripheral blood film - a review. *Ann Ibadan Postgrad Med*. 2014;12(2):71-79. https://www.ncbi.nlm.nih.gov/pmc/articles/PMC4415389/

44. Vira S, Mekhedov E, Humphrey G, Blank PS. Fluorescent-labeled antibodies: Balancing functionality and degree of labeling. *Anal Biochem*. 2010;402(2):146-150. doi:10.1016/j.ab.2010.03.036

45. Fox A, Dutt TS, Karger B, Obregón-Henao A, Anderson GB, Henao-Tamayo M. Acquisition of High-Quality Spectral Flow Cytometry Data. *Curr Protoc Cytom*. 2020;93(1). doi:10.1002/cpcy.74

46. Niewold P, Ashhurst TM, Smith AL, King NJC. Evaluating spectral cytometry for immune profiling in viral disease. *Cytom Part A*. 2020;97(11):1165-1179. doi:10.1002/cyto.a.24211

47. Schenkel JM, Masopust D. Tissue-resident memory T cells. *Immunity*.

2014;41(6):886-897. doi:10.1016/j.immuni.2014.12.007

48. Garratt LW, Wright AKA, Ranganathan SC, et al. Small macrophages are present in early childhood respiratory disease. *J Cyst Fibros*. 2012;11(3):201-208. doi:10.1016/j.jcf.2011.11.008

49. Nguyen R, Perfetto S, Mahnke YD, Chattopadhyay P, Roederer M. Quantifying spillover spreading for comparing instrument performance and aiding in multicolor panel design. *Cytom Part A*. 2013;83 A(3):306-315. doi:10.1002/cyto.a.22251

50. Roederer M. Compensation in flow cytometry. *Curr Protoc Cytom*. 2002;Chapter 1. doi:10.1002/0471142956.cy0114s22

51. Roederer M. Spectral compensation for flow cytometry: Visualization artifacts, limitations, and caveats. *Cytometry*. 2001;45(3):194-205. doi:10.1002/1097-0320(20011101)45:3<194::AID-CYTO1163>3.0.CO;2-C

52. McCausland M, Lin YD, Nevers T, Groves C, Decman V. With great power comes great responsibility: High-dimensional spectral flow cytometry to support clinical trials. *Bioanalysis*. 2021;13(21):1597-1616. doi:10.4155/bio-2021-0201

53. Malmström K, Lehto M, Majuri ML, et al. Bronchoalveolar lavage in infants with recurrent lower respiratory symptoms. *Clin Transl Allergy*. 2014;4(1):1-7. doi:10.1186/2045-7022-4-35

54. Stanzel F. Bronchoalveolar Lavage. In: *Principles and Practice of Interventional Pulmonology*. Springer New York; 2013:165-176. doi:10.1007/978-1-4614-4292-9_16

55. Davis RW, Timlin JA, Kaiser JN, Sinclair MB, Jones HDT, Lane TW. Accurate detection of low levels of fluorescence emission in autofluorescent background: Francisella-infected macrophage cells. In: *Microscopy and Microanalysis*. Vol 16. ; 2010:478-487. doi:10.1017/S1431927610000322

56. Garn H. Specific aspects of flow cytometric analysis of cells from the lung. *Exp Toxicol Pathol*. 2006;57(SUPPL. 2):21-24. doi:10.1016/j.etp.2006.02.009

57. Baráth S, Mezei ZA, Száraz-Széles M, Hevessy Z. Combined use of different antibody clones improves the efficiency of human leukocyte antigen B27 detection by flow cytometry. *Cytom Part B - Clin Cytom*. 2022;102(3):239-245. doi:10.1002/cyto.b.21989

58. Spitzer MH, Nolan GP. Mass Cytometry: Single Cells, Many Features. *Cell*. 2016;165(4):780-791. doi:10.1016/j.cell.2016.04.019

59. Bush A, Saglani S. Management of severe asthma in children. *Lancet*. 2010;376(9743):814-825. doi:10.1016/S0140-6736(10)61054-9

60. Poorebrahim M, Quiros-Fernandez I, Fakhr E, Cid-Arregui A. Generation of CAR-T cells using lentiviral vectors. In: *Methods in Cell Biology*. Vol 167. Academic Press; 2022:39-69. doi:10.1016/bs.mcb.2021.07.001

61. Kirk AD. Antilymphocyte Globulin, Monoclonal Antibodies, and Fusion Proteins. In: *Kidney Transplantation-Principles and Practice: Seventh Edition*. W.B. Saunders; 2013:287-313. doi:10.1016/B978-1-4557-4096-3.00020-9

62. Machura E, Mazur B, Pieniążek W, Karczewska K. Expression of naive/memory (CD45RA/CD45RO) markers by peripheral blood CD4 + and CD8 + T cells in children with asthma. *Arch Immunol Ther Exp (Warsz)*.

2008;56(1):55-62. doi:10.1007/s00005-008-0005-6

63. MORIKAWA K, OSEKO F, MORIKAWA S. The Role of CD45RA on Human B-Cell Function: Anti-CD45RA Antibody (Anti-2H4) Inhibits the Activation of Resting B Cells and Antibody Production of Activated B Cells Independently in Humans. *Scand J Immunol Suppl*. 1991;34(3):273-283. doi:10.1111/j.1365-3083.1991.tb01547.x

64. Nagasawa T, Kobayashi H, Aramaki M, Kiji M, Oda S, Izumi Y. Expression of CD14, CD16 and CD45RA on monocytes from periodontitis patients. *J Periodontal Res*. 2004;39(1):72-78. doi:10.1111/j.1600-0765.2004.00713.x

65. Merad M, Sathe P, Helft J, Miller J, Mortha A. The dendritic cell lineage: Ontogeny and function of dendritic cells and their subsets in the steady state and the inflamed setting. *Annu Rev Immunol*. 2013;31:563-604. doi:10.1146/annurev-immunol-020711-074950

66. Golinski ML, Demeules M, Derambure C, et al. CD11c+ B Cells Are Mainly Memory Cells, Precursors of Antibody Secreting Cells in Healthy Donors. *Front Immunol*. 2020;11:32. doi:10.3389/fimmu.2020.00032

67. Van Acker HH, Capsomidis A, Smits EL, Van Tendeloo VF. CD56 in the immune system: More than a marker for cytotoxicity? *Front Immunol*. 2017;8(JUL):1. doi:10.3389/fimmu.2017.00892

68. Recio MJ, Moreno-Pelayo MA, Kiliç SS, et al. Differential Biological Role of CD3 Chains Revealed by Human Immunodeficiencies. *J Immunol*. 2007;178(4):2556-2564. doi:10.4049/jimmunol.178.4.2556

69. Shi Z, Zhang Q, Yan H, et al. More than one antibody of individual B cells

revealed by single-cell immune profiling. *Cell Discov*. 2019;5(1):1-13. doi:10.1038/s41421-019-0137-3

70. Yeap WH, Wong KL, Shimasaki N, et al. CD16 is indispensable for antibodydependent cellular cytotoxicity by human monocytes. *Sci Rep*. 2016;6(1):1-22. doi:10.1038/srep34310

71. Létourneau S, Krieg C, Pantaleo G, Boyman O. IL-2- and CD25-dependent immunoregulatory mechanisms in the homeostasis of T-cell subsets. *J Allergy Clin Immunol*. 2009;123(4):758-762. doi:10.1016/j.jaci.2009.02.011

72. Pavlasova G, Mraz M. The regulation and function of CD20: An “enigma” of B-cell biology and targeted therapy. *Haematologica*. 2020;105(6):1494-1506. doi:10.3324/haematol.2019.243543

73. Carrette F, Surh CD. IL-7 signaling and CD127 receptor regulation in the control of T cell homeostasis. *Semin Immunol*. 2012;24(3):209-217. doi:10.1016/j.smim.2012.04.010

74. Couture A, Garnier A, Docagne F, et al. HLA-class II artificial antigen presenting cells in CD4+ T cell-based immunotherapy. *Front Immunol*. 2019;10(MAY):1081. doi:10.3389/fimmu.2019.01081

75. Goronzy JJ, Weyand CM. T-cell co-stimulatory pathways in autoimmunity. *Arthritis Res Ther*. 2008;10(SUPPL. 1):1-10. doi:10.1186/ar2414

76. Morandi F, Airoldi I, Marimpietri D, Bracci C, Faini AC, Gramignoli R. Cd38, a receptor with multifunctional activities: From modulatory functions on regulatory cell subsets and extracellular vesicles, to a target for therapeutic strategies. *Cells*. 2019;8(12). doi:10.3390/cells8121527

77. Kenney-Herbert E, Al-Mayhani T, Piccirillo SGM, et al. CD15 Expression Does Not Identify a Phenotypically or Genetically Distinct Glioblastoma Population. *Stem Cells Transl Med*. 2015;4(7):822-831. doi:10.5966/sctm.2014-0047

78. Simon S, Labarriere N. PD-1 expression on tumor-specific T cells: Friend or foe for immunotherapy? *Oncoimmunology*. 2018;7(1). doi:10.1080/2162402X.2017.1364828

79. Rajaram MVS, Arnett E, Azad AK, et al. M. tuberculosis-Initiated Human Mannose Receptor Signaling Regulates Macrophage Recognition and Vesicle Trafficking by FcRγ-Chain, Grb2, and SHP-1. *Cell Rep*. 2017;21(1):126-140. doi:10.1016/j.celrep.2017.09.034

80. Nurieva RI, Chung Y. Understanding the development and function of T follicular helper cells. *Cell Mol Immunol*. 2010;7(3):190-197. doi:10.1038/cmi.2010.24

81. Kiwamoto T, Kawasaki N, Paulson JC, Bochner BS. Siglec-8 as a drugable target to treat eosinophil and mast cell-associated conditions. *Pharmacol Ther*. 2012;135(3):327-336. doi:10.1016/j.pharmthera.2012.06.005

82. Luckheeram RV, Zhou R, Verma AD, Xia B. CD4 +T cells: Differentiation and functions. *Clin Dev Immunol*. 2012;2012:12. doi:10.1155/2012/925135

83. Konduri V, Oyewole-Said D, Vazquez-Perez J, et al. CD8+CD161+ T-Cells: Cytotoxic Memory Cells With High Therapeutic Potential. *Front Immunol*. 2021;11. doi:10.3389/fimmu.2020.613204

84. Hintzen RQ, Lens SMA, Koopman G, Pals ST, Spits H, Van Lier RAW. CD70 represents the human ligand for CD27. *Int Immunol*. 1994;6(3):477-480.

doi:10.1093/intimm/6.3.477

85. Hendrickx A, Bossuyt X. Quantification of the leukocyte common antigen (CD45) in mature B-cell malignancies. *Commun Clin Cytom*. 2001;46(6):336-339. doi:10.1002/cyto.10032

86. Barrios CS, Johnson BD, Henderson JD, Fink JN, Kelly KJ, Kurup VP. The costimulatory molecules CD80, CD86 and OX40L are up-regulated in Aspergillus fumigatus sensitized mice. *Clin Exp Immunol*. 2005;142(2):242-250. doi:10.1111/j.1365-2249.2005.02905.x

87. Sahoo NC, Rao KVS, Natarajan K. CD80 expression is induced on activated B cells following stimulation by CD86. *Scand J Immunol*. 2002;55(6):577-584. doi:10.1046/j.1365-3083.2002.01093.x

88. Mak TW, Saunders ME. The T Cell Receptor: Structure of Its Proteins and Genes. In: *The Immune Response*. Academic Cell; 2006:311-340. doi:10.1016/b978-012088451-3.50014-4

89. Khan SQ, Khan I, Gupta V. CD11b activity modulates pathogenesis of lupus nephritis. *Front Med*. 2018;5(MAR):15. doi:10.3389/fmed.2018.00052

90. Santos AF, Bécares N, Stephens A, Turcanu V, Lack G. The expression of CD123 can decrease with basophil activation: Implications for the gating strategy of the basophil activation test. *Clin Transl Allergy*. 2016;6(1):1-11. doi:10.1186/s13601-016-0100-4

91. MacLean Scott E, Solomon LA, Davidson C, Storie J, Palikhe NS, Cameron L. Activation of th2 cells downregulates crth2 through an nfat1 mediated mechanism. *PLoS One*. 2018;13(7). doi:10.1371/journal.pone.0199156

92. Arroyo-Espliguero R, Avanzas P, Jeffery S, Kaski JC. CD14 and toll-like receptor 4: A link between infection and acute coronary events? *Heart*. 2004;90(9):983-988. doi:10.1136/hrt.2002.001297

93. Jenkinson SE, Whawell SA, Swales BM, Corps EM, Kilshaw PJ, Farthing PM. The αE(CD103)β7 integrin interacts with oral and skin keratinocytes in an E-cadherin-independent manner. *Immunology*. 2011;132(2):188-196. doi:10.1111/j.1365-2567.2010.03352.x

94. Lu Y, Kared H, Tan SW, et al. Dynamics of helper CD4 T cells during acute and stable allergic asthma. *Mucosal Immunol*. 2018;11(6):1640-1652. doi:10.1038/s41385-018-0057-9

95. Cosgrove PR, Redhu NS, Tang Y, Monuteaux MC, Horwitz BH. Characterizing T cell subsets in the nasal mucosa of children with acute respiratory symptoms. *Pediatr Res*. Published online 2021. doi:10.1038/s41390-021-01364-2

96. Hapuarachchi T, Lewis J, Callard RE. A mechanistic model for naive CD4 T cell homeostasis in healthy adults and children. *Front Immunol*. 2013;4(NOV):2-7. doi:10.3389/fimmu.2013.00366

97. Yu N, Li X, Song W, et al. CD4+CD25+CD127low/- T cells: A more specific treg population in human peripheral blood. *Inflammation*. 2012;35(6):1773-1780. doi:10.1007/s10753-012-9496-8

98. Rouas R, Merimi M, Najar M, et al. Human CD8+CD25 +CD127 low regulatory T cells: microRNA signature and impact on TGF-β and IL-10 expression. *J Cell Physiol*. 2019;234(10):17459-17472. doi:10.1002/jcp.28367

99. Meyer EH, DeKruyff RH, Umetsu DT. T cells and NKT cells in the pathogenesis of asthma. *Annu Rev Med*. 2008;59:281-292. doi:10.1146/annurev.med.59.061506.154139

100. Kim JH, Jang YJ. Role of natural killer cells in airway inflammation. *Allergy, Asthma Immunol Res*. 2018;10(5):448-456. doi:10.4168/aair.2018.10.5.448

101. Hamelmann E. The rationale for treating allergic asthma with anti-IgE. In: *European Respiratory Review*. Vol 16. ; 2007:61-66. doi:10.1183/09059180.00010401

102. Oliveria JP, Agayby R, Gauvreau GM. Regulatory and IgE+ B cells in allergic asthma. In: *Methods in Molecular Biology*. Vol 2270. Humana Press Inc.; 2021:375-418. doi:10.1007/978-1-0716-1237-8_21

103. Carsetti R, Terreri S, Conti MG, et al. Comprehensive phenotyping of human peripheral blood B lymphocytes in healthy conditions. *Cytom Part A*. 2022;101(2):131-139. doi:10.1002/cyto.a.24507

104. Wu YCB, Kipling D, Dunn-Walters DK. The relationship between CD27 negative and positive B cell populations in human peripheral blood. *Front Immunol*. 2011;2(DEC):1-12. doi:10.3389/fimmu.2011.00081

105. Ajaz B, Akhtar A, Chang CC, Solh M, Tangonan K, Khaled Y. Plasma cell CD20 expression: Primary aberrant expression or receptor up-regulation. *Leuk Lymphoma*. 2014;55(2):444-446. doi:10.3109/10428194.2013.802782

106. Byrne AJ, Powell JE, O'Sullivan BJ, et al. Dynamics of human monocytes and airway macrophages during healthy aging and after transplant. *J Exp Med*. 2020;217(3). doi:10.1084/jem.20191236

107. Kapellos TS, Bonaguro L, Gemünd I, et al. Human monocyte subsets and phenotypes in major chronic inflammatory diseases. *Front Immunol*. 2019;10(AUG):2035. doi:10.3389/fimmu.2019.02035

108. Grainger JR, Konkel JE, Zangerle-Murray T, Shaw TN. Macrophages in gastrointestinal homeostasis and inflammation. *Pflugers Arch Eur J Physiol*. 2017;469(3-4):527-539. doi:10.1007/s00424-017-1958-2

109. Bain CC, Bravo-Blas A, Scott CL, et al. Constant replenishment from circulating monocytes maintains the macrophage pool in the intestine of adult mice. *Nat Immunol*. 2014;15(10):929-937. doi:10.1038/ni.2967

110. Balhara J, Gounni AS. The alveolar macrophages in asthma: A double-edged sword. *Mucosal Immunol*. 2012;5(6):605-609. doi:10.1038/mi.2012.74

111. Dewhurst JA, Lea S, Hardaker E, Dungwa J V., Ravi AK, Singh D. Characterisation of lung macrophage subpopulations in COPD patients and controls /631/250/2504/342/1927 /692/699/1785/4037 /13/31 /13/51 /13/106 /38/77 article. *Sci Rep*. 2017;7(1):1-12. doi:10.1038/s41598-017-07101-2

112. Vroman H, Tindemans I, Lukkes M, et al. Type II conventional DCs of asthmatic patients with frequent exacerbations have an altered phenotype and frequency. *Eur Respir J*. 2020;55(5):8-11. doi:10.1183/13993003.00859-2019

113. Brugha R, Mushtaq N, Mccarthy NE, Stagg AJ, Grigg J. Respiratory tract dendritic cells in paediatric asthma. *Clin Exp Allergy*. 2015;45(3):624-631. doi:10.1111/cea.12457

114. Bartemes KR, Kita H. Roles of innate lymphoid cells (ILCs) in allergic diseases: The 10-year anniversary for ILC2s. *J Allergy Clin Immunol*.

2021;147(5):1531-1547. doi:10.1016/j.jaci.2021.03.015

115. Martin Alonso A, Fainardi V, Saglani S. Severe therapy resistant asthma in children: translational approaches to uncover sub-phenotypes. *Expert Rev Respir Med*. 2017;11(11):867-874. doi:10.1080/17476348.2017.1368391

116. Zein JG, Erzurum SC. Asthma is Different in Women. *Curr Allergy Asthma Rep*. 2015;15(6). doi:10.1007/s11882-015-0528-y

117. Saglani S, Payne DN, Zhu J, et al. Early detection of airway wall remodeling and eosinophilic inflammation in preschool wheezers. *Am J Respir Crit Care Med*. 2007;176(9):858-864. doi:10.1164/rccm.200702-212OC

118. Anderson HM, Lemanske RF, Arron JR, et al. Relationships among aeroallergen sensitization, peripheral blood eosinophils, and periostin in pediatric asthma development. *J Allergy Clin Immunol*. 2017;139(3):790-796. doi:10.1016/j.jaci.2016.05.033

119. Horvath G, Wanner A. Inhaled corticosteroids: Effects on the airway vasculature in bronchial asthma. *Eur Respir J*. 2006;27(1):172-187. doi:10.1183/09031936.06.00048605

120. FABBRI L, MELARA R. Systemic effects of inhaled corticosteroids are milder in asthmatic patients than in normal subjects. *Thorax*. 2001;56(3):165 LP - 166. doi:10.1136/thorax.56.3.165

121. Jia Y, Fang X, Zhu X, et al. IL-13+ Type 2 innate lymphoid cells correlate with asthma control status and treatment response. *Am J Respir Cell Mol Biol*. 2016;55(5):675-683. doi:10.1165/rcmb.2016-0099OC

122. Schulz-Kuhnt A, Greif V, Hildner K, et al. ILC2 Lung-Homing in Cystic Fibrosis

Patients: Functional Involvement of CCR6 and Impact on Respiratory Failure. *Front Immunol*. 2020;11(May):1-19. doi:10.3389/fimmu.2020.00691

123. Hussain SMA, Sen A, Barraclough BC, McCarthy JS, Cousins DJ, Gaillard EA. Blood levels of type-2 innate lymphoid cells in preschool children with acute wheeze. *Eur Respir J*. 2017;50(suppl 61):PA1335. doi:10.1183/1393003.congress-2017.PA1335

124. Holmes-Liew CL, Holmes M, Beagley L, et al. Adoptive T-cell immunotherapy for ganciclovir-resistant CMV disease after lung transplantation. *Clin Transl Immunol*. 2015;4. doi:10.1038/cti.2015.2

125. Kilpatrick RD, Rickabaugh T, Hultin LE, et al. Homeostasis of the Naive CD4 + T Cell Compartment during Aging. *J Immunol*. 2008;180(3):1499-1507. doi:10.4049/jimmunol.180.3.1499

126. Yang Y-L, Pan Y-Q, He B-S, Zhong T-Y. Regulatory T cells and Th1/Th2 in peripheral blood and their roles in asthmatic children. *Transl Pediatr*. 2013;2(1):27-33. doi:10.3978/j.issn.2224-4336.2012.04.03

127. Hartl D, Koller B, Mehlhorn AT, et al. Quantitative and functional impairment of pulmonary CD4+CD25hi regulatory T cells in pediatric asthma. *J Allergy Clin Immunol*. 2007;119(5):1258-1266. doi:10.1016/j.jaci.2007.02.023

128. Martin H, Taube C. *Regulatory T Cells and Regulation of Allergic Airway Disease*. Vol 1.; 2012. www.ajcei.us/ISSN:2164-7712/AJCEI1210004

129. Pérez-Lara JC, Espinosa E, Santos-Argumedo L, et al. CD38 correlates with an immunosuppressive treg phenotype in lupus-prone mice. *Int J Mol Sci*. 2021;22(21):1-13. doi:10.3390/ijms222111977

130. Valentine KM, Davini D, Lawrence TJ, et al. CD8 Follicular T Cells Promote B Cell Antibody Class Switch in Autoimmune Disease. *J Immunol*. 2018;201(1):31-40. doi:10.4049/jimmunol.1701079

131. Valentine KM, Hoyer KK. CXCR5+ CD8 T cells: Protective or pathogenic? *Front Immunol*. 2019;10(JUN):1322. doi:10.3389/fimmu.2019.01322

132. Meyer EH, Goya S, Akbari O, et al. Glycolipid activation of invariant T cell receptor+ NK T cells is sufficient to induce airway hyperreactivity independent of conventional CD4+ T cells. *Proc Natl Acad Sci U S A*. 2006;103(8):2782-2787. doi:10.1073/pnas.0510282103

133. Wang C, Liu X, Li Z, et al. CD8+NKT-like cells regulate the immune response by killing antigen-bearing DCs. *Sci Rep*. 2015;5. doi:10.1038/srep14124

134. Bicer S, Giray T, Çöl D, et al. Virological and clinical characterizations of respiratory infections in hospitalized children. *Ital J Pediatr*. 2013;39(1):2-11. doi:10.1186/1824-7288-39-22

135. Kratofil RM, Kubes P, Deniset JF. Monocyte conversion during inflammation and injury. *Arterioscler Thromb Vasc Biol*. 2017;37(1):35-42. doi:10.1161/ATVBAHA.116.308198

136. Ziegler-Heitbrock L, Ancuta P, Crowe S, et al. Nomenclature of monocytes and dendritic cells in blood. *Blood*. 2010;116(16):5-7. doi:10.1182/blood-2010-02-258558

137. Rhodes JW, Tong O, Harman AN, Turville SG. Human dendritic cell subsets, ontogeny, and impact on HIV infection. *Front Immunol*. 2019;10(MAY). doi:10.3389/fimmu.2019.01088

138. Hartmann FJ, Babdor J, Gherardini PF, et al. Comprehensive Immune Monitoring of Clinical Trials to Advance Human Immunotherapy. *Cell Rep*. 2019;28(3):819-831.e4. doi:10.1016/j.celrep.2019.06.049

139. Van Gassen S, Callebaut B, Van Helden MJ, et al. FlowSOM: Using self-organizing maps for visualization and interpretation of cytometry data. *Cytom Part A*. 2015;87(7):636-645. doi:10.1002/cyto.a.22625

140. Quintelier K, Couckuyt A, Emmaneel A, Aerts J, Saeys Y, Van Gassen S. Analyzing high-dimensional cytometry data using FlowSOM. *Nat Protoc*. 2021;16(8):3775-3801. doi:10.1038/s41596-021-00550-0

141. Mitsi E, Kamng'ona R, Rylance J, et al. Human alveolar macrophages predominately express combined classical M1 and M2 surface markers in steady state. *Respir Res*. 2018;19(1). doi:10.1186/s12931-018-0777-0

142. Sánchez-Torres C, García-Romo GS, Cornejo-Cortés MA, Rivas-Carvalho A, Sánchez-Schmitz G. CD16+ and CD16- human blood monocyte subsets differentiate in vitro to dendritic cells with different abilities to stimulate CD4+ T cells. *Int Immunol*. 2001;13(12):1571-1581. doi:10.1093/intimm/13.12.1571

143. Thomas G, Tacke R, Hedrick CC, Hanna RN. Nonclassical Patrolling Monocyte Function in the Vasculature. *Arterioscler Thromb Vasc Biol*. 2015;35(6):1306-1316. doi:10.1161/ATVBAHA.114.304650

144. Cornwell WD, Kim V, Fan X, et al. Activation and polarization of circulating monocytes in severe chronic obstructive pulmonary disease. *BMC Pulm Med*. 2018;18(1). doi:10.1186/s12890-018-0664-y

145. Cosmi L, Maggi L, Santarlasci V, et al. Identification of a novel subset of

human circulating memory CD4+ T cells that produce both IL-17A and IL-4. *J Allergy Clin Immunol*. 2010;125(1-3):222-230.e4. doi:10.1016/j.jaci.2009.10.012

146. Poggi A, Canevali P, Contatore M, Ciprandi G. Higher frequencies of CD161 + circulating T lymphocytes in allergic rhinitis patients compared to healthy donors. *Int Arch Allergy Immunol*. 2012;158(2):151-156. doi:10.1159/000330903

147. Xu ZJ, Gu Y, Wang CZ, et al. The M2 macrophage marker CD206: a novel prognostic indicator for acute myeloid leukemia. *Oncoimmunology*. 2020;9(1). doi:10.1080/2162402X.2019.1683347

148. Yamauchi K, Kasuya Y, Kuroda F, et al. Attenuation of lung inflammation and fibrosis in CD69-deficient mice after intratracheal bleomycin. *Respir Res*. 2011;12(1):1-10. doi:10.1186/1465-9921-12-131

149. Zhang B, Zhang Y, Xiong L, et al. CD127 imprints functional heterogeneity to diversify monocyte responses in inflammatory diseases. *J Exp Med*. 2022;219(2). doi:10.1084/jem.20211191

150. Topham DJ, Reilly EC. Tissue-resident memory CD8+ T cells: From phenotype to function. *Front Immunol*. 2018;9(MAR). doi:10.3389/fimmu.2018.00515

151. Yuan R, Yu J, Jiao Z, et al. The Roles of Tissue-Resident Memory T Cells in Lung Diseases. *Front Immunol*. 2021;12. doi:10.3389/fimmu.2021.710375

152. Luangrath MA, Schmidt ME, Hartwig SM, Varga SM. Tissue-Resident Memory T Cells in the Lungs Protect against Acute Respiratory Syncytial Virus

Infection. *ImmunoHorizons*. 2021;5(2):59-69. doi:10.4049/immunohorizons.2000067

153. Bara I, Ozier A, Tunon De Lara JM, Marthan R, Berger P. Pathophysiology of bronchial smooth muscle remodelling in asthma. *Eur Respir J*. 2010;36(5):1174-1184. doi:10.1183/09031936.00019810

154. Huster KM, Busch V, Schiemann M, et al. Selective expression of IL-7 receptor on memory T cells identifies early CD40L-dependent generation of distinct CD8+ memory T cell subsets. *Proc Natl Acad Sci U S A*. 2004;101(15):5610-5615. doi:10.1073/pnas.0308054101

155. Lambrecht BN, Hammad H, Fahy J V. The Cytokines of Asthma. *Immunity*. 2019;50(4):975-991. doi:10.1016/j.immuni.2019.03.018

156. Stewart JC, Villasmil ML, Frampton MW. Changes in fluorescence intensity of selected leukocyte surface markers following fixation. *Cytom Part A*. 2007;71(6):379-385. doi:10.1002/cyto.a.20392